EUROPEAN Journal of Molecular Biotechnology

Has been issued since 2013.
ISSN 2310-6255. E-ISSN 2409-1332
2016. Vol.(14). Is. 4. Issued 4 times a year

EDITORIAL BOARD

Novochadov Valerii – Volgograd State University, Russian Federation (Editor in Chief)
Goncharova Nadezhda – Research Institute of Medical Primatology, Sochi, Russian Federation
Mosin Oleg – Moscow State University of Applied Biotechnology, Russian Federation
Garbuzova Victoriia – Sumy State University, Ukraine
Ignatov Ignat – Scientific Research Center of Medical Biophysics, Sofia, Bulgaria
Malcevschi Alessio – University of Parma, Italy
Nefedeva Elena – Volgograd State Technological University, Russian Federation
Kestutis Baltakys – Kaunas University of Technology, Lithuania
Tarantseva Klara – Penza State Technological University, Russian Federation
Venkappa S. Mantur – USM-KLE International Medical College, Karnatak, India

The journal is registered by Federal Service for Supervision of Mass Media, Communications and Protection of Cultural Heritage (Russia). Registration Certificate **ПИ № ФС77-55114** 26.08.2013.

Journal is indexed by: **Chemical Abstracts Service** (USA), **CiteFactor** – Directory of International Reseach Journals (Canada), **Cross Ref** (UK), **EBSCOhost Electronic Journals Service** (USA), **Global Impact Factor** (Australia), **International Society of Universal Research in Sciences** (Pakistan), **Journal Index** (USA), **Electronic scientific library** (Russian Federation), **Open Academic Journals Index** (Russian Federation), **Sherpa Romeo** (Spain), **ULRICH's WEB** (USA), **Universal Impact Factor** (Australia).

All manuscripts are peer reviewed by experts in the respective field. Authors of the manuscripts bear responsibility for their content, credibility and reliability.

Editorial board doesn't expect the manuscripts' authors to always agree with its opinion.

Postal Address: 26/2 Konstitutcii, Office 6
354000 Sochi, Russian Federation

Website: http://ejournal8.com/
E-mail: ejm2013@mail.ru

Founder and Editor: Academic Publishing House *Researcher*

Passed for printing 16.12.16.
Format 21 × 29,7/4.

Headset Georgia.
Ych. Izd. l. 4,5. Ysl. pech. l. 4,2.

Order № 14.

© European Journal of Molecular Biotechnology, 2016

European Journal of Molecular Biotechnology

2016

Is. 4

European Journal of Molecular Biotechnology

2016

№ 4

EUROPEAN Journal of Molecular Biotechnology

Издается с 2013 г.
ISSN 2310-6255. E-ISSN 2409-1332
2016. № 4 (14). Выходит 4 раза в год.

РЕДАКЦИОННЫЙ СОВЕТ

Новочадов Валерий – Волгоградский государственный университет, Волгоград, Российская Федерация (Гл. редактор)
Гончарова Надежда – Научно-исследовательский институт медицинской приматологии РАМН, Сочи, Российская Федерация
Мосин Олег – Московский государственный университет прикладной биотехнологии, Москва, Российская Федерация
Венкаппа С. Мантур – Международный медицинский колледж, Карнатака, Индия
Гарбузова Виктория – Сумский государственный университет, Сумы, Украина
Игнатов Игнат – Научно-исследовательский центр медицинской биофизики, София, Болгария
Кястутис Балтакис – Каунасский технологический университет, Литва
Малкевсчи Алессио – Университет города Парма. Парма, Италия
Нефедьева Елена – Волгоградский государственный технический университет, Волгоград, Российская Федерация
Таранцева Клара – Пензенский государственный технологический университет, Пенза, Российская Федерация

Журнал зарегистрирован Федеральной службой по надзору в сфере массовых коммуникаций, связи и охраны культурного наследия (Российская Федерация). Свидетельство о регистрации средства массовой информации ПИ № ФС77-55114 от 26.08.2013 г.

Журнал индексируется в: **Chemical Abstracts Service** (США), **CiteFactor** – Directory of International Reseach Journals (Канада), **Cross Ref** (Великобритания), **EBSCOhost Electronic Journals Service** (США), **Global Impact Factor** (Австралия), **International Society of Universal Research in Sciences** (Пакистан), **Journal Index** (США), **Научная электронная библиотека** (Россия), **Open Academic Journals Index** (Россия), **Sherpa Romeo** (Испания), **ULRICH's WEB** (США), **Universal Impact Factor** (Австралия).

Статьи, поступившие в редакцию, рецензируются. За достоверность сведений, изложенных в статьях, ответственность несут авторы публикаций.
Мнение редакции может не совпадать с мнением авторов материалов.

Адрес редакции: 354000, Российская Федерация, г. Сочи, ул. Конституции, д. 26/2, оф. 6
Сайт журнала: http://ejournal8.com/
E-mail: ejm2013@mail.ru

Учредитель и издатель: ООО «Научный издательский дом "Исследователь"» - Academic Publishing House *Researcher*

Подписано в печать 16.12.16.
Формат 21 × 29,7/4.

Гарнитура Georgia.
Уч.-изд. л. 4,5. Усл. печ. л. 4,2.
Заказ № 14.

© European Journal of Molecular Biotechnology, 2016

CONTENTS

Articles and Statements

Copyright © 2016 by Academic Publishing House *Researcher*

Published in the Russian Federation
European Journal of Molecular Biotechnology
Has been issued since 2013.
ISSN: 2310-6255
E-ISSN: 2409-1332
Vol. 14, Is. 4, pp. 117-124, 2016

DOI: 10.13187/ejmb.2016.14.117
www.ejournal8.com

Articles and Statements

Lateral flow Immunoassay of Sudan I with Direct Calibration Dependence Based on the use of two Kinds of Conjugated Gold Nanoparticles

Anna N. Berlina [a], Dmitry V. Sotnikov [a, *], Sergei A. Eremin [a, b], Liqiang Liu [c], Chuanlai Xu [c], Anatoly V. Zherdev [a]

[a] A.N. Bach Institute of Biochemistry, Research Center of Biotechnology of the Russian Academy of Sciences, Moscow 119071, Russian Federation
[b] Department of Chemical Enzymology, Faculty of Chemistry, M.V. Lomonosov Moscow State University, 119991 Moscow, Russian Federation
[c] School of Food Science and Technology, Jiangnan University, 214122 Wuxi, Jiangsu, China

Abstract

A novel lateral flow immunoassay based on the use of two kinds of conjugated gold nanoparticles' preparations was developed and applied to the detection of the toxic food colorant Sudan I. The gold nanoparticles were conjugated with monoclonal antibodies specific to Sudan and a Sudan-ovalbumin conjugate. Before the immunochromatographic process, the two conjugates were incubated with a tested sample. The results obtained a direct calibration curve for the detection of low-molecular-weight antigen, in contrast to common reverse concentration dependencies. In the absence of the target compound, minimal coloration of the test line was observed. An increase in the Sudan content led to staining and the appearance of a test line, which could be observed by the naked eye. The total duration of the assay is 15 minutes. The visual limit of Sudan I detection was 0.25 ng/mL, and the instrumental limit of detection (LOD) was 7.6 pg/mL. These values were at least three-four points lower than the established permissible level of the contaminant content in foodstuffs. This reserve in sensitivity provides the possibility of working with highly diluted samples and thus excludes the influence of their matrixes on the assay results. The direct dependence of the coloration on the concentration of Sudan I in the proposed assay means it is easy to identify the presence of the contaminant at extremely low concentrations. The common nature of the proposed approach allows its use in lateral flow immunoassays of different compounds.

Keywords: immunoassay, lateral flow tests, gold nanoparticles, immunochromatography, on-site tests, Sudan I.

* Corresponding author
E-mail addresses: berlina.anna@gmail.com (A.N. Berlina), sotnikov-d-i@mail.ru (D.V. Sotnikov), zherdev@inbi.ras.ru (A.V. Zherdev), saeremin@gmail.com (S.A. Eremin), murel@163.com (L. Liu), xcl@jiangnan.edu.cn (C. Xu), zherdev@inbi.ras.ru (A.V. Zherdev)

1. Introduction

Sudan I and related compounds (Sudans II-IV) are illegal food additives. Their intense red hue improves the coloration of food products and, correspondingly, their market potential. They are classified as class 3 carcinogens according to the International Agency for Research on Cancer. Thus, most countries have banned their use in food production (European Food Safety Authority). The EC maximum allowable level for Sudans is 0.5–1 mg/kg (European Food Safety Authority). However, they are often detected in chilli-, curry-, curcuma-, and palm oil-containing foodstuffs (Calbiani et al., 2004; Calbiani et al., 2004a; Oplatowska-Stachowiak, Elliott, 2015), indicating that unscrupulous manufacturers continue to use Sudans.

Many methods have been proposed for the determination of Sudan dyes in foodstuffs as recently reviewed (Oplatowska-Stachowiak, Elliott, 2015; Rebane et al., 2010): HPLC (Liu et al., 2007; Ertaş et al., 2007; Yu et al., 2015; Khalikova et al., 2015), electrochemical sensors (Li et al., 2015; Li et al., 2015a; Wang et al., 2015), and capillary electrophoresis (Mejia et al., 2007). The main disadvantages of the approaches listed above are the high cost of the equipment, the significant duration of one analysis, and difficulties in screening a large number of samples.

Immunoassay techniques, due to their simplicity and productivity, are often used in food control laboratories. Among these, lateral flow immunoassays (LFIAs) focus on screening out-of-laboratory purposes because of they are faster and less labor-intensive compared with alternate immunotechniques (Wong, Tse, 2009; Quesada-González, Merkoçi, 2015). Despite the availability of ELISA for Sudan dyes (Chang et al., 2011; Liu et al., 2012; Shan et al., 2012; Anfossi et al., 2009; Qi et al., 2015), only two LFIAs for Sudan I have been developed, namely a semi-quantitative assay in the work of Wang et al. (Wang et al., 2013), and a quantitative photometric assay in the work of Berlina et al. (Berlina et al., 2016).

Both assays rely on a traditional competitive scheme when hapten conjugated with protein is immobilized on the membrane and an anti-hapten antibody is conjugated with gold nanoparticles. This format is typical for the LFIA of low-molecular-weight compounds. In this case, the brightest test line occurs in the absence of analyte and thus the limit of detection is determined when the color intensity in the test area decreases. However, this method of data processing is suitable when there is a detector. For out-of-laboratory conditions, the best choice is a cut-off test, i.e. control of the coloration disappearance, but such assay protocols have significantly worse sensitivity.

To resolve this problem, we propose an assay involving the application of two kinds of conjugated gold nanoparticles. It allows receipt of direct calibration dependence when an absence of the competitor leads to an absence of coloration.

2. Materials and methods

2.1. Chemicals and reactants

Mouse monoclonal antibodies of Sudan I and Sudan–ovalbumin conjugate (synthesized using succinimide/carbodiimide technique) were obtained as described previously (Berlina et al., 2016). Goat polyclonal antibodies against mouse immunoglobulins G were from IMTEK (Moscow, Russia). Gold (III) chloride hydrate was purchased from Fluka (St. Louis, MO, USA). Methanol was purchased from Fluka (St. Gallen, Switzerland). Sodium citrate dihydrate, potassium carbonate, Tris, and Tween-20 were purchased from Sigma–Aldrich (St. Louis, MO, USA). Bovine serum albumin (BSA) was purchased from MP Biomedicals (Santa Ana, CA, USA). All other reagents were from Chimmed (Moscow, Russia). Deionized water, with a resistance of 18.2MΩ·cm at 22°C (Simplicity Water Purification system, Millipore, Bedford, MA, USA) was used to prepare all the aqueous solutions for the syntheses and assays. The Amicon Ultra (30 kDa) ultracentrifugation tubes were from Millipore (Bedford, MA, USA).

CNPH-backed nitrocellulose membranes (CNPH90)were purchased from Advanced Microdevices (MDI, Ambala Cantt, India). The following membrane compounds for manufacturing test strips were purchased from Millipore (Bedford, MA, USA): CFSP223000 adsorption pads and fiberglass macroporous CFCP203000 conjugate pads.

2.2. Synthesis of gold nanoparticles (Ji et al., 2007)

0.2 mL of 5% $HAuCl_4$ was added to 97.5 mL of water (filtered through a 0.22-μm filter). The solution was heated to its boiling point, and then 1.5 mL of 1 % sodium citrate was added. The resulting mixture was boiled for 20 minutes and then cooled.

2.3. Conjugation of antibodies or Sudan-ovalbumin with gold nanoparticles

In this step, 3 μL of anti-Sudan antibody with a concentration of 3.8 mg/mL, or 0.3 mL of Sudan–ovalbumin with a concentration 3.5 mg/mL were dialyzed against a 50 mM carbonate buffer, pH 9.0 using Amicon Ultra (30 kDa) ultracentrifugation tubes. The volume upper the separation membrane was added to 1 mL of freshly synthesized gold nanoparticle solution and this mixture was left for 45 minutes to incubate at room temperature with stirring. Then, 15μL of a 10 % BSA aqueous solution was added to the mixture, followed by incubation for 15 minutes under the same conditions. The conjugate was separated by centrifugation at 10,000 g at +4° C for 15 minutes. For the stabilization and long-term storage 50 mL of 50 mM potassium phosphate buffer, pH 7.4, with 0.1 M NaCl, 0.25% BSA, 0.25% Tween-20, 1% saccharose, and 0.05% NaN_3 (TTBSA) were added to the resulting product.

2.4. Manufacturing of test strips

Goat anti-mouse IgG polyclonal antibody (0.5 mg/mL in Milli-Q water) was immobilized onto the nitrocellulose CNPH 90membrane as the test line, as described previously (Berlina et al., 2013). The volume of the reagent loaded zone was 0.1 μL per 1 mm. The membranes were dried at room temperature overnight. The multi-membrane composite was then assembled and cut into individual 3-mm wide strips. The strips were packed and stored at +4 °C. The antibody and Sudan-ovalbumin conjugate with colloidal gold with OD_{520nm} = 10 were mixed in 10% BSA in a 1:10 v/v ratio and used when blending with samples with and without Sudan I.

2.5. Lateral flow immunoassay

The assay was carried out at room temperature. A sample was added to an Eppendorf tube containing the mixture of conjugates and left for 5 minutes. The test strip was then submerged in the tested sample, incubated for 5 minutes, removed, and placed horizontally for 5-minutes to dry. After the removal of the test strip, 50 μL of 50 mM PBSwith 0.05% Triton X-100 were added dropwise to the lower part of the test strip (sample pad) to remove the conjugates from the pad.

The resulting appearance of the test line was determined by the naked eye, and the lowest concentration leading to coloration was taken as the visual limit of detection (LOD_v). To plot a calibration curve, the color intensity was determined by processing the scanned digital images of the strips using TotalLab software (Nonlinear Dynamics, Newcastle upon Tyne, UK) under a 1D regime. The instrumental limit of detection (LOD_i) was calculated as the concentration that resulted in a reliable difference in color from the background value, i.e., the color intensity in the absence of the analyte was three times higher compared with the standard deviation of the background color.

3. Results and Discussion

3.1. Lateral flow immunoassay design

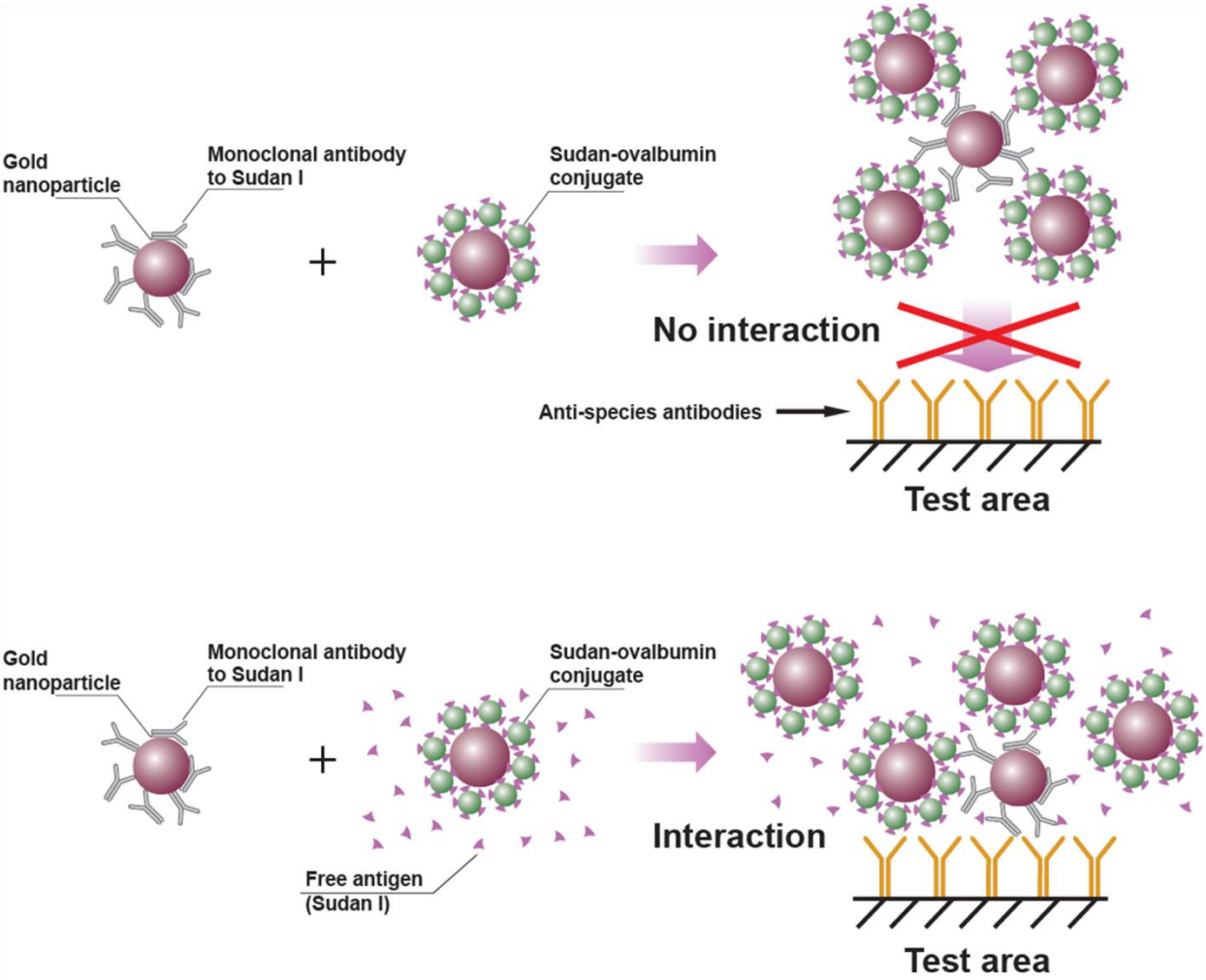

Fig. 1. Scheme of the proposed immunochromatographic assay for Sudan I with the use of two kinds of conjugates.

The mixed conjugates reacted due to an interaction between the Fab fragment of the immobilized antibody on the surface of one gold nanoparticle and a Sudan I derivative conjugated with ovalbumin (Sudan–ovalbumin) on another gold nanoparticle. Thus, the conjugated Sudan–ovalbumin covered the antibodies on the surface of the gold nanoparticle on all sides and prevented the Fc fragment interacting with the anti-mouse IgG immobilized in the test area. This resulted in the absence of visible coloration and is considered as a negative result of the testing. The added Sudan I started to compete with the Sudan-ovalbumin conjugated with gold nanoparticles for the binding sites of antibodies. Thus, Sudan I displaced the Sudan–ovalbumin conjugated to the gold nanoparticles and blocked the Fab-fragments. As a result of this reaction, Fc-binding antibody fragments that were previously blocked by such a big Sudan-ovalbumin conjugate with gold nanoparticles became available for an interaction with an anti-mouse antibody. The result is the binding of mouse anti-Sudan antibodies to goat anti-mouse antibodies immobilized in the test area and the appearance of a colored test line (Fig. 1). The latter signified a positive result of the testing.

For this assay two conjugates of gold nanoparticles were synthesized: the first with an antibody to Sudan I, and the second with a Sudan–ovalbumin conjugate. Both conjugates were mixed in a ratio with 10-fold excess (Sudan-ovalbumin towards antibody) to protect the maximal amount of antibody on the gold nanoparticles. The antibody conjugated to the gold nanoparticles interacted with the target hapten in the conjugate. In the absence of Sudan I in the solution interactions occurred only between the conjugates, and no bright test line was observed (Fig. 2, test strip 1). With an increase in the Sudan I content, the color started to appear due to the opportunity of Fc-fragments antibodies interacting with the anti-species antibody in the membrane's test zone (Fig. 2, test strips 2–4).

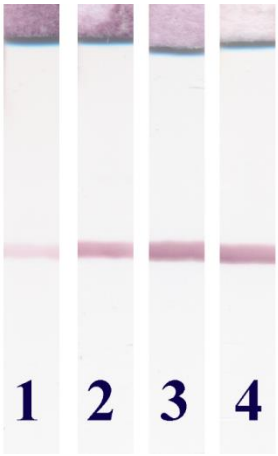

Fig. 2. Test strips images for different Sudan I concentrations in the samples. Strips 1-4 correspond to Sudan I concentrations of 0 pg/mL, 250 pg/mL, 250 ng/mL, and 1 μg/mL, respectively.

Such a novel and untraditional approach is the way to develop LFIA with a direct calibration for better perception of the obtained data by the naked eye. The effect of steric factors, such as the presence of major competitors (in this case Sudan-ovalbumin conjugated to colloidal gold) and the gradual replacement by the molecules of a low molecular competitor applied in the proposed approach, allow for the adjustment of the interaction with the required parameters. Unlike a traditional competitive scheme, the main difference is the inherent movement of the assay sensitivity to low concentrations of analyte. Visually, the appearance of staining in the case of a low positive result is much better perceived in contrast to the slight decrease of staining intensity in the test zone using a traditional format (Berlina et al., 2016). Moreover, no equipment is needed and this can be used as a cut-off test for the detection of Sudan I by ordinary consumers that are not experts.

3.2. Determination of analytical parameters for the proposed LFIA

Various Sudan I solutions were prepared to produce a competitive interaction. The intensity of the color depended directly on the Sudan I concentration (Fig. 3). The LOD_v (when the test line appeared) was 0.25 ng/mL (which corresponds to 1 μg/kg of food taking into account a sample preparation including dilution used in our previous investigation (Berlina et al., 2016)) despite residual staining in the absence of the competitor (Fig. 3A). Analytical characteristics were calculated in accordance with the obtained linear equation (Fig. 3B) and the LOD_i was considered as 7.6 pg/mL (which corresponds to 0.03 μg/kg of food with the same sample pretreatment, n=3). The average deviation of detection varied from 0.2 to 3.5 %. The total duration of the assay was 15 minutes.

This study describes the highest sensitivity in lateral flow assay (and immunoassays at all) for Sudan I detection. Compared to the permissible level established by EC 0.5–1 mg/kg of food (Chailapakul et al., 2008) the developed test system is highly sensitive (more than 1,000 times for visual and 33,000 for instrumental detection). Therefore, the developed assay is suitable for screening samples with low levels of contamination or diluted samples containing Sudan I. The application of two conjugates improved the sensitivity of the assay, and showed new prospects in the development of lateral flow assays.

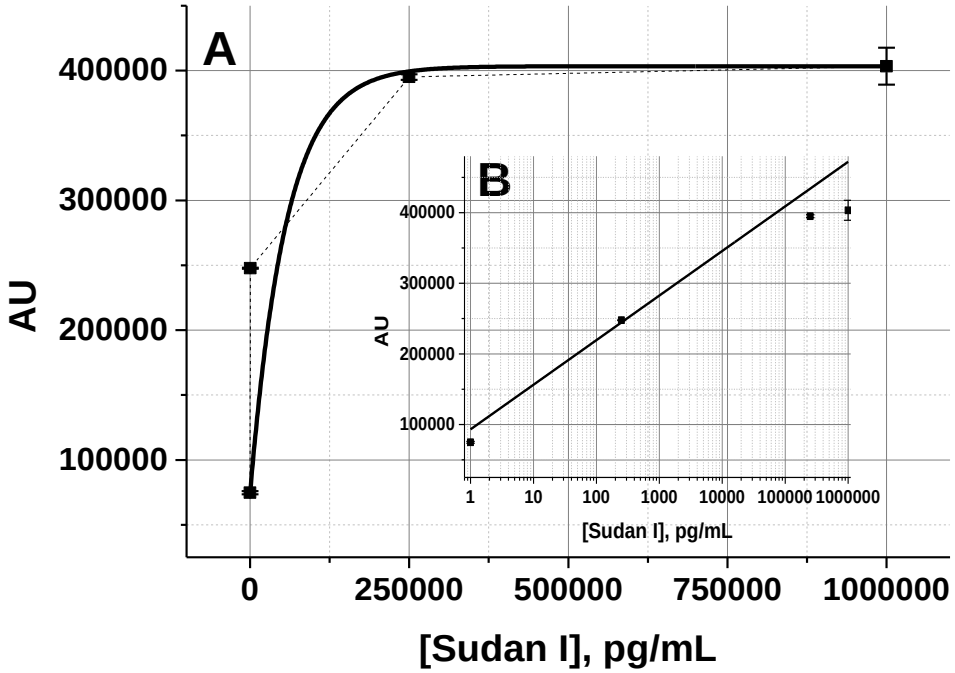

Fig. 3. Concentration dependence of the test line coloration in the LFIA for Sudan I: A – exponential calibration curve, B – its linear region.

4. Conclusion

A novel lateral flow immunoassay for Sudan I was developed using two gold nanoparticles conjugates. Interaction of both conjugates at the first stage of assay with followed competition under the influence of steric factors and ultimately binding with anti-species antibody immobilized in the test area are the basis for the new proposed LFIA format with direct calibration of Sudan I. Unlike traditional competitive schemes, the main difference is the inherent movement of the assay sensitivity to low concentrations of analyte. Visually, the difference between negative and positive results is clearer and based on the corresponding absence or presence of the staining in the test zone of the strip. The developed LFIA allows the detection of Sudan I with LOD_v (when the test line appeared) at 0.25 ng/mL of final solution that corresponds to 1 μg/kg of food before the sample pretreatment. An instrumental limit of detection is 7.6 pg/mL. This level corresponds to 0.03 μg of Sudan I per kg of food.

The application of two conjugates allowed the sensitivity to increase and showed new prospects in the development of immunoassays, especially highly sensitive lateral flow assays. The developed lateral flow assay is suitable for a rapid, non-expensive tool for Sudan I detection even in out-of-laboratory conditions. The proposed approach with the application of two conjugates can be used for further LFIA developments of other food contaminants, including organic hydrophobic compound by the analogy with Sudan I.

5. Acknowledgements

This work was financially supported by the Russian Foundation for Basic Research, project no. 14-03-00753_a.

References

Anfossi et al., 2009 – *Anfossi L., Baggiani C., Giovannoli C., Giraudi G.* (2009). Development of enzyme-linked immunosorbent assays for Sudan dyes in chilli powder, ketchup and egg yolk. *Food Addit. Contam.* 26(6), pp. 800-807.

Berlina et al., 2013 – *Berlina A.N., Taranova N.A., Zherdev A.V., Vengerov Y.Y., Dzantiev B.B.* (2013). Quantum dot-based lateral flow immunoassay for detection of chloramphenicol in milk. *Anal. Bioanal. Chem.* 405(14), pp. 4997-5000.

Berlina et al., 2016 – *Berlina A.N., Zherdev A.V., Xu C., Eremin S.A., Dzantiev B.B.* (2016). Development of lateral flow immunoassay for rapid control and quantification of the presence of the colorant Sudan I in spices and seafood. *Food Control*. (In Press).

Calbiani et al., 2004 – *Calbiani F., Careri M., Elviri L., Mangia A., Pistara L., Zagnoni I.* (2004). Development and in-house validation of a liquid chromatography–electrospray–tandem mass spectrometry method for the simultaneous determination of Sudan I, Sudan II, Sudan III and Sudan IV in hot chilli products. *J. Chromatogr. A*. 1042(1), pp. 123-130.

Calbiani et al., 2004a – *Calbiani F., Careri M., Elviri L., Mangia A., Zagnoni I.* (2004). Accurate mass measurements for the confirmation of Sudan azo-dyes in hot chilli products by capillary liquid chromatography–electrospray tandem quadrupole orthogonal-acceleration time of flight mass spectrometry. *J. Chromatogr. A*. 1058(1), pp. 127-135.

Chailapakul et al., 2008 – *Chailapakul O., Wonsawat W., Siangproh W., Grudpan K., Zhao Y., Zhu Z.* (2008). Analysis of sudan I, sudan II, sudan III, and sudan IV in food by HPLC with electrochemical detection: Comparison of glassy carbon electrode with carbon nanotube-ionic liquid gel modified electrode. *Food Chemistry*. 109(4), pp. 876-882.

Chang et al., 2011 – *Chang X.C., Hu X.Z., Li Y.Q., Shang Y.J., Liu Y.Z., Feng G., Wang J.P.* (2011). Multi-determination of Para red and Sudan dyes in egg by a broad specific antibody based enzyme linked immunosorbent assay. *Food Control*. 22(11), pp. 1770-1775.

European Food Safety Authority – *European Food Safety Authority (EFSA)*. (2005). Opinion of the Scientific Panel on Food Additives, Flavourings, Processing Aids and Materials in Contact with Food on a request from the Commission to Review the toxicology of a number of dyes illegally present in food in the EU. *The EFSA Journal*, 263, pp. 1–71.

Ertaş et al., 2007 – *Ertaş E., Özer H., Alasalvar C.* (2007). A rapid HPLC method for determination of Sudan dyes and Para Red in red chilli pepper. *Food Chem*. 105(2), pp. 756-760.

Ji et al., 2007 – *Ji X., Song X., Li J., Bai Y., Yang W., Peng X.* (2007). Size control of gold nanocrystals in citrate reduction: the third role of citrate. *J. Am. Chem. Soc*. 129(45), 13939-13948.

Khalikova et al., 2015 – *Khalikova M.A., Šatínský D., Solich P., Nováková L.* (2015). Development and validation of ultra-high performance supercritical fluid chromatography method for determination of illegal dyes and comparison to ultra-high performance liquid chromatography method. *Anal. Chim. Acta*. 874, pp. 84-96.

Liu et al., 2007 – *Liu W., Zhao W.J., Chen J.B., Yang, M.M.* (2007). A cloud point extraction approach using Triton X-100 for the separation and preconcentration of Sudan dyes in chilli powder. *Anal. Chim. Acta*. 605(1), pp. 41-45.

Liu et al., 2012 – *Liu J., Zhang H., Zhang D., Gao F., Wang J.* (2012). Production of the monoclonal antibody against Sudan 2 for immunoassay of Sudan dyes in egg. *Anal. Biochem*. 423(2), pp. 246-252.

Li et al., 2015 – *Li B.L., Luo J.H., Luo H.Q., Li N.B.* (2015). A novel conducting poly (p-aminobenzene sulphonic acid)-based electrochemical sensor for sensitive determination of Sudan I and its application for detection in food stuffs. *Food Chem*. 173, pp. 594-599.

Li et al., 2015a – *Li J., Feng H., Li J., Feng Y., Zhang Y., Jiang J., Qian D.* (2015). Fabrication of gold nanoparticles-decorated reduced graphene oxide as a high performance electrochemical sensing platform for the detection of toxicant Sudan I. *Electrochim. Acta*. 167, pp. 226-236.

Mejia et al., 2007 – *Mejia E., Ding Y., Mora M.F., Garcia C.D.* (2007). Determination of banned sudan dyes in chili powder by capillary electrophoresis. *Food Chem*. 102(4), pp. 1027-1033.

Oplatowska-Stachowiak, Elliott, 2015 – *Oplatowska-Stachowiak M., Elliott C.T.* (2015). Food Colours: Existing and Emerging Food Safety Concerns. *Crit. Rev. Food Sci. Nutr*. (just-accepted), pp. 00-00.

Qi et al., 2015 – *Qi Y.H., Zhang H.C., Xu R.T., Liu J., Zhang L., Wang J.P.* (2015). Immunoassay of red dyes based on the monoclonal antibody of β-naphthol. *J. Environ. Sci. Health B*. 50(9), pp. 645-653.

Quesada-González, Merkoçi, 2015 – *Quesada-González D., Merkoçi A.* (2015). Nanoparticle-based lateral flow biosensors. *Biosens. Bioelectron*. 73, pp. 47-63.

Rebane et al., 2010 – *Rebane R., Leito I., Yurchenko S., Herodes K.* (2010). A review of analytical techniques for determination of Sudan I–IV dyes in food matrixes. *J. Chromatogr. A*. 1217(17), pp. 2747-2757.

Shan et al., 2012 – *Shan W.C., Xi J.Z., Sun J., Zhang Y.J., Wang, J.P.* (2012). Production of the monoclonal antibody against Sudan 4 for multi-immunoassay of Sudan dyes in egg. *Food Control*. 27(1), pp. 146-152.

Wang et al., 2013 – *Wang J., Wang Z., Liu J., Li H., Li Q.X., Li J., Xu T.* (2013). Nanocolloidal gold-based immuno-dip strip assay for rapid detection of Sudan red I in food samples. *Food Chem*. 136(3), pp. 1478-1483.

Wang et al., 2015 – *Wang M., Chen Z., Chen Y., Zhan C., Zhao J.* (2015). New synthesis of self-assembly ionic liquid functionalized reduced graphene oxide–gold nanoparticle composites for electrochemical determination of Sudan I. *J. Electroanal. Chem*. 756, pp. 49-55.

Wong, Tse, 2009 – *Wong R., Tse H.* (2009) Lateral flow immunoassay: Humana Press, New York, 223 p.

Yu et al., 2015 – *Yu W., Liu Z., Li Q., Zhang H., Yu Y.* (2015). Determination of Sudan I–IV in candy using ionic liquid/anionic surfactant aqueous two-phase extraction coupled with high-performance liquid chromatography. *Food Chem*. 173, pp. 815-820.

Copyright © 2016 by Academic Publishing House *Researcher*

Published in the Russian Federation
European Journal of Molecular Biotechnology
Has been issued since 2013.
ISSN: 2310-6255
E-ISSN: 2409-1332
Vol. 14, Is. 4, pp. 125-138, 2016

DOI: 10.13187/ejmb.2016.14.125
www.ejournal8.com

Comparative Modeling the Thermal Transfer in Tissues with Volume Pathological Focuses and Tissue Engineering Constructs: a Pilot Study

Valery V. Novochadov [a], Alexander A. Shiroky [a, *], Alexander V. Khoperskov [a], Alexander G. Losev [a]

[a] Volgograd State University, Russian Federation

Abstract

The goal of this study was to conduct the computing experiments on the use of the spatial temperature distribution and heat flow in biological tissues obtained on the basis of microwave radiometry, and to develop the predictive algorithm of their specific properties and conditions.

In the first stage, the data about the surface and deep temperature in different parts of the mammary glands of healthy women were used to build the model of heat flow in this body, proved that there is a lateral heat transfer from one part to another. Accounting for this phenomenon in the analysis of the spatial distribution of temperature in the breast with verified malignant tumours with installed localization made it possible to prove a several decision rules with a potentially high diagnostic efficiency.

Based on the assumption about spatial variation of the dielectric constant and electrical conductivity in biological tissue at the installation site and subsequent remodeling of tissue-engineered constructs to develop in similar patterns, and to be capable of the same impact on brightness temperature of the tissues under the antenna of a microwave radiometer, we conducted simulation in the second phase of the study. The crucial equations, being able to differentiate different states of adaptation (remodeling) of tissue-engineered constructs were offered, that can be used in tissue engineering as creating data structures, also for monitoring postimplantation period.

Keywords: microwave thermography, spatial temperature distribution, thermal transfer, brightness temperature, mammary glands, breast cancer, tissue engineering constructs, mathematical modeling, thermal simulation.

1. Introduction

New approaches to the reconstruction of organs and tissues, which were lost or irreversibly damaged as a result of illness, based on the use of tissue-engineered constructs (TEC) and cellular technologies, described in aggregate as TERM (tissue engineering and regenerative medicine) technologies. Biomimetic and biocompatible properties are fundamental for these products. Their presence provides complete or partial replacement of implant material by proper own tissue without any inflammatory reactions within the projected time (Wang et al., 2014; Maitz, 2015). In other cases, as a result, only a dense integration between the implant and surrounding tissues seems to be a general task of implantation (Jang et al., 2011; Albertini et al., 2015).

* Corresponding author
E-mail addresses: shiroky.aa@volsu.ru (A.A. Shiroky)

The undoubted purpose of the innovation in the field of manufacturing a variety of TEC is to make a more accurate reproduction of the structural and functional characteristics for prosthetic tissue. However, most studies usually focus on the structural biomimetics, which implied the restoration of the required functional characteristics after remodeling TEC in native host tissue (O'Brien, 2011; Park et al., 2016). This explains the comparative scarcity of works devoted to the analysis of the recovery of the functional status of an implantation region in the dynamics (Lu et al., 2013; Hwang et al., 2015). Typically, this analysis is carried out using specially designed options, which were not directly determined by real biochemical and physiological processes in the place of TEC installation (Guliak et al., 2014).

Research of heat transfer in system 'TEC – the surrounding tissue' due to remodeling is strongly important to explain these processes from the standpoint of the biochemistry and physiology of regeneration. First, the TEC remodeling is the phase process, which key points established as cell seeding, growth of blood vessels, resorption of the scaffold matter, and the synthesis of new extracellular matrix (Fitzpatrick, 2015; Mao, 2015). All of these components are differently connected to the heat input in the system and to own heat production in it. Second, the change of physico-chemical properties of the scaffold matter, as its transition in the host extracellular matrix, affects the characteristics of thermal conductivity, which is complicated by the spatial heterogeneity of tissues.

In this paper we analyze the possibility to simulate three-dimensional heat transfer, determine the spatial distribution of temperatures in the system 'TEC – the surrounding tissue', and build predictive algorithms for tissues, containing TEC at different stages of remodeling in host one. This approach is constructed by analogy with the cases for tissues with volume pathological focuses based on spatial heterogeneity of thermal distribution in tissues (Khoperskov et al., 2014; Losev et al., 2015).

2. Material and Methods

2.1. The measuring the spatial temperature distribution of in biological tissues

As a dataset, in the first phase of the study we used the results of measurements of surface and deep temperatures in different breast areas by microwave radiometry (MWR) is combined with surface infrared thermometry. This method is an important tool for breast cancer diagnosis, although it has a low enough nosological specificity (Leroy et al., 1998; Wurst et al., 2006; Kelly et al., 2011). Both most dangerous fast-growing tumors, and cases of marked proliferation, mastopathy, or inflammatory processes in mammary gland may be included in 'red group' after cohort survey (Kelly et al. 2012). To increase the sensitivity and specificity of this method, the spatial heterogeneity of the temperature distribution, their variances, or mirror asymmetry may be realized in several automated algorithms (Bardati, 2008; Vesnin et al., 2008; Shin et al., 2013).

We choose application MWR-method (Filatov et al., 2013), which allowed a direct contact between antenna and human body during the measurement. The technique was realized using radiometer RTM-01-RES Imaging system (RES Ltd., Russia). At frequencies of 1.1–1.6 GHz MWR demonstrated sufficient sensitivity to distinguish clinically significant temperature changes in tissues up to 4 cm depth in biological tissue (Umadevi et al., 2011). Modeling the thermal and electromagnetic processes in kidneys and brain showed a good agreement with the experimental MWR results (Gouzouasis et al., 2010; Stauffer et al., 2014). The use of this method for early diagnosis of vascular diseases such as atherosclerosis and varicose veins of the lower extremities, have received encouraging professional responses (Toutouzas et al., 2012; Stavrov et al., 2013).

The control sample included the results of measurements in healthy women 20-48 years without any breast pathology on clinical examination. The following exclusion criteria were established: any information about breast pathology in anamnesis (1), pregnancy (2), lactation (3), inner genital pathology (4), hormonal disorders (5), chronic infectious diseases or acute infections of less than 1 month before the survey (6), insufficiency of blood circulation (7). In the end, the sample included the results of an examination of 31 women. All calculations were carried out separately for the right and left mammary glands, given the presence of a physiological bilateral asymmetry (Vesnin et al., 2008).

The main sample included MWR data of the 78 women of the same age range, which had clinically proven breast cancer in the form of three-dimensional focus of accurate localization. Primary-dissociated, neglected, and doubtful cases were excluded from this sample.

Quantitative data were processed using Statistica 8.0 (StatSoft Inc., USA). Results were shown as Median [1st quartile ÷ 3rd quartile]. To prove the validity of differences for multiple groups the non-parametric ANOVA criterion was used; P values < 0.05 were considered statistically significant.

2.2. Modeling the heat transfer

Numerical simulation of electromagnetic radiation of tissues, including tumors, was based on the equations of heat conduction and Maxwell in the stationary approximation (Vesnin et al., 2010):

$$\vec{\nabla}\{k(x,y,z)\vec{\nabla}T(x,y,z)\} = -Q_{bl}(x,y,z) - Q_{met}(x,y,z), \quad (1)$$

$$\nabla^2\vec{E}(x,y,z) + \omega_0\mu_0\varepsilon_0\varepsilon(x,y,z)\vec{E}(x,y,z) = 0 \quad (2)$$

where k is the thermal conductivity coefficient; T – temperature; Q_{bl} – heat input with blood flow (determined by the balance of the arterial Q_a and venous Q_v heat transfer); Q_{met} is the heat source connected to metabolic processes in tissues (Fig. 1); $\vec{E}$ – vector of the electric field; ε – dielectric permittivity; ∇ is the nabla operator, and ω_0 is the radiation frequency.

Heat transfer from biological tissue to air at the interface, specified unit normal to the surface vector, defined by the condition:

$$\left(\vec{n},\vec{\nabla}T\right) = \frac{h_{air}}{k(x,y,z)}\left(T(x,y,z) - T_{air}\right). \quad (3)$$

Complex geometries and multi-component structure by using the methods of finite-difference approximations of the differential equations requires special numerical unstructured grids (Ng, 2004; Lin et al., 2009) and tasks of the boundary conditions (3) on a complex surface. The use of tetrahedra as elements of the grid is convenient for the simulation of radiation propagation in biotissue (Seteikin et al., 2010).

Fig. 1 shows the scheme of heat exchange between the biological tissues and the environment with the temperature T_{air}. It significantly depends on the heat transfer coefficient h_{air}, which can be taken equal to $h_{air} \approx 13.5$ W/(m·°C) for our case. A strong spatial heterogeneity of physical parameters is the distinctive feature of these biological tissues (Losev et al., 2015).

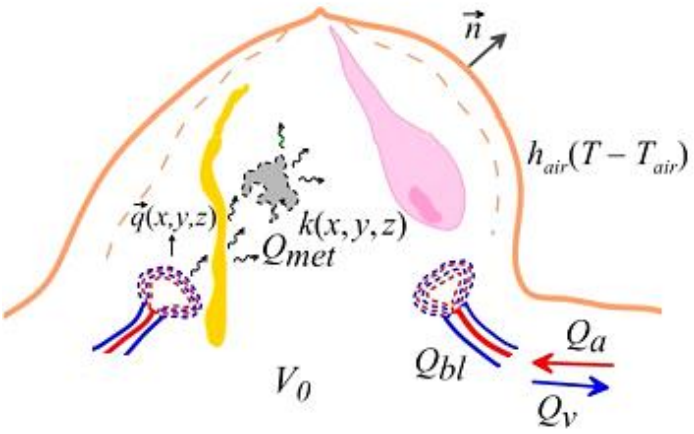

Fig. 1. The heat input Q_{bl}, own heat generation Q_{met}, heat exchange with air, and the internal heterogeneity of the structure are the fundamental processes characterizing the spatial features of heat transfer in the volume of breast tissue V_0. Explanations are following in the text.

Coefficient of thermal conductivity of tissues varies in the range of 0.15–0.7 W/(m·°C). The most important factor is the specific water content due to the strong dependence of tissue density, heat capacity and thermal conductivity from the value of this indicator (Table 1).

The presence of a malignant tumor to the greatest extent modifies the distribution of the specific heat generation $Q_{met} \approx 250\text{-}70000$ W/m^3 and flow parameters.

Table 1. The main physical characteristics of biological tissues, necessary to calculate the volumetric heat transfer in the body, generally at (Herman I.P., 2007; Afrin et al., 2011; Li et al., 2014)

Human tissues	Density, g/sm^3	Heat capacity, J/(g·°C)	Termal conductivity, W/(m·°C)
Skin	1.10 – 1.50	2.93 – 3.45	0.45 – 0.50
Blood	1.05 – 1.06	3.60 – 3.90	0.53 – 0.55
Adipose tissue	0.85 – 0.92	2.25 – 2.30	0.20
Connective tissue and muscles	1.04 – 1.10	3.30 – 3.36	0.50
Human body in common	1.04	3.35	0.48

Features of use of these general formulas and its approximation to specific calculations in the case of heat transfer in the tissues with the pathological focus or the TEC, following if result statement.

3. Results

3.1. Spatial temperature distribution in mammary glands

Table 2 shows the sample characteristics for control group of healthy women. Since the distribution in the samples is not parameterized, the median characteristics in quartiles 1 – 3 were presented.

The dispersion of inside temperatures at the measuring points 0 – 8 are in the range from 0.14 (point 0) to 0.37 (point 2). One way ANOVA shows that the sample with 95% probability does not differ. However, sampling of measurement results in point 9 (axillary region) has significant differences from the results in the breast.

In the case of surface temperature differences are brighter. The dispersion values are from 0.39 (measuring point 1) to 0.95 (point 0), which was probably due to differences in external conditions in examination procedure. U-test (Mann-Whitney) for the measurement data in pairs of adjacent points revealed no differences, although the ANOVA test showed that the alternative hypothesis was true. In a similar way the difference of external and internal temperatures manifested themselves.

Table 2. Spatial distribution and gradient of temperature in intact mammary glands of practically healthy women (Me [Q1 ÷ Q3])

Points	Surface temperature ˚C	Inner temperature ˚C	Temperature gradients
Left breast			
0 (Mamilla)	32.8 [32.6 ÷ 33.7]	34.5 [34.3 ÷ 34.8]	1.5 [1.0 ÷ 2.1]
1	32.9 [32.7 ÷ 33.3]	34.6 [34.1 ÷ 35.0]	1.6 [1.2 ÷ 2.1]
2	33.2 [32.7 ÷ 33.7]	34.6 [34.2 ÷ 34.9]	1.5 [1.0 ÷ 1.9]
3	33.4 [32.6 ÷ 33.8]	34.7 [34.3 ÷ 34.9]	1.2 [0.8 ÷ 2.1]
4	33.2 [32.7 ÷ 33.5]	34.4 [34.2 ÷ 34.8]	1.3 [1.0 ÷ 1.7]
5	32.9 [32.1 ÷ 33.3]	34.4 [34.1 ÷ 34.7]	1.7 [1.1 ÷ 2.3]
6	32.5 [31.9 ÷ 33.1]	34.3 [33.9 ÷ 34.7]	2.0 [1.5 ÷ 2.4]
7	32.5 [32.2 ÷ 33.0]	34.4 [34.0 ÷ 34.8]	1.9 [1.5 ÷ 2.3]

8	33.0 [32.4 ÷ 33.4]	34.5 [34.2 ÷ 35.0]	1.7 [1.2 ÷ 2.1]
9 (Axillary)	33.1 [32.7 ÷ 33.5]	34.9 [34.4 ÷ 35.3]	1.8 [1.4 ÷ 2.2]
Right breast			
0 (Mamilla)	32.7 [32.2 ÷ 33.2]	34.5 [34.1 ÷ 35.0]	1.6 [1.2 ÷ 2.4]
1	33.1 [32.8 ÷ 33.6]	34.6 [34.1 ÷ 35.0]	1.3 [0.8 ÷ 2.1]
2	32.9 [32.2 ÷ 33.6]	34.5 [34.2 ÷ 34.8]	1.6 [1.1 ÷ 2.2]
3	32.7 [32.1 ÷ 33.3]	34.3 [34.1 ÷ 34.7]	1.6 [1.0 ÷ 2.2]
4	33.1 [32.4 ÷ 33.7]	34.5 [34.1 ÷ 34.7]	1.4 [0.9 ÷ 2.0]
5	33.0 [32.4 ÷ 33.4]	34.3 [34.1 ÷ 34.6]	1.5 [1.1 ÷ 1.9]
6	32.4 [31.8 ÷ 33.1]	34.2 [33.8 ÷ 34.6]	1.8 [1.4 ÷ 2.4]
7	32.7 [32.2 ÷ 33.0]	34.4 [34.1 ÷ 34.6]	1.7 [1.5 ÷ 2.1]
8	32.8 [32.6 ÷ 33.2]	34.5 [34.0 ÷ 35.0]	1.5 [1.2 ÷ 2.0]
9 (Axillary)	33.1 [32.6 ÷ 33.6]	35.0 [35.3 ÷ 35.3]	1.7 [1.3 ÷ 2.1]

Statistically insignificant differences of inner temperatures in healthy women related to the fact that the heat input to the breast came from the evenly heated chest muscles and also the blood close to the temperature, while the foci of abnormally high metabolic activity of cells (with a corresponding increase in temperature) do not exist in its tissue.

Fig. 2 shows that a relatively uniform distribution of inner temperatures, at the surface we can see a fairly large range of temperatures, which corresponded to the fluctuations of the vertical temperature gradient from 1.2 to 2.0 °C.

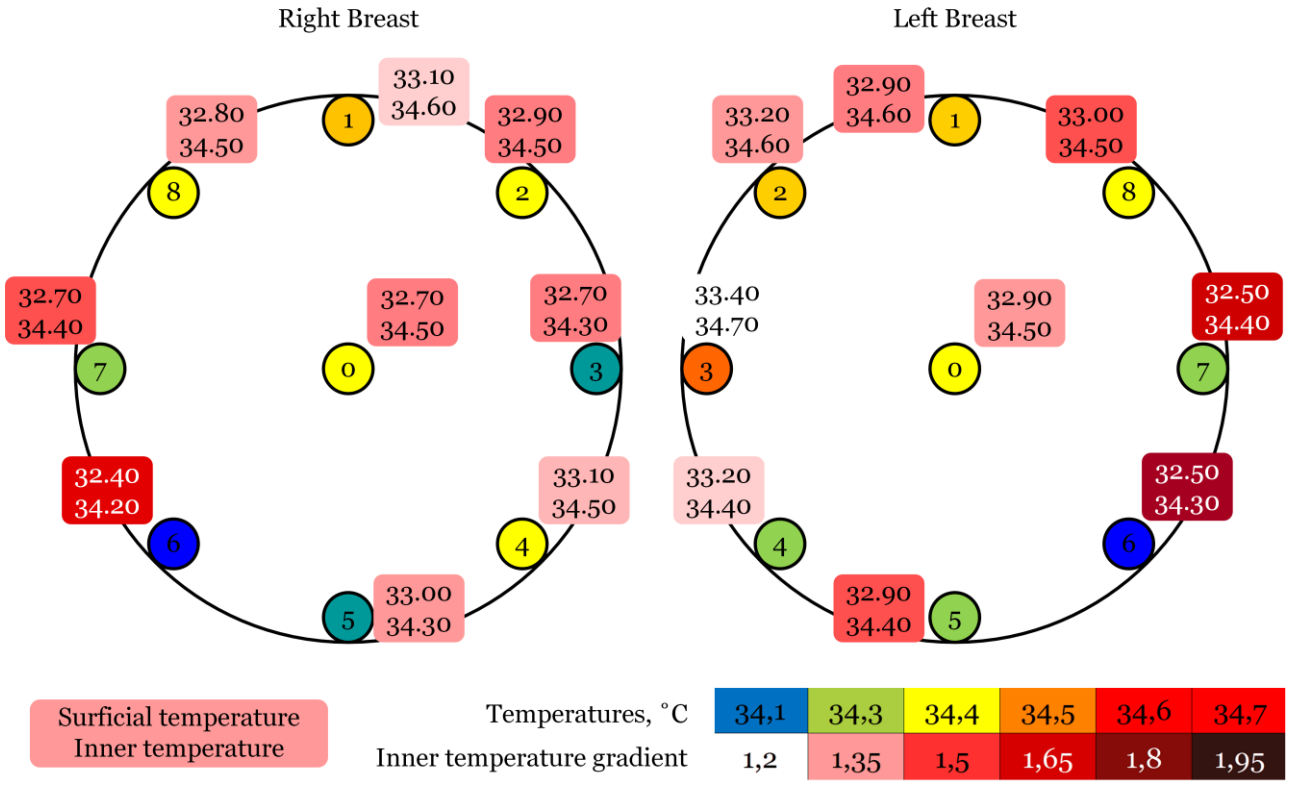

Fig. 2. The spatial distribution of temperatures (°C) inside the right and left breasts of healthy women based on the MWR results. Numbers '0-9' represent the point of withdrawal of surface and inner temperatures according to the methodology of the breast survey (Vesnin et al., 2008).

One of important feature of method used to measure the internal temperatures, is that the average temperature of the tissues inside the cylinders with a depth of 5-7 cm and a diameter equal to the diameter of the applicator antenna became an index for measurement. The surface temperature measured by contact method using combined sensor – that is, the measurements were carried out exactly on the axis of the cylinder. With this approach, increased spread of surface temperatures in the breast can be explained only by redistribution (lateral transfer) of heat inside the body, between the cylinders of the measurement.

3.2. The calculation of the lateral thermal transfer in normal mammary glands

Thermal radiation of biotissue consists of heat introduced with the blood flow, and also of metabolic energy. The value of the latter in breast is ten times smaller in absolute value, and the difference between arterial and venous temperature is almost exclusively a reflection of the magnitude of heat transfer from the surface of the body (Rodrigues et al., 2013). In this regard, the contributions of the metabolic processes (Q_{met}) to the spatial distribution of heat transfer in unchanged mammary gland, are comparable to the measurement error, and therefore they will continue to be excluded from consideration.

Thus, breast without the pathological focus primarily receives heat from the blood flow, and lose it through heat output to the environment. Since the quantity of blood in the tissue under physiological conditions, is equal to the quantity leaving the body all the difference in stored thermal energy to be dissipated into the environment through the skin. From these positions, the points of the breast with the greatest difference of deep and surface temperatures correspond to the zones with the most intensive heat transfer to the environment.

The radiometer measures the average temperature in the cylinder with a diameter of about 5 cm and depth of 5-7 cm. This corresponds to a volume of tissue greater than 450 cm^3. In this connection within the space, measured in the projection of any point MWR, quite correct to highlight in the breast the conditional cylinder from the pectoral muscle to the skin a mass of 100 g. Totality of these nine volumes was adopted for building the spatial model.

To calculate the volume of the spatial heat transfer in the mammary gland, we use the fact that, according to adopted minimize the Q_{met} contribution and approximate process to stationary state in time that is commensurate with the measurement period, all surplus energy from the inner core of the body is equal to the energy transfer to the skin. It, in turn, is equal to the amount of heat transfer into the surrounding tissue.

Calculations it is more convenient to start from the transfer of energy inside the breast. The total amount of heat given to the conventional cylinder Q_i (J) we find by the formula:

$$Q_i = m \cdot C \cdot \Delta T / t_{cap} , (6)$$

where m is the mass of the conditional cylinder of tissue, g; C – thermal conductivity, J/(g·°C); ΔT – the difference of surface and inner temperatures, °C; t_{cap} – average time of capillary blood flow, numerically equal to the duration of one cycle of heat transfer, c.

Since the average specific heat of tissue is 3.35 J/(g·°C), and the average time of capillary blood flow t_{cap} is approximately 30 seconds, the total quantity of heat given to the conventional cylinder weight of 100 g per unit time, will be $Q_i(\Delta T) = 3.35 \cdot 100 \cdot \frac{\Delta T}{30} = 11.17\Delta T$, J.

Fig. 3 demonstrates a vertical flow of heat energy after their calculation in the literal expression. It is clearly seen that the system has both areas with very moderate heat transfer from the deep tissues to the skin, and a relatively large ones, with fluctuations of values from 14.5 to 21.2 J. A similar pattern can be partially explained by the spatial heterogeneity of small-scale structure of mammary gland, and of course, it influences the interstitial heat transfer processes in this organ.

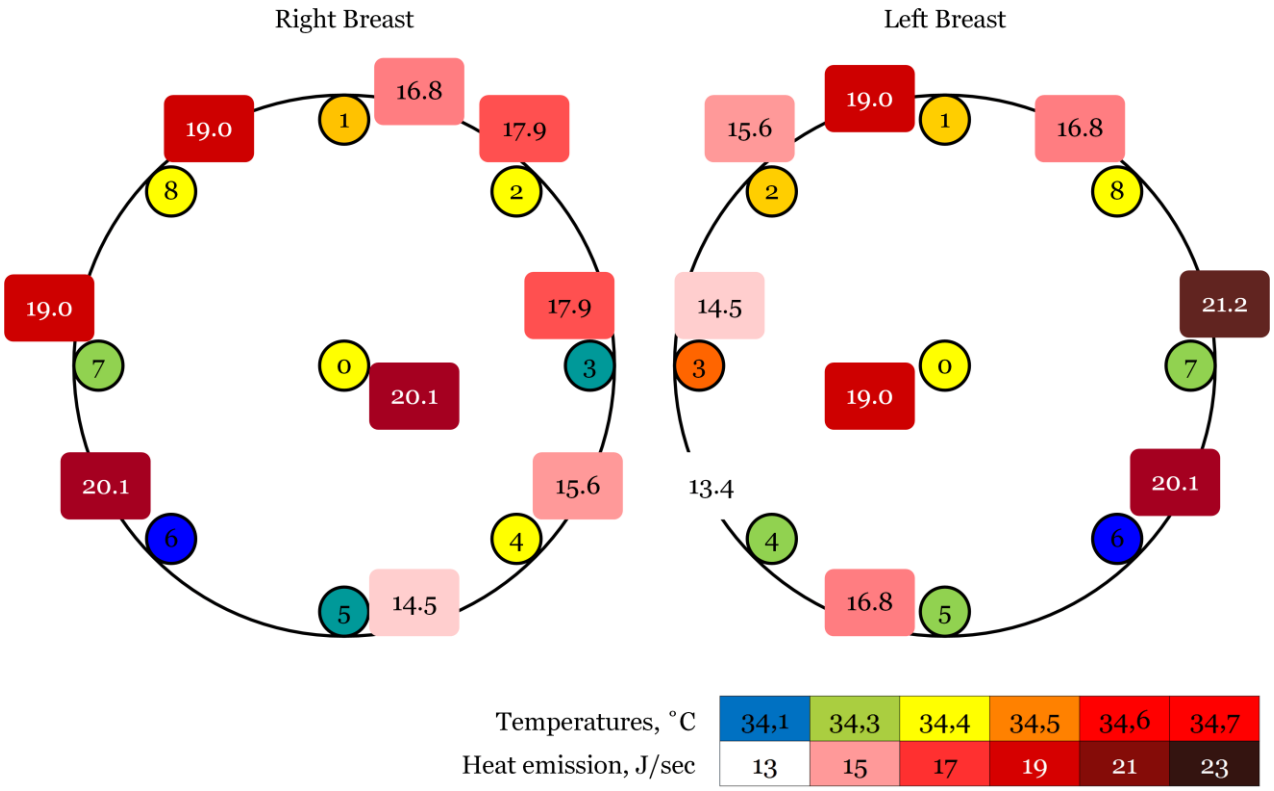

Fig. 3. Heat transfer (J) moved every second from the depths to the surface in the conventional areas in the right and left breast mass of 100 g in the projection points of the MWR.

Assume that the breast can be divided into nine non-overlapping segments corresponding to cylinders with axes perpendicular to the skin surface and passing through the point of measurement 0 – 8. Assume also that the mass of the tissues inside these segments is equal to 100 grams.

Then, knowing the difference between external and internal temperatures in the cylinders of measurement, it is possible to obtain the total amount of heat dissipated into the environment: $Q = \sum_i Q_i$. Since the process is stationary, then the quantity of heat flowing into the breast is also equal to Q.

Let us now consider the heat transfer inside the cylinder. Most of the energy passes along the cylinder from the depths to the surface of body. Constantly there is an exchange of energy between adjacent cylinders. Since both inner and surface temperatures of the cylinders are different, the amount of heat, adopted and diffused by them will also be different. We calculate them as follows:

$$Q_i^{in} = \frac{1}{9}Q + Q_i\left(T_{mean}^{in} - T_i^{in}\right)$$

$$Q_i^{out} = \frac{1}{9}Q + Q_i\left(T_{mean}^{sf} - T_i^{sf}\right) \text{ или } Q_i^{out} = \frac{1}{9}Q - Q_i\left(T_{mean}^{sf} - T_i^{sf}\right),$$

where T_i^{in}, T_i^{sf} is, respectively, inner and surface temperature of the ith cylinder, $T_{mean}^{in}, T_{mean}^{sf}$ – average temperatures in the cylinders 0 – 8.

Here is an example of calculated data for right breast of the healthy woman 36 years old (Table 3).

Table 3. Evaluation data of heat transfer between measurement cylinders for one case (healthy woman, 36 years)

	0	1	2	3	4	5	6	7	8	Mean
Inner temperature ˚C	35.2	34.6	35.2	34.7	34.6	35	34.6	34.5	34.5	34.8
Surface temperature ˚C	32.9	32.8	33.6	32.7	32.4	33.1	32.3	32.1	32.5	32.7
Inner temperature gradient	2.3	1.8	1.6	2.0	2.2	1.9	2.3	2.4	2.0	—
Heat emission of cylinder, J/sec	25.7	20.1	17.9	22.3	24.6	21.2	25.7	26.8	22.3	23.0
Evaluated cylinder heat income, J/sec	27.8	21.1	27.8	22.2	21.1	25.6	21.1	20.0	20.0	—
Evaluated cylinder heat outcome, J/sec	25.1	24.0	32.9	22.8	19.5	27.3	18.4	16.1	20.6	—
Heat excess, J/sec	2.7	-2.9	-5.1	-0.6	1.6	-1.7	2.7	3.8	-0.6	—
Average cylinder temperature, ˚C	34.1	33.7	34.4	33.7	33.5	34.1	33.5	33.3	33.5	—

Fig. 4 shows the main directions of heat transfer in the breast of this woman. Note that the average temperature of the cylinder 2 is the highest. Temperature points {0, 5}, {1, 3}, and {4, 6, 7, 8} are within the error of the measuring instrument RTM-01-RES. The direction of possible lateral heat transfer is oriented from the outer portions of the breast (the cylinders corresponding to points 6 and 7 during the MWT) to the upper-medial quadrant (point 2).

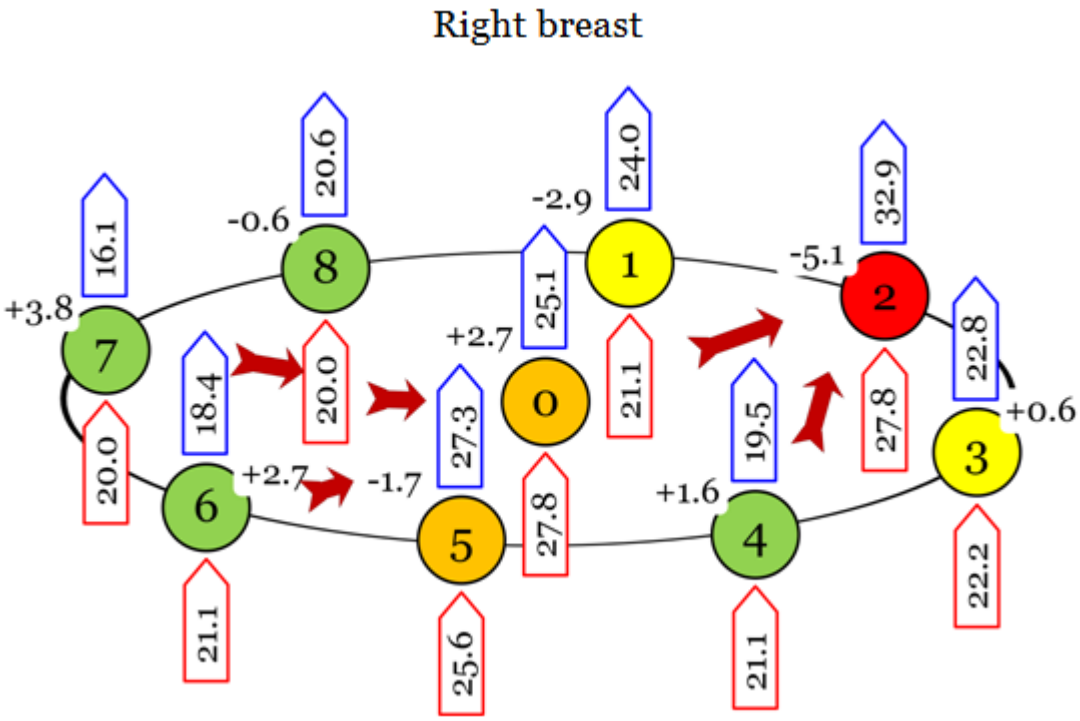

Fig. 4. Probable heat transfer routes in right breast for one case (healthy female, 36 years).

The calculation of the actual values of heat transfer will require, apparently, three-dimensional models to build which is necessary to make a series of additional measurements. Therefore, this aspect remains beyond the scope of this article.

3.3. Calculation of heat transfer in the presence of the pathological focus

Table 3 presents the following statistics on the temperature in the healthy breast and breast with the diagnosed cancers: the inner temperature of the hottest point given to internal axillary temperature (1); the inner temperature of a point on the opposite side of the body (2); the temperature difference between the hottest point and its opposite (3).

Table 4. Spatial distribution and temperature gradients in the mammary glands in the presence of malignant tumors of the installed localization (Me [Q1 ÷ Q3])

Breast	Healthy women	Breast cancer
Left breast		
Most hot point temperature, ˚C	34.9 [34.7 ÷ 35.2]	35.2 [34.6 ÷ 35.9]
Opposite point temperature, ˚C	34.5 [34.0 ÷ 34.8]	34.5 [33.6 ÷ 35.2]
Temperature difference between axillary and most hot point, ˚C	–0.1 [–0.4 ÷ 0.1]	0.1 [–0.4 ÷ 0.6]
Temperature difference between axillary and opposite point, ˚C	0.4 [–0.2 ÷ 0.8]	0.8 [0.4 ÷ 1.4]
Most hot point and its opposite difference, ˚C	0.4 [0.1 ÷ 1.0]	0.7 [0.4 ÷ 1.1]
Right breast		
Most hot point temperature, ˚C	35.05 [34.2 ÷ 35.7]	35.1 [34.2 ÷ 35.7]
Opposite point temperature, ˚C	34.4 [34.0 ÷ 34.9]	34.3 [33.5 ÷ 35.0]
Temperature difference between axillary and most hot point, ˚C	0.1 [–0.3 ÷ 0.3]	0.2 [–0.2 ÷ 0.5]
Temperature difference between axillary and opposite point, ˚C	0.4 [0.1 ÷ 0.9]	1.1 [0.5 ÷ 1.4]
Most hot point and its opposite difference, ˚C	0.6 [0.1 ÷ 0.8]	0.8 [0.4 ÷ 1.2]

Analysis of variance revealed no significant differences between samples. The temperature distribution was largely dependent on the individual structure of the body; any regularities between the structure of the gland and the area of disease were also not installed. However, it is quite obvious that the additional source of heat may change the structure of the heat transfer inside the body.

Here is an example of calculated data for the right breast women 38 years with diagnosed cancer focus (Table 5).

Table 5. Evaluation data of heat transfer between measurement cylinders for one case (woman with breast cancer, 38 years)

	0	1	2	3	4	5	6	7	8	Mean
Inner temperature ˚C	34.3	34.5	34.8	34.4	34.1	34.7	34.7	35	34.4	34.5
Surface temperature ˚C	33	32.9	33.2	32.8	32.8	33	32.9	33.8	33	33.0
Inner temperature gradient	1.3	1.6	1.6	1.6	1.3	1.7	1.8	1.2	1.4	—
Heat emission of cylinder, J/sec	14.5	17.9	17.9	17.9	14.5	19.0	20.1	13.4	15.6	16.8
Evaluated cylinder heat income, J/sec	14.0	16.3	19.6	15.1	11.8	18.5	18.5	21.8	15.1	—
Evaluated cylinder heat outcome, J/sec	16.3	15.1	18.5	14.0	14.0	16.3	15.1	25.2	16.3	—
Heat excess, J/sec	-2.2	1.1	1.1	1.1	-2.2	2.2	3.4	-3.4	-1.1	—
Average cylinder temperature, ˚C	33.7	33.7	34.0	33.6	33.5	33.9	33.8	34.4	33.7	—

Note that the average temperature of the cylinders 7 and 2 is the highest. Cylinders {0, 1, 5, 6, 8} are somewhat colder, and the temperature in the MWR points {3, 4} markedly (by about half a degree) is below.

Fig. 5 shows that the direction of possible lateral transfer in the same way as in the case with a healthy body, directed from the cylinders corresponding to points 5 and 6 at MWR. But now the lateral heat transfer occurs in two quadrants – lower-medial (point 2) and the left one, where the pathology was focused (point 7). Note that the average temperature of the cylinders 7 and 2 is the highest. Cylinders {0, 1, 5, 6, 8} are somewhat colder, and the temperature in the MWR points {3, 4} is markedly (by about half a degree) below.

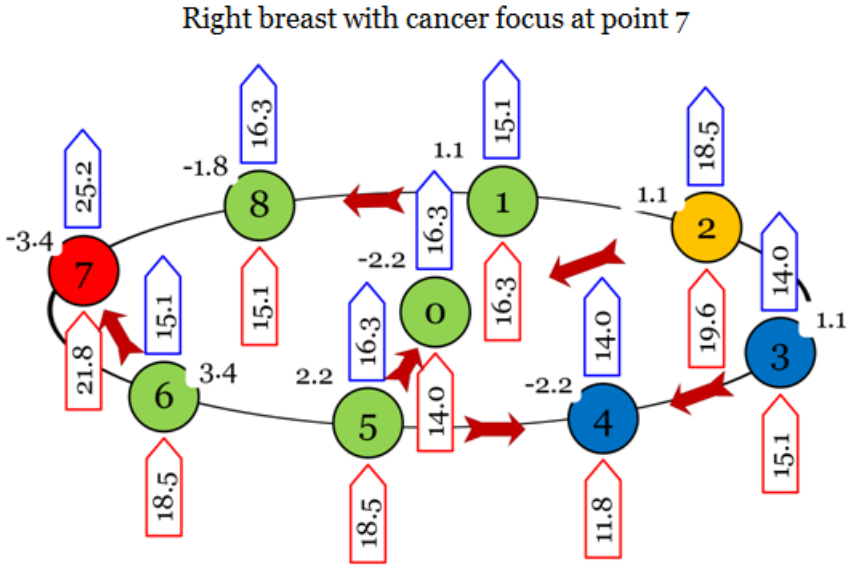

Fig. 5. Probable heat transfer routes in right breast for one case (woman with breast cancer, 38 years).

3.4. Transformation models for the case with TEC presence

Let us consider the use of such building for the analysis of heat transfer in tissue containing TEC. If the scaffold has a cylindrical shape, covering the soft tissue defects with a fairly uniform distribution of properties, only three positions can be vary in its properties: the soft tissues outside of the scaffold (point 0), the border 'soft tissue – scaffold' (point 1), and its geometric center (point 2).

As the remodeling, the ratio of the individual components (substances scaffold, blood vessels and host tissues), in points 1 and 2 will change. To calculate the heat capacity and thermal

conductivity of the newly formed tissue, we used the ratio of the components obtained in the experimental study, where scaffolds based on natural polymers chitosan and polycaprolactone have been successfully installed (Novochadov et al., 2013; Ivanov et al., 2015; Modulevsky et al., 2016); the basic design characteristics are given in Table 5. From these data it is clearly seen that as scaffold remodeling is accompanied by decrement of heat capacity, while the conductivity increased.

Table 5. The design physical characteristics of biological tissue due to scaffold remodeling

	Surrounding soft tissues (point 0)	Time of remodeling	The TEC edge (point 1)	The TEC centre (point 2)
TEC, %	0	Installation 4 week 12 week	100 67 0	100 88 9
Vessels, %	5	Installation 4 week 12 week	0 9 7	0 3 6
Soft tissues, %	95	Installation 4 week 12 week	0 24 93	0 10 85
The estimated heat capacity, J/(g·°C)	3.35	Installation 4 week 12 week	3.85 3.72 3.34	3.85 3.83 3.37
The estimated termal conductivity, W/(m·°C)	0.50	Installation 4 week 12 week	0.35 0.40 0.50	0.35 0.37 0.46

Fig. 5 shows the calculated values of the relevant thermal transfers, which direction, to the extent of scaffold remodeling, have been reversed.

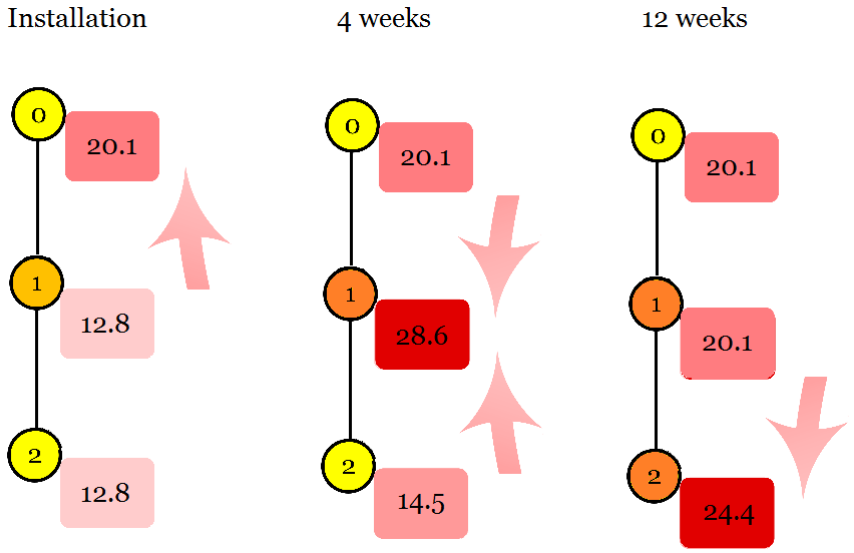

Fig. 5. The amount of energy (J) that is moved every second of the depths to the surface in the field of installation of tissue-engineered cylindrical constructs (diameter 5 cm; height 0.5 cm) as replacement of its material by host tissues. Number '0' shows point in the surrounding tissue; number '1' is the point at the border of the structure and surrounding tissue; number 2 shows the place in the center of the TEC. Arrows indicate the path of lateral heat transfer.

The revealed regularities can be considered as in tissue engineering when setting properties of the newly developed structures (Gu et al., 2016; Li et al., 2016), and for monitoring postimplantation period where it could obtain a non-invasive way information about the most likely mechanobiology properties of the implanted object in the dynamics of its remodeling (Giorgi et al., 2016).

4. Conclusion

This study demonstrates the presence of lateral heat transfer from one part of the breast to other ones and the ability to determine its most probable vectors in the real bodies of healthy women and cases with presence of malignant neoplasms. It was shown the identification and calculation of such heat flow vectors had independent diagnostic potential.

The algorithm of calculations for tissue with pathological focus, with minor modifications, is applicable for analyzing heat transfer in tissue containing TEC. Calculations of heat transfer for such systems in different periods after the TEC installation demonstrate the presence of a lateral heat transfer, and as scaffold remodeling in the host tissue the direction of heat transfer changes from a predominantly centrifugal to centripetal. This transition is well marked and can be used for non-invasive monitoring of adaptation in the postimplantation period.

5. Acknowledgements

The study was carried out with financial support of Russian Foundation for Basic Research in the framework of a research projects No. 15–47–02475–Povolzhie and No. 15–47–02642–Povolzhie.

References

Afrin et al., 2011 – *Afrin N., Zhang Y., Chen J.K.* (2011). Thermal lagging in living biological tissue based on nonequilibrium heat transfer between tissue, arterial and venous bloodsInternational. *J. Heat Mass Transfer.* 54(11–12), 2419–2426. doi: 10.1016/j. ijheatmasstransfer. 2011.02.020

Albertini et al., 2015 – *Albertini M., Fernandez-Yague M., Lázaro P., et al.* (2015). Advances in surfaces and osseointegration in implantology. Biomimetic surfaces. *Med. Oral Patol. Oral Cir. Bucal.* 20(3), e316–e325. doi: 10.4317/medoral.20353.

Bardati, 2008 – *Bardati F., Iudicello S.* (2008). Modeling the visibility of breast malignancy by a microwave radiometer. *IEEE Trans. Biomed. Eng.* 55(1), 214-221. doi: 10.1109/TBME.2007.899354

Filatov et al., 2013 – *Filatov A.V., Ubaichin A.V., Bombizov A.A.* (2013). A two-receiver microwave radiometer with high transfer characteristic linearity. *Measurement Techniques.* 55(11), pp. 1281–1286. doi: 10.1007/s11018-013-0121-5

Fitzpatrick, 2015 – *Fitzpatrick L.E., McDevitt T.C.* (2015). Cell-derived matrices for tissue engineering and regenerative medicine applications. *Biomater. Sci.* 3(1), 12–24. doi: 10.1039/C4BM00246F

Giorgi et al., 2016 – *Giorgi M., Verbruggen S.W., Lacroix D.* (2016). In silico bone mechanobiology: modeling a multifaceted biological system. *Wiley Interdiscip. Rev. Syst. Biol. Med.* 8(6), 485–505. doi: 10.1002/wsbm.1356

Gouzouasis et al., 2010 – *Gouzouasis I.A., Karathanasis K.T., Karanasiou I.S., Uzunoglu N.K.* (2010). Contactless passive diagnosis for brain intracranial applications: a study using dielectric matching materials. *Bioelectromagnetics.* 31(5), 335–349. doi: 10.1002/bem.20572

Gu et al., 2016 – *Gu B.K., Choi D.J., Park S.J., et al.* (2016). 3-Dimensional bioprinting for tissue engineering applications. *Biomater Res.* 20: 12. doi: 10.1186/s40824-016-0058-2

Guliak et al., 2014 – *Guilak F., Butler D.L., Goldstein S.A., Baaijens F.P.T.* (2014). Biomechanics and mechanobiology in functional tissue engineering. *J. Biomech.* 47(9): 1933–1940. doi: 10.1016/j.jbiomech.2014.04.019

Herman I.P., 2007 – *Herman I.P.* (2007). Physics of the Human Body. Berlin; Heidelberg: Springer-Verlag, 880 p.

Hwang et al., 2015 – *Hwang J., Jeong Y., Park J.M., et al.* (2015). Biomimetics: forecasting the future of science, engineering, and medicine. *Int. J. Nanomedicine.* 10: 5701–5713. doi: 10.2147/IJN.S83642

Ivanov et al., 2015 – *Ivanov A.N., Kozadaev M.N., Bogomolova N.V., et al.* (2015). Biocompatibility of polycaprolactone and hydroxyapatite matrices in vivo. *Cell Tissue Biol.* 9(5), 422-429. doi:10.1134/S1990519X15050077

Jang et al., 2011 – *Jang H.W., Kang J.K., Lee K., et al.* (2011). A retrospective study on related factors affecting the survival rate of dental implants. *J. Adv. Prosthodont.* 3(4), 204-215. doi: 10.4047/jap.2011.3.4.204

Kelly et al., 2011 – *Kelly P., Sobers T., Peter B.S., et al.* (2011). Temperature anomaly detection and estimation using microwave radiometry and anatomical information. *Proc. SPIE.* e79614. doi: 10.1117/12.878136

Kelly et al., 2012 – *Kelly, P. Sobers T., Peter B. S. et al.* (2012). Microwave radiometric signatures of temperature anomalies in tissue. *Proc. SPIE 2012.* e831368. doi: 10.1117/12.910785.

Khoperskov et al., 2014 – *Khoperskov A.V., Khrapov S.S., Novochadov V.V., Burnos D.V.* (2014). The effect of small-scale mammary glands structure on the distribution of the deep temperature using the microwave radiometry diagnostics. *J. Volgograd State Univ. 1: Mathematics. Physics.* 5 (25), 60-68. [in Rus., Eng. abstr.]

Leroy et al., 1998 – *Leroy Y., Bocquet B., Mammouni A.* (1998). Non-invasive microwave radiometry thermometry. *Physiol. Means.* 19, 127-148.

Li et al., 2014 – *Li L., Liang M., Yu B., Yang S.* (2014). Analysis of thermal conductivity in living biological tissue with vascular network and convection. *Int. J. Thermal Sci.* 86, 219–226. doi: 10.1016/j.ijthermalsci.2014.07.006

Li et al., 2016 – *Li J., Chen M., Fan X., Zhou H.* (2016). Recent advances in bioprinting techniques: approaches, applications and future prospects. *J. Transl. Med.* 14, e271. doi: 10.1186/s12967-016-1028-0

Lin et al., 2009 – *Lin Q.Y., Yang H.Q., Xie S.S., et al.* (2009) Detecting early breast tumour by finite element thermal analysis. *J. Med. Eng. Technol.* 33(4), 274-280. doi: 10.1080/03091900802106638

Losev et al., 2015 – *Losev A.G., Khoperskov A.V., Astakhov A.S., Suleymanova Kh.M.* (2015). Problems of measurement and modeling of thermal and radiation fields in biological tissues: analysis of microwave thermometry data. *J. Volgograd State Univ. 1: Mathematics. Physics.* 6 (31), 31-71. [in Rus., Eng. abstr.] doi: 10.15688/jvolsu1.2015.6.3

Lu et al., 2013 – *Lu T., Li Y., Chen T.* (2013). Techniques for fabrication and construction of three-dimensional scaffolds for tissue engineering. *Int. J. Nanomedicine.* 8, 337–350. doi: 10.2147/IJN.S38635

Maitz, 2015 – *Maitz M.F.* (2015) Applications of synthetic polymers in clinical medicine. *Biosurf. Biotribol.* 1(3), 161–176.

Mao, 2015 – *Mao A.S., Mooney D.J.* (2015). Regenerative medicine: Current therapies and future directions. *Proc. Natl. Acad. Sci. U. S. A.* 112(47), 14452–14459. doi: 10.1016/ j.bsbt.2015.08.002

Modulevsky et al., 2016 – *Modulevsky D.J., Cuerrier C.M., Pelling A.E.* (2016). Biocompatibility of subcutaneously implanted plant-derived cellulose biomaterials. *PLoS One.* 11(6): e0157894. doi: 10.1371/journal.pone.0157894

Ng, Sudharsan, 2004 – *Ng E.Y.-K., Sudharsan N.M.* (2004). Computer simulation in conjunction with medical thermography as an adjunct tool for early detection of breast cancer. *BMC Cancer.* 4(17), e6. doi: 10.1186/1471-2407-4-17.

Novochadov et al., 2013 – *Novochadov V.V., Semenov P.S., Lyabin M.P.* (2013). [Innovative approaches to scaffold technology optimization based on chitosan, in tissue engineering of articular cartilage]. *J. Volgograd State Univ. 10: Innovations.* (2), pp. 135-143. [in Rus., Eng. abstr.]

O'Brien, 2011 – *O'Brien F.J.* (2011) Biomaterials and scaffolds for tissue engineering. *Mater. Today.* 14, 88–95. doi: 10.1016/S1369-7021(11)70058-X

Park et al. 2016 – *Park K.D., Wang X., Lee J.Y., et al.* (2016). Research trends in biomimetic medical materials for tissue engineering: commentary. *Biomater Res.* 20: 8. doi: 10.1186/s40824-016-0053-7

Rodrigues et al., 2013 – *Rodrigues D.B., Maccarinia P.F., Salahic S., et al.* (2013). Numerical 3D modeling of heat transfer in human tissues for microwave radiometry monitoring of brown fat metabolism *Proc. SPIE 2013.* e8584. doi: 10.1117/12.2004931.

Seteikin et al., 2010 – *Seteikin A.Yu., Krasnikov I.V., Pavlov M.S.* (2010). [3-Dimentional model of light propagation in biological tissues]. [J. Saint Petersburg University. 11: Medicine]. (3), 166–172. [in Rus.]

Shin et al., 2013 – *Shin S.-W., Kim K.-S., Lee J.-W., et al.* (2013). Implementing graphic user interface system for microwave radiometry data to utilize breast cancer diagnosis. Transact. Korean Inst. Electr. Eng. 62(6), 818–824.

Stavrov et al., 2013 – *Stavrov T.A., Bukina E.V., Losev A.G., Zamechnik T.V.* (2013). [Mathematical verification of early recurrence of the varicose disease after the endovascular laser obliteration of the great saphenous vein according to data of the radiothermometry]. *J. New Med. Technol. (Tula).* 20(2), 14–18. [in Rus., Eng. abstr.]

Stauffer et al., 2014 – *Stauffer P.R., Rodrigues D.B., Maccarini P.F.* (2014). Utility of microwave radiometry for diagnostic and therapeutic applications of non-invasive temperature monitoring. *IEEE BenMAS (Benjamin Franklin Symposium on Microwave and Antenna Sub-systems).* doi: 10.13140/2.1.3762.0487.

Toutouzas et al., 2012 – *Toutouzas K., Drakopoulou M., Siores E. et al.* (2012). In vivo measurement of plaque neovascularisation and thermal heterogeneity in intermediate lesions of human carotid arteries. *Heart.* 98, 1716-1721. doi: 10.1136/heartjnl- 2012-302507

Umadevi et al., 2011 – *Umadevi V., Raghavan S.V., Jaipurkar S.* (2011). Framework for estimating tumour parameters using thermal imaging. *Indian J. Med. Res.* 134(5), 725–731. doi: 10.4103/0971-5916.91012.

Vesnin et al., 2008 – *Vesnin S.G., Kaplan A.M., Avakyan R.S.* (2008). [Advanced microwave radiometry of the breast]. *Meditzinskiy Al'manakh [Med. Almanac].* (3), 82–87.

Vesnin et al., 2010 – *Vesnin S.G., Sedankin M.K.* (2010). [Mathematical modeling of own radiation of human tissues in the microwave range]. *Biomeditzinskaya Radioelektronika [Biomedical Radio Electronics].* (9), 33–43. [in Rus., Eng. abstr.]

Wang et al., 2014 – *Wang J., Lü D., Mao D., Long M.* (2014). Mechanomics: an emerging field between biology and biomechanics. *Protein Cell.* 5(7), 518–531. doi: 10.1007/s13238-014-0057-9

Wust et al., 2006 – *Wust P., Cho C. H., Hildebrandt B., Gellermann J.* (2006). Thermal monitoring: invasive, minimal-invasive and non-invasive approaches. *Int. J. Hyperthermia.* 22(3), 255–262. doi: 10.1080/02656730600661149

Copyright © 2016 by Academic Publishing House *Researcher*

Published in the Russian Federation
European Journal of Molecular Biotechnology
Has been issued since 2013.
ISSN: 2310-6255
E-ISSN: 2409-1332
Vol. 14, Is. 4, pp. 139-147, 2016

DOI: 10.13187/ejmb.2016.14.139
www.ejournal8.com

The Functionalizing Bioactive Surface of Screw Titanium Implants with Chitosan: Fabrication and Surface Features

Valery V. Novochadov [a, *], Anna S. Krylova [a], Nikita A. Anikeev [a],
Victor I. Shemonaev [b], Angelina O. Zekiy [c]

[a] Volgograd State University, Russian Federation
[b] Volgograd State Medical University, Russian Federation
[c] Sechenov First Moscow State Medical University, Russian Federation

Abstract

The necessity to develop different approaches to increasing dental implant osseointegration should be of high prevalence of dental diseases in current world, the massive expansion of dental implantation technologies, and the advent of technical possibilities to functionalize bioactive surfaces using modern molecular biotechnology.

To improve bioactive surface of dental implants by functionalization, we selected chitosan because it had the properties of biocompatibility and osteoinductive effect, also we had literature data about the possibility of its application as nano-films and nano-coating. Chitosan, applied using epy cathodic sputtering technique, significantly altered nano-surface topography of dental implants. Using atomic force microscopy it is shown that after chitosan applying, the nano-roughness parameter has 5.6-fold increase, and the developed surface area ratio has increased 3.7 times in comparison with surface properties of commercial titanium screw implant without chitosan spraying.

The application of chitosan on bioactive surface of the screw titanium implants was shown to improve the morphological characteristics of osseointegration after implantation into the rat femoral bone. The bone volume fraction in osseointegration zone exceeded at different periods of the experiment the value of the same parameter in the comparison group 1.56-1.64 times. Implants with a surface chitosan-based functional coating provided the additional osteoconductive effect appeared in more intensive and rapid osteogenesis around implants, and the more expressed remodeling and thickening of the surrounding trabecular bone.

Keywords: dental implantation, titanium implants, functional coating, bioactive surface, chitosan, osseointegration, atomic force microscopy

1. Introduction

Biomimetic approach to the principles of maximum biocompatibility and as full compensation for the missing functional properties is crucial for solving the major problems of tissue engineering and regenerative medicine (TERM) (Wang et al., 2014; Hwang et al., 2015; Park

* Corresponding author
E-mail addresses: novovv@rambler.ru (V.V. Novochadov)

et al. 2016). With regard to dental implants, this approach can be deciphered as the establishment of artificial or semi-artificial structures that could completely support a function of the tooth for a long time. This paradigm is formulated in the concept of complete osseointegration (Jang et al., 2011; Albertini et al., 2015; Trindade et al., 2015).

From the biomedical standpoint, the osseointegration represents the implantation of the implant, that is, forming a strong bond between its surface and the surrounding bone. The remodeling of this bone is necessary to sustain the loads after the prosthesis. Currently, titanium is the most commonly used material for intraosseous implants, also its alloys with nickel, aluminum, and vanadium used also, alloys with other metals used less frequently (Chang et al., 2010; Mas-Moruno et al., 2015; Ogle, 2015).

Active modification of the implant surface, providing maximum contact area with the adjacent bone and, simultaneously, stimulating the remodeling in this bone, that is, possessing osteoconductive effect, is a fundamental approach to improve osseointegration of the implants. Technically this is achieved through a lot of methods creating three-dimensional porous surface (sandblasting, sintering, deposition, electric arc or plasma spraying, micro-implosion technique, chemical etching, etc.) (Coelho et al., 2009; Chang et al., 2010; Stanford, 2010).

The number of analytic reviews described technique to improve the osseointegration through creation of biomimetic micro-relief of surfaces, and the implant coating by various materials with high osteoinductive properties. The particles of the same alloy, the oxides of titanium, tantalum, hydroxyapatite, or other substances, which were similar to bone mineral matrix, may be useful for improvement of implant surface (Beutner et al., 2010; van Oirschot et al., 2013; Xuereb et al., 2015; Kalita et al., 2016).

A new possibility to produce implants and to control their surface properties at the nanoscale level deserves a special attention and offer great opportunities for fundamental improvement in these properties (Dzenis, 2008; Tomsia et al., 2011; Gao et al., 2015). The idea of this use is in a controlled fixation on the implant surface of molecules with biological effects (adhesive, growth factors, etc.), allowing to achieve the most rapid initialization of osteogenesis on the entire implant surface (Dohan Ehrenfest et al., 2010; Luo et al., 2012; Berglundh, 2013; Correa et al., 2015).

Chitosan proved to be one of the most promising components for this procedure, because it is non-toxic, has complete biocompatibility, bioresorbability, and moderate antibacterial properties.

The use of chitosan as a material for TERM technologies has been documented in an article written by scientific group from Italy led by R. Muzzarelli and published in 'Biomaterials' in May 1988. In subsequent years, these researchers successfully applied chitosan scaffolds for replacement of defects of the Dura mater, the wound surface and the fibrous cartilage, noting the adequate morphological reconstruction of defects without any functional disorders. The authors believe that the start of chitosan application for recovery of lost supporting tissue has opened a new milestone in tissue engineering (Kumar et al., 2004; Muzzarelli, 2011).

The availability of raw materials for chitosan production (exoskeleton of arthropods, fungi etc.) and lightness improvement of its physico-chemical properties with enzymatic treatment are a major reason to consider chitosan to be a very promising basis for the fabrication of modern scaffolds. The strong chondroinductive and osteoinductive effects of three-dimensional porous chitosan were shown experimentally (Di Martino et al., 2005; Abarrategi et al., 2010; Yang, 2011).

Chitosan-based scaffolds have a high ability to induce cellular migration, adhesion, proliferation and induction of necessary chondral or osteogenic phenotype, resulting in intensive remodeling bone and cartilage, it does not activate the resorption of surrounding tissue (Venkatesan, 2010; Correia et al., 2011). The material has adequate wettability and degree of bioresorption, it able to induce bone formation in osteoblast culture (Park et al., 2012). We previously also showed a positive effect of chitosan on the osseointegration of titanium implants (Novochadov et al., 2013).

The goal of this work was to study structural features of nano-sized chitosan-based bioactive coating and opportunities to improve the osseointegration of implants with such procedure.

2. Material and Methods

Chitin as a raw material for chitosan production was extracted from external skeleton of crustaceans (genus Pandalus) by rinsing with tap water, followed by 10 % $NaHCO_3$ solution in the presence of surfactants. The cleaning included being re-deproteinization, washing the intermediate

product, demineralization, final rinse and lyophilization to dry-air condition. The chitosan was obtained by deacetylation of chitin, previously milled to sizes not exceeding 2 mm in diameter. Vacuum conditions promoted the minimum concentration of oxygen in the reaction zone to prevent the oxidative degradation of chitin. The filtered chitosan was a highly hydrated product with a water content of more than 70%. To prevent keratinization this material was dried in a thermostat at 35,0-40,0 °C to a dry-air state (Lyabin, 2012). The obtained chitosan met the Russian standart (Technical Specification 9289-067-00472124-03), it had a mass moisture fraction of 9.4 %, pH of 1% solution in 2 % CH3COOH of 3.85, and the deacetylation degree of 93 %.

As initial products for fabrication of functional coatings we used commercial screw titanium implants for dentistry (MIS BioCom, Israel). Before the chitosan coating all implants were ultrasonically cleaned in MilliQ water and organic solvents. The procedure of deposition was consistently provided to form a finely porous film of chitosan using the freeze-drying technology (1), 1 % suspension in 2 % acetic acid (2), grinding the film with separation of the fraction of microparticles 10-20 microns in diameter (3), ultrasonic dispersion of fragments with a diameter of 1 μm from the surface of micro-particles (4), and cathode coating on the implant surface (5).

Four implants with or without functionalization were used to characterize their surface. Qualitative visualisation of the implant surface morphology was performed using atomic force microscope Solver Pro, equipped with conductive cantilevers coated with diamond DCP-11 (NT–MDT, Zelenograd, Russia). Before each experiment the calibration was performed in the mechanical properties of the tip using NT-MDT software. Images were obtained in Nova software, using semi-contact mode, in which the tip of the cantilever oscillates with a high frequency over the sample and its deformation is captured by the reflected laser beam. Typical digital images contain up to 256 x 256 dpi, 2048 points on curves. Length of curves correspond to a 9.8 microns, the speed of image formation was in the range of 0.7 to 2.1 lines per second. The interaction of the 'tip – sample' was deemed valid, since the maximum height of nano-roughness did not exceed 25 nm.

For quantitative assessment of surface topography, several parameters were investigated at the top and valley regions of the implant threads, on two implants of each type. In accordance with known schemes of analyzing the implants topography (Dohan Ehrenfest, 2011; Shah et al., 2016), we used the following indices of surfase: the maximum peak height (SP, μm), arithmetic mean deviation (SD, nm), ten point height (S10, μm), and developed surface area ratio (SDR, %).

Tissue samples of femur of twenty white skeletally-mature male Wistar rats were used for study in vivo. The Protocol of the experiments conformed to the ethical standards set out in Directive 2010/63/EU on the protection of animals used for scientific purposes. In main group the implants with chitosan-based coating were placed in distal femoral metaphyses of eight skeletally-mature Wistar rats (one implant in each femur) and were followed for four or eight weeks. In comparison group (six rats) the same surgery was using non-coated-implants. Prior to surgery, all animals were anaesthetised by intra-peritoneal injection of Zoletil (20 mg/kg BW; Virbac Sante Animale, France). The animals were fed ad libitum. As a control, we investigated 8 tissue samples of four intact femoral bones from the rats, which have been all the time of the experiment in standard vivarium conditions. The animals were euthanised with an intraperitoneal overdose of Zoletil (200 mg/kg BW; Virbac Sante Animale, France).

After removing the skin, the superficial soft tissue, and careful out-twisting of implants, the remaining tissue specimens of femoral bone, were prefixed by neutral formalin for one week, underwent by decalcification in EDTA solution, dehydrated in a graded series of ethanol, and paraffin embedded. Then we used the staining with toluidine blue for qualitative histology using optical microscopy (Leica DM 4000 (Germany). Quantitative analysis included determining and estimation of following bone structure indicators: the cortical bone thickness (μm), cancellous bone volume fraction (%), trabecular thickness (μm), osseointegration zone thickness (μm), and bone volume fraction in this zone (%).

Immunohistochemical study was to identify CD68 as markers of macrophages/osteoclasts and osteonectin as marker of the osteogenic series using monoclonal antibodies (Novocastra, UK). The numerical density of these cells (103/mm3) was a quantitative parameter for this analysis. For video documentation and quantitative morphological analysis the software Image J (U.S.A) was applied, which allowed determining values of the above parameters in semi-automatic mode.

Quantitative data were processed using with the calculation of the indices adopted to characterize the non-parametric samples in biomedical research. Results were shown as Median

[1st quartile ÷ 3rd quartile]. To prove the validity of differences for multiple groups was applied. P values less than 0.05 were considered significant. The non-parametric Mann-Whitney U and Friedman criterions were used for all statistical analyses between the implant types for atomic force microscopy and quantitative histomorphometry (Statistica 10.0, StatSoft Inc., USA); P values < 0.05 were considered statistically significant. Mean values ± standard deviations are presented.

3. Results

The functionalization of implant surface using chitosan does not affect the properties at the macro level, they were indistinguishable from ordinary commercial samples of these products.

Atomic force microscopy allowed characterizing the nano-relief of the implant surface with or without chitosan coatings. Visualization by NT-MDT software allows us to see that the chitosan application onto implant surface was associated with a considerable alteration of the surface nano-relief. It became nano-rough, while basic micro-relief was almost unchanged (Fig. 1).

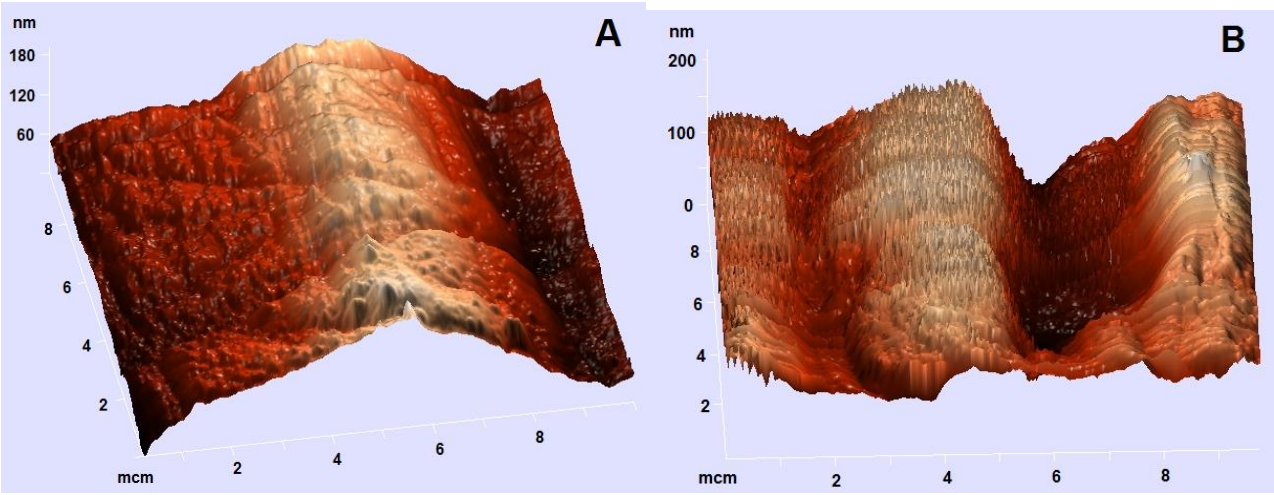

Fig. 1. Functionalization of titanium implants by chitosan-based coating leads to a significant complication of the surface nano-relief, as seen on three-dimensional reconstructions, obtained using atomic force microscopy. A. Non-coated screw titanium implant MIS BioCom (Israel). B. The same implant with chitosan-based coating.

Quantitative characteristics of the surface topography presented in Table 1, confirm and detail these observations. The maximum peak height did not differ between implants with or without surface functionalization; in 75 % of cases its value was in the range from 1.02 to 2.08 μm. Parameter named as ten point height indicating the homogeneity of micro-relief, was also the similar in two variants of implants; it ranged from 1.19 to 2.71 μm. The nano-roughness, estimated from SD parameter, has 5.6-fold increase, and the meaning of SDR has increased 3.7 times in comparison with surface properties of titanium screw implant without chitosan spraying.

Table 1. Surface topography characterization of commercial screw titanium implants for dentistry with or without functional chitosan-based coating (Median [1st quartile ÷ 3rd quartile])

Parameter	Non-coated implants	Chitosan-coated implants
Maximum peak height of the surface, μm	1.44 [1.02 ÷ 1.90]	1.49 [1.14 ÷ 2.08]
Arithmetic mean deviation of the surface, nm	49 [34 ÷ 75]	274 [195 ÷ 340] *
Ten point height of the surface, μm	1.85 [1.19 ÷ 2.62]	1.97 [1.16 ÷ 2.71]
Developed surface area ratio, %	11.34 [6.85 ÷ 15.21]	41.75 [29.71 ÷ 55.84] *

* – Mann-Whitney criterion is less than < 0.05

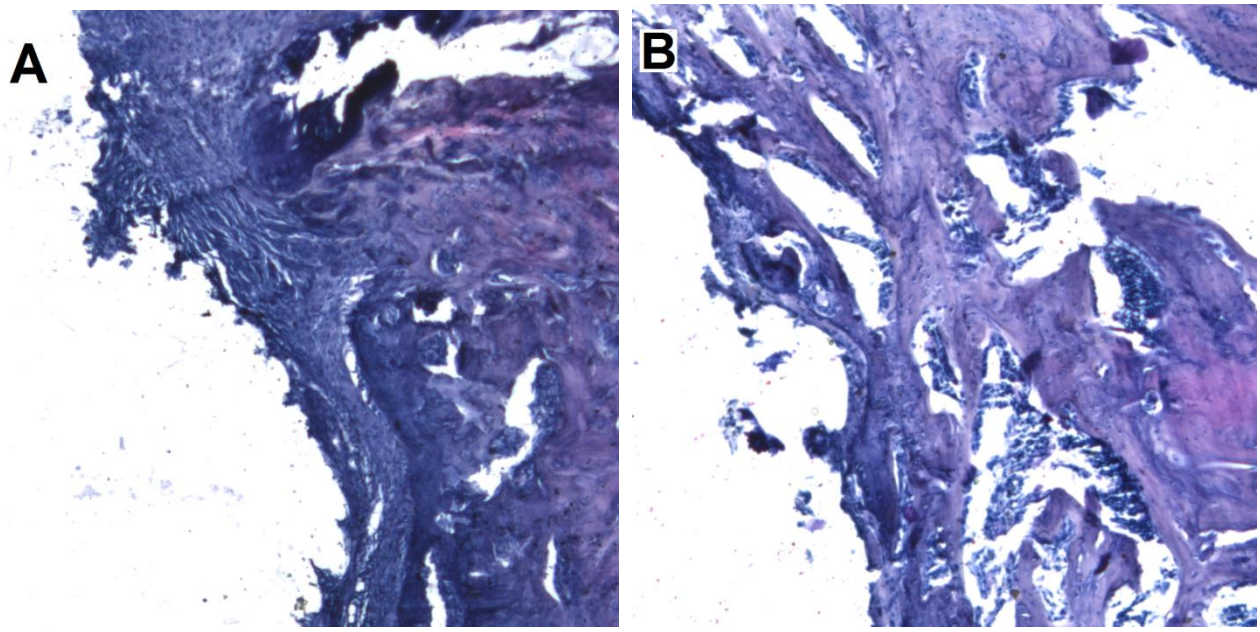

Fig. 2. Histological data at 4 weeks demonstrate the prevalence of osteogenic processes around titanium implants with chitosan-based coating, while osseointegration of implants without coating provided osseointegration through temporary connective tissue layer. A. Osseointegration zone after removing non-coated screw titanium implant MIS BioCom (Israel). B. The same, but implant had chitosan-based coating. Stain with toluidine blue, × 120.

Histological study confirmed the successful osseointegration after setting the titanium implants onto rat femoral bone. Four weeks after installation around the implants without chitosan-based coating we can see a thin layer of connective tissue. It contained a lot of blood vessels and small foci of osteogenic cells. In adjacent bone the simultaneous presence of small osteoresorption areas and chains of osteoblasts at the edges of the osseous beams testified about the active bone remodeling (Fig. 2A). Around implants coated by chitosan, a layer of formed connective tissue contained a variety of osteogenic and chondrogenic foci. The border of tissue after implant removing was irregular in shape, with partial separation of tissue, indicating successful osseointegration. The restoration and remodeling of the surrounding bone was very intense (Fig. 2B).

At 8 weeks, the zone around the implants in the comparison group was presented by a mixed regenerate in the form of connective tissue and fibrous bone with concentric direction of the fibers around the implant. On the border with the surrounding cancellous bone, this regenerate more resembled the structure of the bone. The cancellous bone demonstrated the traits of remodeling. The shape and structure the border with the cavity after implant showed a high degree of osseointegration. In the main group the zone around implants remained appearance of mixed osteogenesis. The fibrous tissue was thin, and the bulk of osseointegration zone look like a dense cover of the newly formed bone surrounding the implant. Adjacent trabecular bone was in a state of intense remodeling, with a clear increase of bone formation.

The data of quantitative analysis are shown in Table 2 and Fig. 3, indicate that the surface coating of the implant with chitosan was accompanied by a significant increase in the thickness of the zone of integration. The bone volume fraction in osseointegration zone exceeded at different periods of the experiment the value of the same parameter in the comparison group 1.56-1.64 times. Changes in the adjacent cancellous bone in group with using chitosan-based coating revealed the activation of osteosynthesis, which is clearly prevailed over osteoresorption. By the 8th week of the experiment, in the main group the cortical bone thickness near the osseointegration zone was 1.21 times higher than in the comparison group; at the same time the cancellous bone volume fraction was exceeded values in the comparison group 1.24 times; and the trabecular thickness was higher than 1.32 times (all differences were significant).

Table 2. Surface topography characterisation of commercial screw titanium implants for dentistry with or without functional chitosan-based coating (Median [1st quartile ÷ 3rd quartile])

Parameter	Control group	Time	Experimental groups	
			Main	Comparison
Osseointegration zone				
Osseointegration zone thickness, μm	-	4 weeks	255 # [198 ÷ 319]	150 [127 ÷ 179]
		8 weeks	412 # [373 ÷ 361]	244 [212 ÷ 270]
Bone volume fraction in osseointegration zone, %	-	4 weeks	44.8 # [41.6 ÷ 47.5]	27.3 [24.1 ÷ 31.0]
		8 weeks	59.9 # [52.8 ÷ 63.1]	38.2 [35.9 ÷ 40.4]
Surrounding bone				
Cortical bone thickness, μm	1035 [945 ÷ 1123]	4 weeks	1195 * [1040 ÷ 1332]	1070 [971 ÷ 1157]
		8 weeks	1384 *# [1210 ÷ 1538]	1136 [1005 ÷ 1275]
Cancellous bone volume fraction, %	41.0 [36.8 ÷ 47.1]	4 weeks	45.0 [41.2 ÷ 50.4]	40.7 [38.3 ÷ 43.4]
		8 weeks	58.6 *# [52.0 ÷ 55.9]	47.2 * [45.4 ÷ 52.5]
Trabecular thickness, μm	238 [214 ÷ 252]	4 weeks	284 [239 ÷ 302]	249 [205 ÷ 289]
		8 weeks	355 * [298 ÷ 410]	268 [220 ÷ 306]

* = p < 0.01 by Friedman test (comparing control group); #= p< 0.05 by Mann-Whitney test (between experimental groups)

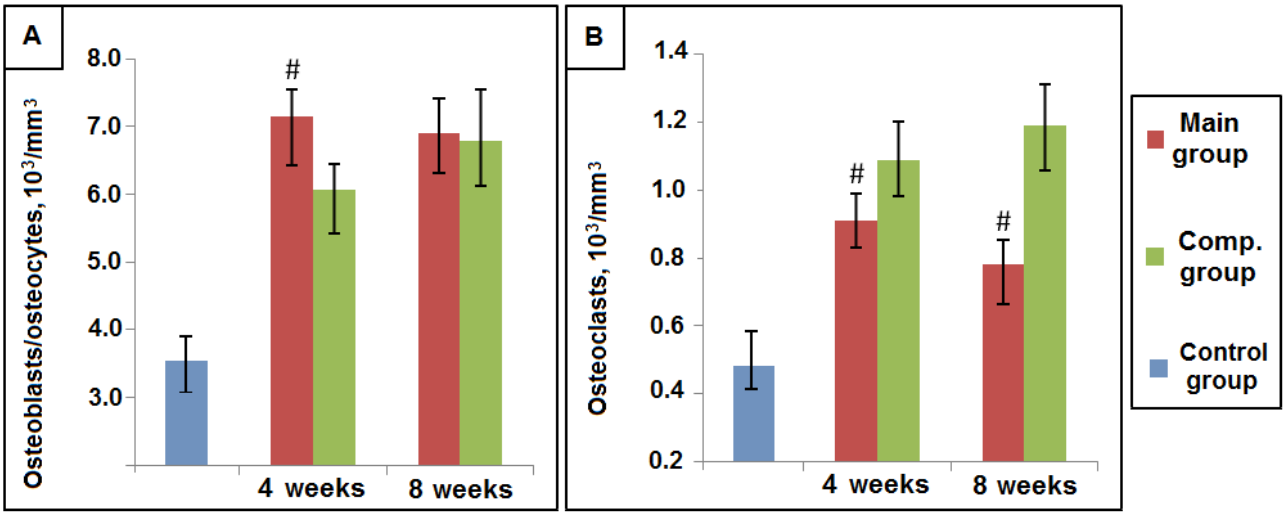

Fig. 3A. The cellular composition of osseointegration zone around of dental implants with chitosan-based coating in rat femur demonstrates more rapid arising the pool of osteogenic cells and more intensive increment of osteoclasts, comparing the dynamics of the same indices in group with non-coated implants. A. Numeral density of osteoblast and osteocytes. B. Numeral density of osteoblast. Data are represented as Me [Q1 ÷ Q3], mark '#' means p<0,01.

Fig. 3B. demonstrates the friendly increase in the numerical density of osteoblasts, osteocytes and osteoclasts, a few more intensive at the 4th week of the experiment in main group. In contrast, the number of osteoclasts in the primary group was significantly lower than in the comparison group, which showed relatively lower capacity of ostertibble in this group.

4. Discussion

According to modern concepts, osseointegration involves a series of events, including the activation of several protein cascades, cell apposition, vascular invasion, de novo bone formation and maturation to achieve the result of primary and secondary stability of the endosseous implants (Sailaja, 2016). This process is successfully accelerated by changing the surface roughness of the implant and the development of a biomimetic interface (Chang et al., 2010; O'brien, 2011). The available preclinical and clinical evaluation of the biomechanical properties showed an ambiguous dependence between the structural parameters of implants, preimplantation tissues, and indicators of functional integration of the implant (Tonetti et al., 2012; Bassi et al., 2013; Morachini et al., 2015). As a result, very little commercial implants contain nanostructures (e.g. Osseospeed, AstraTech, Sweden and Ossean, Intra-Lock, USA), and the prevalence micro-relief coatings (e.g., Bicon, USA) is relatively low (Coehlo, 2009; Dohan Ehrenfest, 2011). The main reason seems to be impossible to fabricate dental implants with enough efficiency in the experiment and clinics, using all suitable nanotechnologies.

We obtained coverage will definitely improve the ability of dental implants to osseointegration. But at the same time, they are still very far from ideal, and need to be studied from the standpoint of uniformity of the obtained properties, repeatability, storage stability, and other important characteristics in the transition to clinical implementation. Most likely, the ideal functional coatings are not manufactured with any one procedure or material, and by combining several approaches, taking into account all (from chemical to macroscopic) levels of interaction between implant and host tissue. The future the problem can be solved based on the principles of functional tissue engineering, which considered the osseointegration as the formation of hybrid biomechanical systems with the construction of computational models based on the principle of achieving the desired end results of the operation (Guliak et al., 2014).

5. Conclusion

Chitosan is a suitable agent for bioactive functionalization of the surface of dental implants. The original functional coating based on chitosan, applied using the technique of cathodic sputtering, alter significantly the surface nano-relief of dental implants. The results of atomic force microscopy confirm that implants with chitosan-based coating had a record of nano- roughness 7.7 times more than non-coated products, and the rate of development of the surface was increased by coating 4.5 times.

The obtained experimental results indicate that after setting the screw titanium implants with bioactive functionalization of their surface with chitosan in the femur of rats, an additional osteoconductive effect is revealed. As a result, more intense and anticipating the timing the formation of bone tissue is in the area of osseointegration, it combines with morphological signs of intensive remodeling and compaction of the surrounding bone. In the end, to 8 weeks after installation, the complete osseointegration is present. This suggests for this method of surface functionalization to be promising for implementation in the dental practice.

References

Abarrategi et al., 2010 – *Abarrategi A., Lópiz-Morales Y., Ramos V., et al.* (2010). Chitosan scaffolds for osteochondral tissue regeneration. *J. Biomed. Mater. Res.* A. 95(4), 1132-1141.

Albertini et al., 2015 – *Albertini M., Fernandez-Yague M., Lázaro P., et al.* (2015). Advances in surfaces and osseointegration in implantology. Biomimetic surfaces. *Med. Oral Patol. Oral Cir. Bucal.* 20(3), e316–e325. doi: 10.4317/medoral.20353.

Bassi et al., 2013 – *Bassi F., Carr A.B., Chang T.L., et al.* (2013). Clinical outcomes measures for assessment of longevity in the dental implant literature: ORONet approach. *Int. J. Prosthodont.* 26(4), 323-330. doi: 10.11607/ijp.3402.

Berglundh, 2013 – *Berglundh T., Giannobile W.V.* (2013). Investigational clinical research in implant dentistry: beyond observational and descriptive studies. *J. Dent. Res.* 92(12 Suppl): 107S–108S. doi: 10.1177/0022034513510531.

Beutner et al., 2010 – *Beutner R., Michael J., Schwenzer B., Scharnweber D.* (2010). Biological nano-functionalization of titanium-based biomaterial surfaces: a flexible toolbox. *J. Royal Soc. Interface.* 7, S93–S105.

Chang et al., 2010 – *Chang P.-C., Lang N.P., Giannobile W.V.* (2010). Evaluation of functional dynamics during osseointegration and regeneration associated with oral implants: a review. *Clin. Oral Implants Res.* 21(1), 1–12. doi: 10.1111/j.1600-0501.2009.01826.x

Coelho et al., 2009 – *Coelho P.G., Granjeiro J.M., Romanos G.E., et al.* (2009). Basic research methods and current trends of dental implant surfaces. *J. Biomed. Mater. Res. B. Appl. Biomater.* 88(2), 579–596. doi: 10.1002/jbm.b.31264.

Correa et al., 2015 – *Corrêa J.M., Mori M., Sanches H.L., et al.* (2015). Silver nanoparticles in dental biomaterials. *Int. J. Biomater.* e485275. doi: 10.1155/2015/485275

Correia et al., 2011 – *Correia C.R., Moreira-Teixeira L.S., Moroni L., et al.* (2011). Chitosan scaffolds containing hyaluronic acid for cartilage tissue engineering. *Tissue Eng. Part C. Methods.* 17(7), 717-730. doi: 10.1089/ten.tec.2010.0467

Di Martino et al., 2005 – *Di Martino A., Sittinger M., Risbud M.V.* (2005). Chitosan: a versatile biopolymer for orthopaedic tissue-engineering. *Biomaterials.* 26(30), 5983-5990.

Dohan Ehrenfest, 2011 – *Dohan Ehrenfest D.M., Vazquez L., Park Y.J., et al.* (2011). Identification card and codification of the chemical and morphological characteristics of 14 dental implant surfaces. *J. Oral Implantol.* 37(5): 525-542. doi: 10.1563/AAID-JOI-D-11-00080.

Dohan Ehrenfest et al., 2010 – *Dohan Ehrenfest D.M., Coelho P.G., Kang B.S., et al.* (2010). Classification of osseointegrated implant surfaces: materials, chemistry and topography. *Trends Biotechnol.* 28(4): 198-206. doi: 10.1016/j.tibtech.2009.12.003.

Dzenis, 2008 – *Dzenis Y.* (2008). Materials science - structural nanocomposites. *Science.* 319 (5862): 419–420. doi: 10.1126/science.1151434.

Gao et al., 2015 – *Gao X., Zhang X., Song J., et al.* (2015). Osteoinductive peptide-functionalized nanofibers with highly ordered structure as biomimetic scaffolds for bone tissue engineering. *Int. J. Nanomedicine.* 10, 7109–7128. doi: 10.2147/IJN.S94045

Guliak et al., 2014 – *Guilak F., Butler D.L., Goldstein S.A., Baaijens F.P.T.* (2014). Biomechanics and mechanobiology in functional tissue engineering. *J. Biomech.* 47(9): 1933–1940. doi: 10.1016/j.jbiomech.2014.04.019

Hwang et al., 2015 – *Hwang J., Jeong Y., Park J.M., et al.* (2015). Biomimetics: forecasting the future of science, engineering, and medicine. *Int. J. Nanomedicine.* 10: 5701–5713. doi: 10.2147/IJN.S83642

Jang et al., 2011 – *Jang H.W., Kang J.K., Lee K., et al.* (2011). A retrospective study on related factors affecting the survival rate of dental implants. *J. Adv. Prosthodont.* 3(4), 204-215. doi: 10.4047/jap.2011.3.4.204

Kalita et al., 2016 – *Kalita V.I., Mamaev A.I., Mamaeva V.A., et al.* (2016). Structure and shear strength of implants with plasma coatings. *Inorganic Materials: Applied Research.* 7(3), 376–387. doi: 10.1134/S2075113316030102

Kumar et al., 2004 – *Kumar M.N., Muzzarelli R.A., Muzzarelli C., et al.* (2004). Chitosan chemistry and pharmaceutical perspectives. *Chem. Rev.* 104(12), 6017-6084.

Luo et al., 2012 – *Luo T., Zhang W., Shi B., et al.* (2012). Enhanced bone regeneration around dental implant with bone morphogenetic protein 2 gene and vascular endothelial growth factor protein delivery. *Clin. Oral Implants Res.* 23(4), 467-473. doi: 10.1111/j.1600-0501.2011.02164.x

Lyabin, 2012 – *Lyabin M.P., Novochadob V.V., Semenov P.S.* (2012). Способ получения хитозана патент на изобретение RUS 2539933 30.03.2012 (in Rus, Engl abstr.)

Mas-Moruno et al., 2015 – *Mas-Moruno C., Garrido B., Rodriguez D., et al.* (2015). Biofunctionalization strategies on tantalum-based materials for osseointegrative applications. *J. Mater. Sci. Mater. Med.* 26(2), 109. doi: 10.1007/s10856-015-5445-z

Morachini et al., 2015 – *Moraschini V., Poubel L.A., Ferreira V.F., Barboza Edos S.* (2015). Evaluation of survival and success rates of dental implants reported in longitudinal studies with a follow-up period of at least 10 years: a systematic review. *Int. J. Oral Maxillofac. Surg.* 44(3), 377-388. doi: 10.1016/j.ijom.2014.10.023.

Muzzarelli, 2011 – *Muzzarelli R.A.* (2011). Biomedical exploitation of chitin and chitosan via mechano-chemical disassembly, electrospinning, dissolution in imidazolium ionic liquids, and supercritical drying. *Mar. Drugs.* 9(9), 1510-1533. doi: 10.3390/md9091510

Novochadov et al., 2013 – *Novochadov V.V., Gaifullin N.M., Zalewski D.A., et al.* (2013). The chitosan-coated implants with bioactive surface demonstrate improved characteristics of

osseointegration in rats. *Rossiyskiy mediko-biologicheskiy vestnik imeni akademika I.P.Pavlova.* (2): 30-35.

O'Brien, 2011 – *O'Brien F.J.* (2011). Biomaterials and scaffolds for tissue engineering. *Mater. Today*. 14, 88–95. doi: 10.1016/S1369-7021(11)70058-X

Ogle, 2015 – *Ogle O.E.* (2015). Implant surface material, design, and osseointegration. *Dent. Clin. North Am.* 59(2), 505-520. doi: 10.1016/j.cden.2014.12.003

Park et al., 2012 – *Park J.H., Wasilewski C.E., Almodovar N., et al.* (2012). The responses to surface wettability gradients induced by chitosan nanofilms on microtextured titanium mediated by specific integrin receptors. *Biomaterials*. 33(30): 7386–7393. doi: 10.1016/j.biomaterials. 2012.06.066.

Park et al. 2016 – *Park K.D., Wang X., Lee J.Y., et al.* (2016). Research trends in biomimetic medical materials for tissue engineering: commentary. *Biomater Res.* 20: 8. doi: 10.1186/s40824-016-0053-7

Sailaja, 2016 – *Sailaja G.S., Ramesh P., Vellappally S., et al.* (2016). Biomimetic approaches with smart interfaces for bone regeneration. *J. Biomed. Sci.* 23, e77. doi: 10.1186/s12929-016-0284-x

Shah et al., 2016 – *Shah F.A., Stenlund P., Martinelli A., et al.* (2016). Direct communication between osteocytes and acid-etched titanium implants with a sub-micron topography. *J. Mater. Sci. Mater. Med.* 27(11): 167. doi: 10.1007/s10856-016-5779-1

Stanford, 2010 – *Stanford C.M.* (2010). Surface modification of biomedical and dental implants and the processes of inflammation, wound healing and bone formation. *Int. J. Mol. Sci.* 11(1): 354–369. doi: 10.3390/ijms11010354.

Tomsia et al., 2011 – *Tomsia A.P., Launey M.E., Lee J.S., et al.* (2011). Nanotechnology approaches for better dental implant. *Oral Maxillofac. Implants*. 26(Suppl): 25–49. PMC3087979.

Tonetti et al., 2012 – *Tonetti M., Palmer R.* Working Group 2 of the VIII European Workshop on Periodontology (2012). Clinical research in implant dentistry: study design, reporting and outcome measurements. Consensus report of Working Group 2 of the VIII European Workshop on Periodontology. *J. Clin. Periodontol.* 39(Suppl 12), 73-80. doi: 10.1111/j.1600-051X.2011.01843.x

Trindade et al., 2015 – *Trindade R., Albrektsson T., Wennerberg A.* (2015). Current concepts for the biological basis of dental implants: foreign body equilibrium and osseointegration dynamics. *Oral Maxillofac. Surg. Clin. North Am.* 27(2): 175-183. doi: 10.1016/j.coms. 2015.01.004.

van Oirschot et al., 2013 – *van Oirschot B.A., Bronkhorst E.M., van den Beucken J.J., et al.* (2013). Long-term survival of calcium phosphate-coated dental implants: a meta-analytical approach to the clinical literature. *Clin. Oral Implants Res.* 24(2), 355–362. doi: 10.1111/clr.12063

Venkatesan, 2010 – *Venkatesan J., Kim S.K.* (2010). Chitosan composites for bone tissue engineering - an overview. *Mar. Drugs*. 8(8), 2252-2266. doi: 10.3390/md8082252

Wang et al., 2014 – *Wang J., Lü D., Mao D., Long M.* (2014). Mechanomics: an emerging field between biology and biomechanics. *Protein Cell.* 5(7), 518–531. doi: 10.1007/s13238-014-0057-9

Xuereb et al., 2015 – *Xuereb M, Camilleri J, Attard NJ.* (2015). Systematic review of current dental implant coating materials and novel coating techniques. *Int. J. Prosthodont.* 28(1): 51-59. doi: 10.11607/ijp.4124

Yang, 2011 – *Yang T.L.* (2011). Chitin-based materials in tissue engineering: applications in soft tissue and epithelial organ. *Int. J. Mol. Sci.* 12(3), 1936-1963. doi: 10.3390/ijms12031936

Copyright © 2016 by Academic Publishing House *Researcher*

Published in the Russian Federation
European Journal of Molecular Biotechnology
Has been issued since 2013.
ISSN: 2310-6255
E-ISSN: 2409-1332
Vol. 14, Is. 4, pp. 148-157, 2016

DOI: 10.13187/ejmb.2016.14.148
www.ejournal8.com

Ancient Paleo-DNA of Pre-Copper Age North-Eastern Europe: Establishing the Migration Traces of R1a1 Y-DNA Haplogroup Part 2. Baikal Episode and Indo-Uralic Framework

Alexander S. Semenov [a, *], Vladimir V. Bulat [a]

[a] Deep Dive Research Group, Russian Federation

Abstract

The work considers the problems of paleogenetics and anthropology connected with pre-Copper Age after-Glacial repopulation process of the North-Eastern Europe. The unified data, obtained in various laboratories in 2010–2016, collects a certain amount of the ancient mt-DNA and Y-DNA haplogroup samples of the considered period, what allows establishing the connection between some of them. The first part of the paper (Semenov, Bulat, 2016) showed the possible connection of R1a1 Y-haplogroup dispersion in Neolithic time with Comb Ware pottery. The second part shows that the recently found R1a1's in Neolithic Baikal cultures also fit the hypothesis and can go along with Indo-Uralic language superfamily hypothesis.

The paper makes an attempt to build a picture of the population of North-Eastern Europe in pre-Copper Age time and to systemize the pale DNA genotyping results into clusters corresponding to different migration waves. The paper can be of use in biomedical purposes also, as some correlations between diseases and haplogroups were noticed in different medical works.

Keywords: Y-DNA haplogroup, R1a1, J2b, mtDNA haplogroups U4 and U5a1, Yuzniy Oleni Ostrov, Khvalynsk, Serteya, Kitoi, Indo-Uralic, paleogenetics, paleolinguistics, subclades.

1. Introduction

The interest in the origin and early localization of carriers of Y-DNA haplogroup R1a1 is serious, since this Y-DNA subclade is inherent to the significant percentage of the population of Central and Eastern Europe, India, Middle East. It is widely recognized and already proven in terms of archeology and paleogenetics that a significant concentration of R1a1 Y-DNA haplogroup was inherent to the population of European Corded Ware culture (authors note that there also existed less famous East Asian Corded Ware culture group (Semenov, Bulat, 2015). However, the location of R1a1 bearers of Pre-Corded Ware horizons causes debates due to a lack of data. However, over the last year such data emerged, allowing formulating a data-based hypothesis. New data from Kitoi also go along with it.

* Corresponding author
E-mail addresses: semyonov1980@mail.ru (A.S. Semenov)

2. Materials and Methods

The main materials for the research are data from paleogenetic samples described in other works, and catalogized in the aggregated list (Ancestral Journeys).

Table 1. R1a1 in pre-Corded Ware sites

Sample	Y-DNA from the site	MitoDNA from the site
Yuzniy Oleni Ostrov burial № 125, 5500-5000 BCE. *Indirect indicators of comb ware possible presence.*	R1a1*-M459+, M198-, J	C1g (formely C1f), U4, U2e, **U5a**, H
Serteya archeological site, middle of V-IV mill. BCE *(Comb ware presence)*	R1a1-M17	H2
Khvalynsk-II burial 5200-4000 BCE. *(Comb ware presence in preceding layers, partial continuity of population)*	R1a1*-M459+, M198-, R1b1, Q	**U5a1i**, U4, H2
Early Neolithic Kitoi culture burials (Baikal, Irkutsk area) (*Comb ware presence, reference later here)* 6000–4500 BCE (Moussa, 2015; Moussa et al, 2016)	R1a1-M17, C3-M217, K-M9	**U5a**, A, C, D,F
Satsurblia burial (Georgia), Upper Paleolithic	J	K3
Kotias burial (Georgia), Mesolithic	J2a	H13c

The main research method of this paper is the interpretation of recently obtained genetic data, which are compared with archaeological cultures distribution.

3. Discussion and Results

In the previous paper we conclude that the presence of haplogroup R1a1 is strongly probable in the cultures of Comb Stamp Ware in the Neolithic context of Eastern Europe, but though the origin and the trace of R1a1 migration is still unclarified and more data are needed. This year the unexpected and striking data from Baikal were obtained, and, as we show, that is in accordance with our previous results and, moreover, that gives some insights on early history of Y-DNA haplogroup R1a1 bearers. So the new Baikal findings should be examined according to our view.

We base our previous findings on the D. L. Gaskevych's view on the origins of Comb Ware. In his long article «North Pontic Impresso: the origin of the Neolithic Pottery with Comb Decoration in the South Eastern Europe» In (Gaskevych, 2010: 246-247) he proposed the origin of this type of pottery in the northern Black Sea coast. «*The absolute data collected over the last 15 years in Kiev Radiocarbon Laboratory, have revealed that such ware appeared in the North-Pontic region earlier than in Upper Dnieper, Volga Region, Kama basin, Trans-Urals. However, in the steppe Pontic region it appeared earlier than in forest-steppe. All these data have proved unreliability of abovementioned hypothesis. As an alternative, the author suggests considering the Pontic region Neolithic area with comb ceramic ornamentation as a part of Neolithic cultures with Impresso ware from the Mediterranean region*»

This way, according to D. Gaskevych, we see in the Eastern Europe only a small episode of a big process, which took place from Sahara to Trans-Urals and from Marocco to the Levant. As D.L. Gaskevich refers to the initial spread of the Neolithic within the Eastern Europe, we should consider the issue of the genetic reflection of this process and specify the genetic map of the North Black Sea Region and the adjust territories in the period, preceding the Mediterranean ware adoption (though, there is another possible address of this initial spread, namely Elshanskaya culture and its derivates up to the Crimea), and the earliest time of intrusion was 6500 BC.

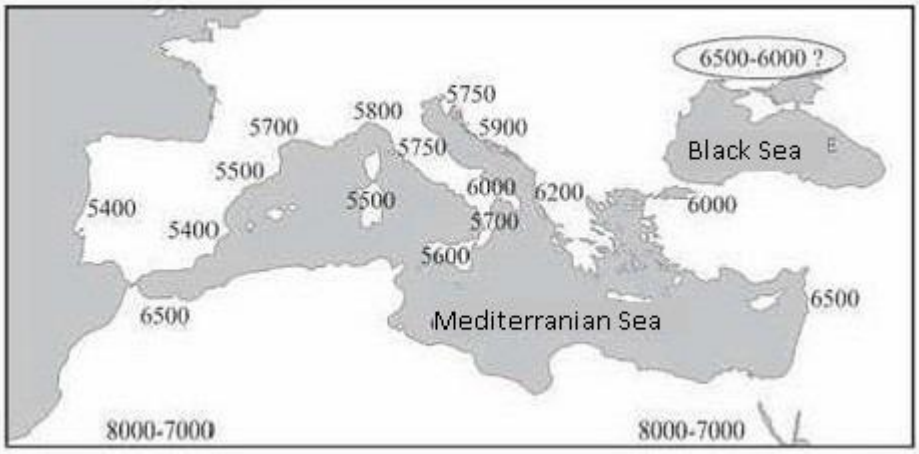

Fig. 1. The time of arrival of the Cardial ceramics, BC (Gaskevych, 2010: 239)

Gaskevych emphasizes the pre-Neolithic Bug-Dniester culture as the transmitter of Comb tradition. In our paper (Semenov, Bulat, 2016:46) we noticed, that this culture was developed on the basis of the Kukrek one. The latter belongs to Epi-Gravettian tradition and the Epi-Gravettian tradition show the presence of J (Satsurblia and Kotias burial grounds) and R1b1 (Villabruna) (Ancestral Journeys).

In our previous paper we discussed the traces of J in Native Eastern European populations (especially Finno-Ugric) and the possible Comb Cultures (Karelia) and conclude that they may have Epi-Gravettian ancestors. And if R1a1 went throughout Eastern Europe Comb Ware areas (as findings of paleoDNA show) from the Epi-Gravettian area, it can be also present in the Epi-Gravettian itself, maybe somewhere near Bug-Dniester area.

First step of this research is to see more precise origins of Corded Ware R1a1 population. According to (Kozintsev, 2016:2) «*Traditional marker of Indo-European migrations is the Corded ornament on vessels. As it is presumed, this tradition started in Dereivka culture of the end of V- beginning of IV mil BC (around 4000 BC), and then entered to Cucuteni-Tripolye areal and more to the South. The most ancient variant of the corded ornament, the caterpillar, is seen on Cucuteni C ceramics. The first its appearance in Balkans is the same, the early Eneolithic. But at first it is met rarely and the wide dispersal of it starts from the end of IV mil. BC*». We notice, that Serteya's pre-Corded Ware R1a1 belongs also to this time period.

According to (Genofond Thesaurus), the ceramics of Dereivka is hand-made, with the addition of the shells. It has comb ornament, or also stroked, pearled and pitted. Also some corded ware is noticed and the similarity with Funnel Beakers of Germany and Poland by the geometrical shape is also observable (Genofond Thesaurus). So, we see that Dereivka may be the part of the initial area of spread of «Indo-European» subclades of R1a1 (maybe R1a1-M417 and downstream) and has connections and relations with Funnel Beakers. It should be noted that one stage of Serteya culture development is also viewed as the Eastern Branch of Funnel Beakers. Hence, the area of initial spread of R1a1-M417 could be the wide area from Central Europe (Funnel Beakers) to the Black Sea, what correlates with the initial spread of Corded Ware in Early Bronze Age (Fig. 2).

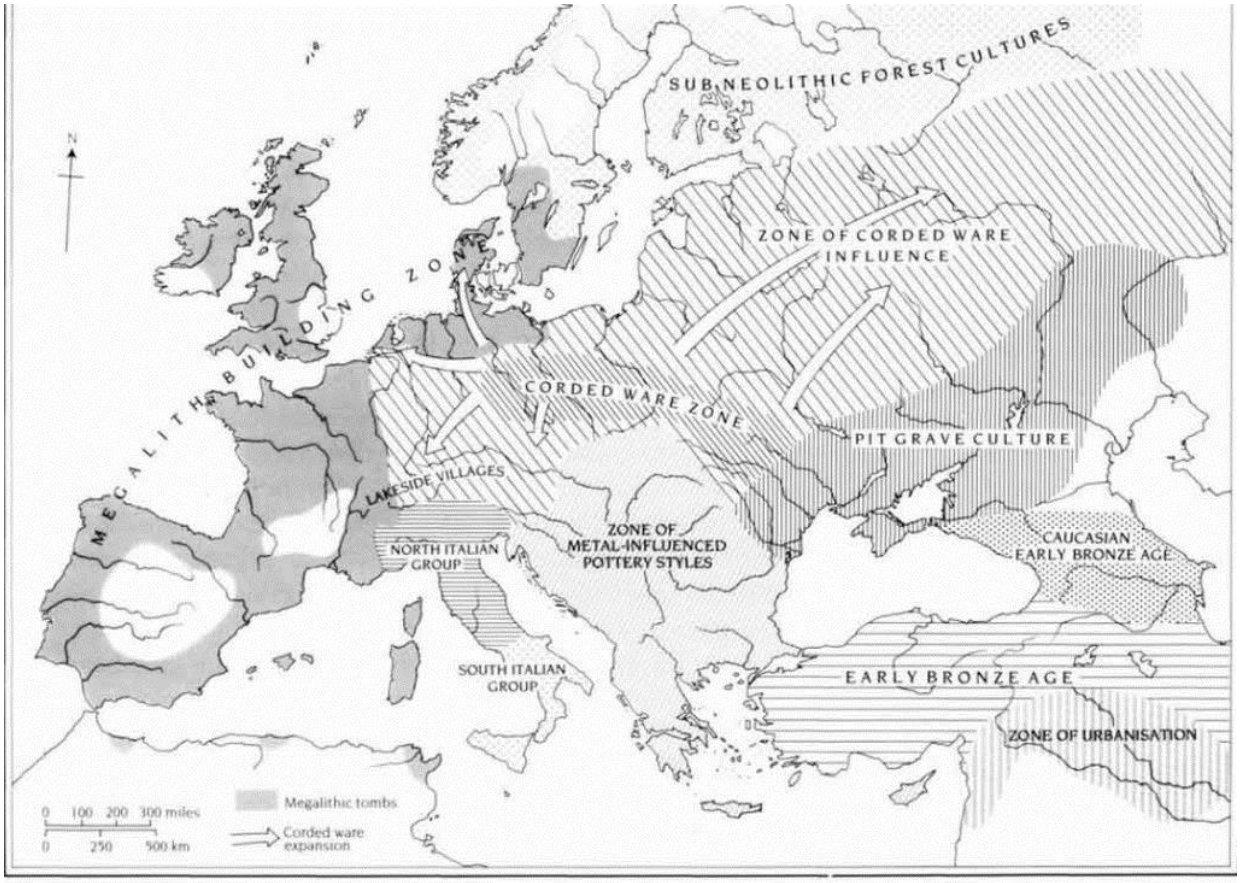

Fig. 2. The initial spread of Corded Ware

So, the new Baikal findings are to be examined according to this starting view, and we here show that they may feet well to the picture.

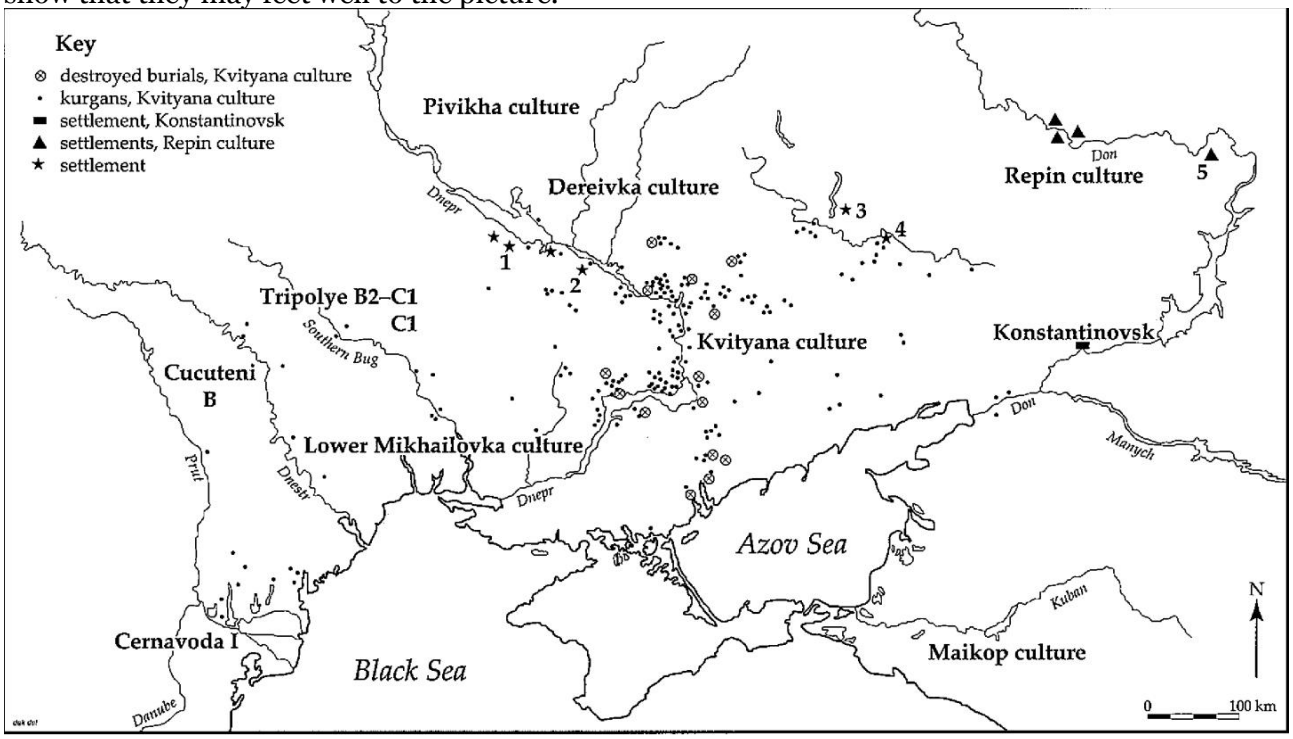

Fig. 3. The place of Dereivka culture, 4500–4000 BC (Genofond Thesaurus)

Of course, the broad range of dating Kitoi's R1a1's (6000–4500 BC) gives certain ambiguity. But we will try to show that the scenario of western migration of Kitoi R1a1 bearers is possible and

fits well with our previous conclusions (Semenov, Bulat, 2016: 51). The first argument of the Western migration to Kitoi area is the Comb Ware character of Kitoi culture (Oxford Archaeology, 1996: 644). The second and stronger is the presence of U5a mtDNA haplogroup, which is found in Paleo-, Meso and Neolithic of Europe to Urals and West Siberia (we describe it later in this paper).

As the possible Kitoi dating is earlier than Serteya-Dereivka, we should look what happened earlier on the Eastern European plain in the epoch prior to Indo-European (4500 BC). In (Kozintsev, 2016: 1, 3) it is mentioned, that the spilt of initial Indo-European had happened in the V mil. BC. (the precise time of Dereivka). So, to understand what happened earlier, we should use the hypothesis of the possible ancestors of the Indo-European language as tools. Of course, Indo-European is considered as a Nostratic branch, but this superfamily is too wide, so we should use narrower grouping. One of that is Indo-Uralic framework (sub-family, or the language union). It is not totally accepted, bud starts becoming a working tool for prominent linguists. The Academician of RAS Vyach.Vs. Ivanov, in his analysis of the names of seasons mentions Uralic materials and Indo-Uralic correspondences (Ivanov, 2006: 1-5). In (Kloekhorst, 2008: 94) it is shown that unique for Hittite languages merger the roots with possessive pronouns has the parallels in Uralics. According (Napolskikh, 2015: 4) the etymology for the Indo-European numeral '4' may be viewed as an extension of root '2' present in Uralic languages.

Let us regard the recent works with dating of language splits. The Dutch linguist Frederik Kortlandt supports a model of Indo-Uralic in which the original Indo-Uralic speakers lived north of the Caspian Sea, and the Proto-Indo-European speakers began as a group that branched off westward from there to come into geographic proximity with the Northwest Caucasian languages, absorbing a Northwest Caucasian lexical blending before moving farther westward to a region north of the Black Sea where their language settled into canonical Proto-Indo-European (2002). Allan Bomhard suggests a similar schema in Indo-European and the Nostratic Hypothesis (1996). Alternatively, the common protolanguage may have been located North of the Black Sea, with Proto-Uralic moving northwards with the climatic improvement of post-glacial times. Continuing this, in the work in (Romanchuk, Semenov, 2014; Klyosov, 2014) it was proposed, that the bearers of Y-DNA haplogroup R used to speak Sino-Caucasian languages, and some of them (including R1a1 bearers) developed proto-Indo-European language later, in the process of migrations.

According to (Kortlandt, 2002: 1) «*C.C. Uhlenbeck made a distinction between two components of Proto-Indo-European, which he called A and B. The first component comprises pronouns, verbal roots, and derivational suffixes, and may be compared with Uralic, whereas the second component contains isolated words, such as numerals and most underived nouns, which have a different source. Though Uhlenbeck objects to the term "substratum" for his B complex, I think that it is a perfectly appropriate denomination*». So, dealing with two substrata, the first is can be «Indo-Uralic», and the second could be «Sino-Caucasic».

Also Kortlandt's link Indo-Uralic and Altaic (Kortlandt, 2004: 4) show the following dating. *«We may conclude that Proto-Indo-Uralic and Proto-Altaic may have been contemporaries (6000–5500 BC), that Proto-Uralic and Proto-Uralo-Yukagir may have been the same thing and contemporaneous with Proto-Indo-Hittite (4500–4000 BC), and that Proto-Finno-Ugric and nuclear Proto-Indo-European may again have been contemporary languages (3500–3000 BC). This puts the dissolution of the Uralo-Siberian language family in the 7th millennium. It now becomes attractive to identify the latter with the abrupt climate change of 8200 BP or 6200 BC, when severe cold struck the northern hemisphere for more than a century. The catastrophic nature of this disastrous event agrees well with the sudden dispersal and large-scale lexical replacement which are characteristic of the Uralo-Siberian languages*».

Our previous hypothesis based on Gaskevych's works, and the Indo-Uralic view of Kortlandt and Bomhard can be matched together and linked with Kitoi results according to the old work of A.Kh. Khalikov (Khalikov, 1967: 27-35). The possibility of application of Indo Uralic-Theory is the findings of Khalikov that Bug-Dniestr culture influenced eastwards. It should be mentioned that Khalikov applies it to Uralic only and the his dating is as latter as possible. He also mentions Indo-Uralic hypothesis, but in earlier and very careful forms, preceding Kortlandt's. And we will show, that it matches well with current mtDNA results.

In (Khalikov, 1967: 27-35) the following scheme of the genesis of Uralic tribes genetics was outlined. Before IV mil. BC the Proto-Uralic tribes with stroked pottery lived in the territories of Volga and Kama, both sides of Urals, from Oka to Ob (and even more eastwards). In cultural and

ethnic point of view they were close related to the tribes of Dnieper-Donets culture, who were either the branch of Uralic or some extinct branch between Indo-European and Finno-Ugric. Khalikov also mentions the remark of G.F. Debets who noticed the Siberian influence on Dnieper-Donets burials. He also mentions that the ceramics looking similarly to Dnieper-Donets was found near Yenisei.

Khalikov also stresses that the Uralic community in IV mil. BC was intersected near Ural into two parts by the tribes similar to Kelteminar culture bearers. Then the Samodian tribes moved eastwards to Yenisei and Finno-Ugric stayed. Then proto-Saami may move northwards to the West.

The more distant roots of Finno-Ugric and Uralic Khalikov places into the mesolitic community in Volga-Kama and Ural regions connected with both Eastern Europe and Siberia. Khalikov avoids the precise dating but the framework supposes VI–V mil. BC. Now we know the mtDNA from Uralic (geographically) burials Chekalino, Lebyazinka IV, and they are predominantly U5a, as some of Kitoi's (the reference is later in this paper).

He mentions that the basics of this culture have the roots in Siberia, but also shows the contacts between the proto-Uralic tribes and the ancestors of Indo-Europeans, and he mentions the early Indo-Uralic theories directly. The connection between Indo-Europeans and Proto-Uralics can be traced by the inclusion the Western microlithic technique in Uralic cultures. So, he points on two substrates in Uralic cultures –Paleo-Siberian and Paleo-European.

Khalikov also mentions that the tribes from Volga and Kama (where he notices Comb pottery) and Ural borrowed the production of pottery from the South (maybe only some of the technologies, as it is seen now) via Dnieper-Donets culture. And the latter borrowed the pottery from Bug-Dniester culture, which, as Khalikov mentions, could be one of the basic of Indo-Europeans (and it was itself influenced by Starchevo-Krish culture).

Now we know the mtDNA haplogroups from Dnieper-Donets circle of cultures and they include U5a (as unique western mtDNA haplogroup present in Kitoi). Though Khalikov mentions stroked pottery only, in fact it can be both comb and stroke as it happens in Dereivka, and we saw the presence of the comb pottery in Kitoi.

The continuity of the space from Baikal to Black Sea in Meso- and Neolithic may also result in possible transfer of Corded Ware techniques to the West (Semenov, Bulat, 2015), possibly with the bearers of mtDNA haplogroup C, as we show earlier (C is present in Dnieper-Donets circle).

So, Khalikov's movement of Uralic people to the East could be that of Kitoi's R1a1 bearers. Also, if we admit the scenario that it could be two waves, one of proto-Altaic and another of Uralic, Kitoi's also could be the first, Altaic wave (the scenario that they are the ancestor of modern Altaic people is mentioned in (Turov, 2003), but there is also shown some arguments against). We stress that (Turov, 2003) also cites G. F. Debets, who admitted that Kitoi burials of the Neolithic were differentiated anthropologically and possessed a substantial European admixture. So their bearers could not be the direct ancestors of Tungusic people. This gives an additional argument for the Uralic migration version.

It is interestion to notice that though S. Starostin gives the common etymology for pot, vessel to all Borean languages we see that the most reliable etymologies are in Indo-European, Uralic, Altaic, and Sino-Caucasic (Starling). (Austric analog mentioned by Starostin also can be explained by 'Boreal' wave of creamics moving westwards from the Far East). So that can be cultural borrowing.

- Indo-European: *pod-
- Altaic: *p`a˘´dì
- Uralic: *pata
- Proto-Sino-Caucasian: *pɦătV

So that gives another argument that Altaic can be the first wave on Bug-Dniester influence eastwards. The common roots for 'pot' in Altaic and Uralic can be the sigh that the Khalikov's scenario can take place in two waves. We see that first appearance of Cardial pottery in Black Sea cost happened is in 7 mill BC, just before Kortlandt's Indo-Uralo-Altaic separated, and both Gaskevych and Khalikov show the migration of pottery cultures deeply eastwards.

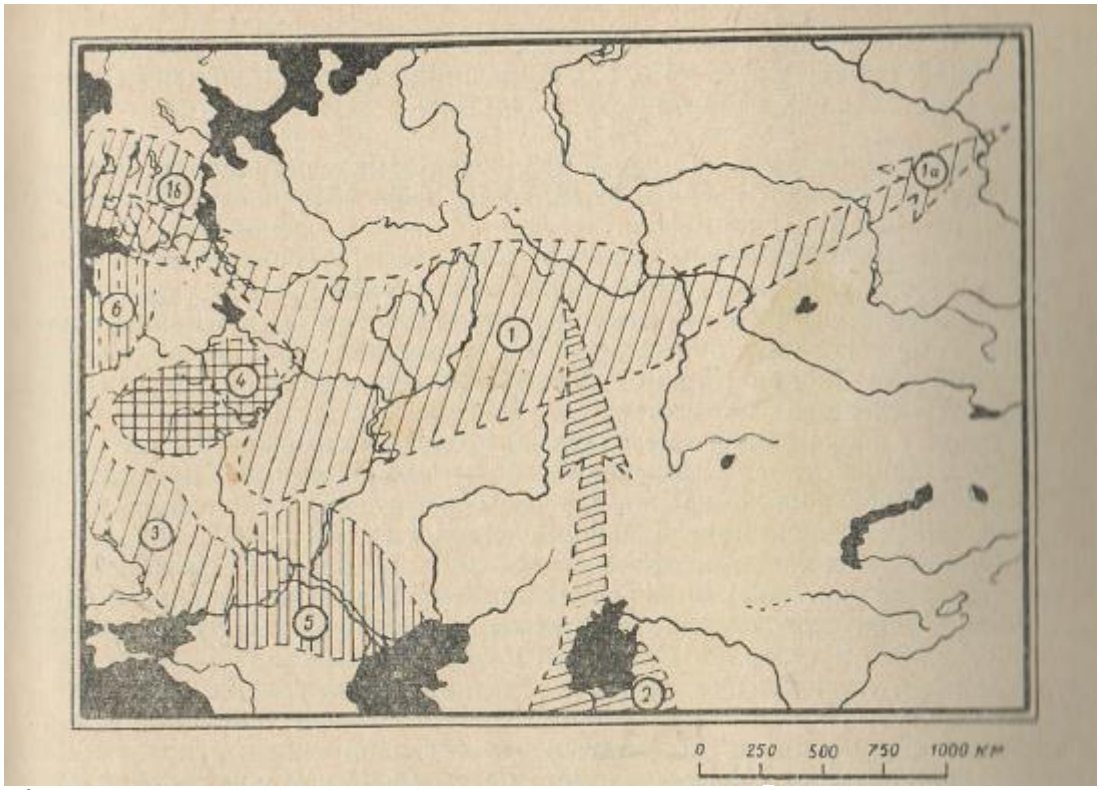

Fig. 4. Early Neolithic of Eurasia (IV mil. BC according to (Khalikov, 1967: 33))

Table 2. Early Neolithic of Eurasia (IV mil. BC according to (Khalikov, 1967: 33))*

Culture (name according to (Khalikov, 1967))	**Known Y-DNA**	**Known mtDNA**
1. Volga-Kama (Uralic)	R1b1 (**Lebyazhinka**-IV)	U5a(**Lebyazhinka**-IV)
1a. Moving Eastwards (Samoedic)		Ust-Tartas (Baraba forest-steppe) U5a, U4, U2e, A, C, Z, D (III mil BC)
1b. Sperrings (moving westwards)	R1a1*-M459+, M198-, J (if Yuzhni Oleni Ostrov is part of it or direct ancestor, question is risen in (Semenov, Bulat, 2016:43)	C1g (formely C1f), U4, U2e, U5a, H (the same)
2. Kelteminar		
3. Dniepro-Donets		U5a1a C, C4a, H, U3 (including Dereivka)
4. Early Pit-Comb (Volga-Oka)	R1a1, N1c1 (outflow to Zhizhitsa, Smolensk area)	H2
5. Dassang, Rakushechny Yar		
6. Narva		U5b

Of course, the bearers of Proto-Indo-Uralic-Altaic language can also have R1a1 and R1b taken from the Epi-Gravettian. And our main conjecture is that if the Indo-Uralic language family or commonwealth existed and dissoluted along with Khalikov's scenario, it can be correlated by the U5a mtDNA dispersion from Central Europe to Kitoi. As we see C in Dnieper-Donets and R1a1 and U5a in Kitoi we can make a hypothesis on connectivity (at least, existence of connections) between

* Some references of findings are hypothetical and shows the opinion of authors according to time and geographical proximity and archeological data.

the areas of Dnieper to Baikal. As G.F. Debets notices Siberian admixture in Dneper-Donets, and European in Kitoi, that looks possible.

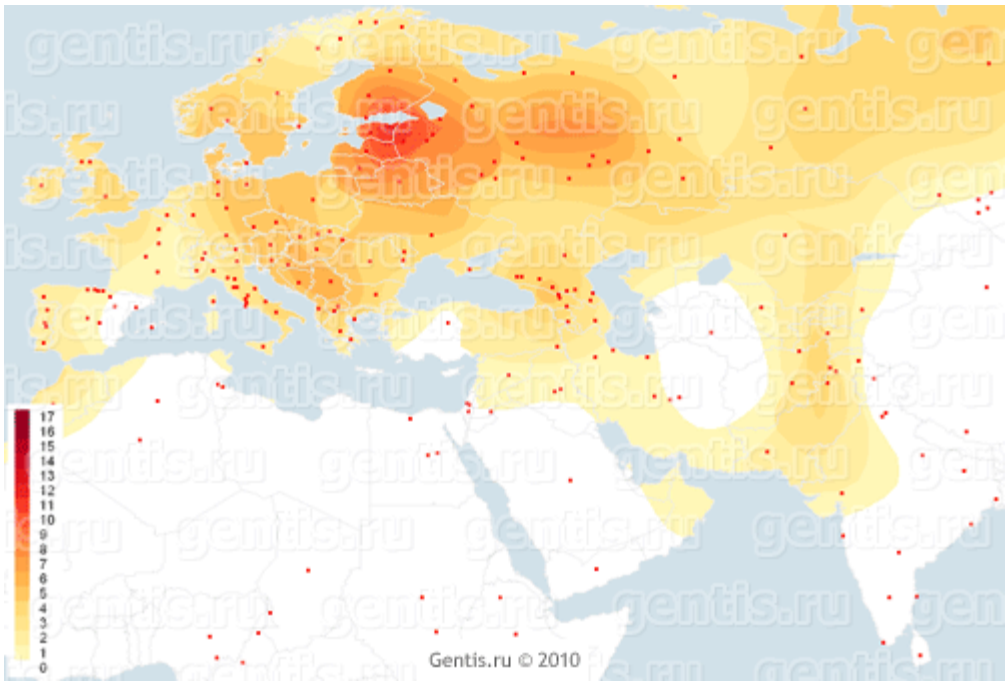

Fig. 5. The modern distribution of U5a mtDNA haplogroup

The modern distribution of U5a fits well with this idea, as it has vector to the East and goes through areals of Uralic people (Gentis)

U5 is the mitochondrial group, typical to the Upper-Paleolithic cultures like Gravettian one (Fu et al., 2013) and the dispersal routes of U5a bearers across Europe are concerned with the Central Europe (U5b prevailed in the west of Europe in Paleolithic-Mesolithic), rather than with the Western one. U5a seems to mark some migration (unknown to the archeologists) of the final Paleolithic or early Mesolithic from the Danube (possibly where Dolni-Vestonice site was located, although this location dates back to the XXV millennium BC) (ibid) to Central Germany, where the route of the U5a bearers divides into two subclades U5a1 and U5a2.

Haplogroup U5a1 is the most probable for the U5a bearer in Yuzniy Oleniy Ostrov. The bearers of U5a spread far beyond Scandinavia and Baltics. Bearers of this haplogroup can be found in Chekalino culture about 7800 BC (Bramanti et al., 2009), Lebyazhinka IV culture of the VI millennium BC (ibid, Ancestral Journeys) at the Volga and Lokomotiv burial ground of the Kitoi culture at the Angara (6100–4900 BC) (Mooder et al., 2006; Moussa, 2015; Moussa et al, 2016; AncestralJourneys). The latter enables to affirm that the Kitoi culture, which some researchers consider as the ancestral for the Altaic-language tribes or at least for the part of them (Turov, 2003), or the Uralic-language tribes, may be connected with some Mesolithic or Neolithic migrations from the more westward regions. The analysis of the burial grounds of Bolshoi Oleniy Ostrov (Sarkissian et al., 2013: 4), Lebyazhinka IV and the later cultures shows the existence of subclade U5a1. The work (Sarkissian et al., 2013: 3) shows similarity of populations of Yuzniy and Bolshoi Oleniy Ostrov. This haplgroup was also found in Mesolithic Sweden (Motala burial). The latter two arguments make the existence of U5a1 in Yuzniy Oleniy Ostrov the most possible.

Swedish burial ground Motala contains burials with a bunch of mitochondrial DNA: U2e, U5a1, U5a2, U5a2d (Ancestral Journeys; Lazaridis et al., 2013). The fixed subclade U5a2 in Les Closeaux (Rueil-Malmaison) location, dated back to 8870 BC (Posth et al., 2016) and German subclade U5a2c3 in Blätterhöhle, dated back to 8638 BC (Bolongino et al., 2013) could be considered as the similar for Motala subclades. It is possible to consider that U5a subclades were brought from the Western or Central Europe in the period, preceding to Yuzniy Oleniy Ostrov burial and the center of it dispersal was continental Western-Central Europe, and then bearers of U5a mover far to the East.

So, according to wide distribution of U5a throughout Mesolitic and Early Neolithic cultures of Eurasia we can make a conjecture that the initial bearers of Indo-European-Uralic-Altaic unity of 7th millennium BC included the bearers of mtDNA U5a, and in Early Neolithic Time R1a1-M17 could be present in proto-Altaic, and proto-Uralic populations, as well as pre-Indo-European. Nevertheless, R1a1-M17 in Proto-Altaic and proto-Uralic populations may reflect the influences from «Old Europe». Also, Uralic-like sister languages could be also present in Meso- and Neolithic Europe, where U5a mitochondrial haplogroup was detected.

4. Conclusion

We can conclude that the Early Neolithic time is characterized by the strong connection of Bug-Dniester and Dnieper-Don culture. The latter was connected with both cultures of European Neolithic and proto-Uralic cultures of Easter Europe and Urals (and, very probably, Altaic). This continuum existed since the late Mesolithic and can be characterized by mtDNA haplogroup U5a presence. Comb Ware cultures could be considered the culture of Indo-Uralic language community. Indo-Uralic community also could have sister branches in Europe, in areas, where U5a was present.

According to F. **Kortlandt**, the dual nature of Indo-European language can be explained by the mix of the Epi-Gravett Black Sea inhabitants initially speaking Sino-Caucasian dialects (maybe some of them connected with Zarzian Groups) and having R1a1, possibly R1b1, J Y-DNA haplogroups and Paleo-European populations having U5a mtDNA haplogroup. Y-haplogroup R1a1-M17 in Proto-Altaic and proto-Uralic populations may reflect the influences from «Old Europe» and Black Sea.

References

Ancestral Journeys – Aggregator http://www.ancestraljourneys.org

Bolongino et al., 2013 – *Bollongino, R. et al.* (2013). 2000 years of parallel societies in Stone Age Central Europe. *Science* 25 Oct 2013: Vol. 342, Issue 6157, 479-481. DOI: http://dx.doi.org/10.1126/science.1245049.

Bramanti et al., 2009 – *Bramanti, B. et al.* (2009). Genetic Discontinuity between Local Hunter-Gatherers and Central Europe's First Farmers. *Science*. 02 Oct 2009: Vol. 326, Issue 5949, 137-140. DOI: 10.1126/science.1176869.

Fu et al., 2013 – *Fu, Q. et al.* (2013). A revised timescale for human evolution based on ancient mitochondrial genomes, *Current Biology*, 21 March 2013. http://www.cell.com/current-biology/abstract/S0960-9822(13)00215-7

Gaskevych, 2010 – *Gaskevych D.L.* (2010). The North-Pontic Impresso: the Origin of Neolithic Patching-comb at the South of West Europe. *Stratum Plus*. No 2.

Genofond Thesaurus – www.генофонд.рф. The Thesaurus of Archaeological Cultures http://xn--c1acc6aafa1c.xn--p1ai/?page_id=9312

Gentis – The Mitochondrial Haplogroup Description http://gentis.ru/info/mtdna-tutorial/hg-u/u5a

Ivanov, 2006 – *Ivanov Vyach. Vs.* (2006). Indoeuropean Words for Seasons. The Conference «Calendar and Chronology Culture and Problems of its Studies». M. RSHU, 2006, pp. 64-70. http://kogni.narod.ru/seasons.pdf

Khalikov, 1967 – *Khalikov A.Kh.* (1967). On the Beginnings of Finno-Urgic Peoples. *The Genesis of Mari People*. Yoshkar-Ola, 1967.

Kloekhorst, 2008 – *Kloekhorst A.* (2008). Some Indo-Uralic Aspects of Hittite, *Journal of Indo-European Studies,* 36, 88-95. http://www.kloekhorst.nl/Publications.html

Klyosov, 2014 – *Klyosov A.A.* (2014). How Europe was Repopulated by the New Europeans. http://pereformat.ru/2014/04/arbins/

Kortlandt, 2002 – *Kortlandt F.*, (2002). The Indo-Uralic Verb. *Finno-Ugrians and Indo-Europeans: Linguistic and Literary Contacts: Proceedings of the Symposium at the University of Groningen, November 22–24, 2001*, 217–227. Maastricht: Shaker Publishing. http://www. kortlandt.nl /publications/art203e.pdf

Kortlandt, 2004 – *Kortlandt F.*, (2004). Indo-Uralic and Altaic, Leiden University, 2004. http://www.kortlandt.nl/publications/art216e.pdf

Kozintsev, 2016 – *Kozintsev A.G.* (2016). The earliest stage of Indo-European history: Evidence of linguistics, paleogenetics, and archaeology. *Vestnik of Tomsk State University, History*, 5.

Lazaridis et al., 2013 – *Lazaridis, I. et al.* (2013). Ancient Human Genomes Suggest Three Ancestral Populations for Europeans. DOI: http://dx.doi.org/10.1038/nature13673.

Mooder et al., 2006 – *Mooder K. et al.* (2006). Population Affinities of Neolithic Siberians: A Snapshot from Prehistoric Lake Baikal, *American Journal of Physical Anthropology*, vol. 129, no. 3 (March 2006), pp. 323-481. https://www.ncbi.nlm.nih.gov/pubmed/16323184

Moussa, 2015 – *Nour Moussa (2015).* Maternal and Paternal Polymorphisms in Prehistoric Siberian Populations of Lake Baikal. PhD. Thesis https://era.library.ualberta.ca /files/ wm117r51m/Moussa_Nour_M_201509_PhD.pdf

Moussa et al., 2016 – *Nour Moussa et al. (2016).* Y-chromosomal DNA analyzed for four prehistoric cemeteries from Cis-Baikal, Siberia. *Journal of Archaeological Science: Reports.* http://dx.doi.org/10.1016/j.jasrep.2016.11.003

Napolskikh, 2015 – *Napolskikh V.V.* (2015). Reconstruction of Numerals and Numeric Bases in Uralic Languages. In *Papers on Ethnical History, Kazan, 2015*, https://www.academia.edu /4918933/_2012.

Oxford Archaeology, 1996 – The Oxford Companion to Archaeology, 1996.

Posth et al., 2016 – *Posth, C. et al.* (2016). Pleistocene Mitochondrial Genomes Suggest a Single Major dispersal of non-Africans and a Late Glacial population turnover in Europe. DOI: http://dx.doi.org/10.1016/j.cub.2016.01.03

Romanchuk, Semenov, 2014 - *Romanchuk A.A., Semenov A.S.* (2014). R and Q haplogroups of Y-chromosome and ProtoNorth Caucasian Substratum of Proto-Indo-Europeans. *Russian Journal of Biological Research*, 2014, Vol. (1), № 1, pp. 46-68

Sarkissian et al, 2013 – *Der Sarkissian C. et al. (2013).* Ancient DNA Reveals Prehistoric Gene-Flow From Siberia in the Complex Human Population History of North East Europe. http://journals.plos.org/plosgenetics/article?id=10.1371/journal.pgen.1003296

Semenov, Bulat, 2015 – *Semenov A.S., Bulat V.V.* (2015). Possible North-Eastern Connections of the R1a1-populations of Corded Ware Culture According to the Archaeologic and Paleogenetic Data. *Russian Journal of Biological Research*, 2015, Vol. (5), Is. 3, pp. 173-194. DOI: 10.13187/ejbr.2015.5.173

Semenov, Bulat, 2016 – *Semenov A.S., Bulat V.V.* (2016). Ancient Paleo-DNA of Pre-Copper Age North-Eastern Europe: Establishing the Migration Traces of R1a1 Y-DNA Haplogroup. *European Journal of Molecular Biotechnology,* Vol.(11), Is. 1. http://ejournal8.com/ journals_n/ 1461227205.pdf

Starling – Etymological Database starling.rinet.ru

Turov, 2003 – *Turov M.G.* (2003) More on the Historical Urheimat and Early Ethnogenesis of Tungusians. Peoples and Cultures of Siberia. Communication as the Factor of Formation and Modernization: (papers). Irkutsk. 147-180. http://mion.isu.ru/filearchive/ mion_publcations /turov/9.html

Copyright © 2016 by Academic Publishing House *Researcher*

Published in the Russian Federation
European Journal of Molecular Biotechnology
Has been issued since 2013.
ISSN: 2310-6255
E-ISSN: 2409-1332
Vol. 14, Is. 4, pp. 158-170, 2016

DOI: 10.13187/ejmb.2016.14.158
www.ejournal8.com

Characterization, Mechanisms and Applications in the Chemistry of Cyanine Dyes: A Review

H. A. Shindy [a, *]

[a] Department of Chemistry, Faculty of Science, Aswan University, Aswan 81528, Egypt

Abstract

In this paper review, some of the important characterizations and mechanisms in the chemistry of cyanine dyes were explained. This include topics like absorption spectral behaviour, general characterization of cyanine dyes, photosensitisation effects of cyanine dyes in silver halide emulsion, photosensitisation-structure correlation of cyanine dyes, colour spectrophotometric measurements of cyanine dyes, fluorescence spectra of cyanine dyes, IR and ^{1}H NMR spectra of cyanine dyes, general view in the visible spectra of cyanine dyes, stability of cyanine dyes, cyanine dyes in photodynamic therapy, synthesis mechanisms of monomethine cyanine dyes and synthesis mechanisms of trimethine cyanine dyes. In addition, in the introduction section of this review paper some light is shed on important uses and applications of cyanine dyes. Reviewing some of the important characterizations and synthesis mechanisms in the chemistry of cyanine dyes is interesting and can be considered as a novel or patent idea to which little attention has been paid in the chemistry literature.

Keywords: cyanine dyes,characterization of cyanine dyes, applications of cyanine dyes, absorption spectra of cyanine dyes, emission spectra of cyanine dyes, stability of cyanine dyes, synthesis mechanisms of cyanine dyes.

1. Introduction

Cyanine dyes (Fasiulla et al., 2008; Deligeorgiev et al., 1998; Champagne et al., 2006; Rongqi, 2006; Kovalska et al., 2010; Kabatc, Paczkowski, 2010; Yakubovskyi et al., 2010; Klochko et al., 2010; Yashchuk et al., 2007; Boto et al., 2008; Gadjev et al., 1999; Keisar et al., 2014; Yi et al., 2014; Owens et al., 2014) occupy an important and vital position in the chemistry of dyes and pigments because of their multiple uses and applications in various fields of science, technology, engineering, pharmacology and medicine. These may include but not limited to determination of carbon–carbon bond length, in textile industry, as corrosion inhibitors, as electrophotographic photoreceptors, in printing inks, as synthetic drugs, as inhibitors for cell growth and division in many biological process, as cosmetic ingredients, as reagents in biomedicine, as indicator for solvent polarity, as suitable model systems to understand and study the colour of organic compounds, as photorefractive materials, dyes for polymers, in laser printers, in histological staining, as intercalating agents and as hormonal effects on plant growth. Numerous publications

* Corresponding author
E-mail addresses: hashindy2@hotmail.com (H. A. Shindy)

in the synthesis, characterisation and applications of cyanine dyes in the present time (Parvathy et al., 2015; Ferreira et al., 2015; Moreira et al., 2015; Upadhyayula et al., 2015; Arjona et al., 2016; Soriano et al., 2016; Shindy et al., 2016; Zielinska et al., 2010; Zanotti et al., 2011; Shindy et al., 2016a; Lynch et al., 2013; Zhao et al., 2013; Park et al., 2013) reflect the positive future and importance of these dyes in modern science and advanced technologies.

Because cyanine dyes have multidisciplinary uses and applications in various fields of science, technology, engineering, pharmacology and medicine, this paper review might be very interesting for the large heterogenous community groups of chemists, biologists, physicists, biotechnologists, pharmacologists and medical scientists. This paper review will also be informative, useful, and an excellent key reference work for chemists and researchers who are keen to have the fundamental understanding, principles and knowledge of cyanine dyes. Also, this paper review can be used and will be most valuable for students, particularly for the post graduate students in the field of heterocyclic and cyanine dyes chemistry. This paper review is recommended to everyone interested in the subject, to chemistry libraries and also for the personal bookshelves of every organic heterocyclic and cyanine dyes chemist.

2. Some characterization of cyanine dyes

2.1. Absorption spectral behavior (Mojzych, Henary, 2008; Shindy et al., 2000; Shindy et al., 2001; Shindy et al., 2002; Shindy et al., 2002a; Shindy, 1999; Shindy et al., 2006):

Absorption spectra bands in the visible region of the spectrum correspond to transitions of electrons from ground state of a molecule to an excited state. Many substances do not absorb light in the visible range of the spectrum. Such substances are not coloured compounds. Compounds that absorb light in the visible region of the spectrum are coloured compounds, and generally have some weakly bound or delocalized electrons. Cyanine dyes are one of these coloured compounds which have delocalized electrons. Cyanine dyes belong to the category of complex organic compounds which have very intense absorption spectra bands in the visible region of the spectrum. This strong absorption of light at particular wavelengths makes solutions of these molecules brightly coloured. A solution of a dye shows the colour of the light that is not absorbed. The strong absorption leads to many applications of these dyes in technology. For example, these dyes are used to colour plastics, fabrics, and hair. They can also be used to filter and produce coloured light and as laser medium in medical applications. The polymethine cyanine dyes generally show absorption bands in the visible region of the spectra, and each extension for the methine units causes a bathochromic shifts for the absorption bands. Depending on the structure absorption of the pentamethine, cyanine dyes can reach a near-infrared region (>700 nm) and heptamethine cyanine dyes may show absorption bands beyond 1000 nm.

2.2. General characterization of cyanine dyes (Mojzych, Henary, 2008; Shindy et al., 2000; Shindy et al., 2001; Shindy et al., 2002; Shindy et al., 2002a; Shindy, 1999; Shindy et al., 2006; Dioxn et al., 2005):

Cyanine dyes are highly coloured compounds, partially soluble in non polar organic solvents and easily soluble in polar organic solvents giving coloured solutions, accompanied in many cases by pale to intense fluorescence. The intensity and colour of the fluorescence depends upon the type of dye and solvent used. The dyes are soluble in concentrated H_2SO_4 liberating iodine vapour on warming. They are also pH-sensitive dyes, and hence their ethanolic solutions give changeable colours in acid and base media being yellow or colourless on acidification and getting back (restore) their permanent intense colour on basification.

In addition, the solutions of cyanine dyes in solvents having different polarities exhibits either general solvent effects (increasing wavelength and/or bathochromic shift with increasing solvent polarity) and/or specific solvent effects (decreasing wavelength and/or hypsochromic shift with increasing solvent polarity). The specific solvent effects of cyanine dyes is illustrated due to hydrogen bond and/or molecular complex formation between the molecules of solvents and cyanine dyes molecules.

Besides, the solutions of cyanine dyes in aqueous universal buffer solutions having varies pH media gives either positive halochromism (increasing wavelength and/or bathochromic shift with changing pH of the buffer solution) and/or negative halochromism (decreasing wavelength and/or hypsochromic shift with changing the pH of the buffer solution). The negative halochromism of

cyanine dyes is explained due to protonation for the lone pair electrons which represents the source of the electronic charge transfer pathways inside the cyanine dye molecule via acidic H proton.

Furthermore, cyanine dyes have unusual optical properties, and high fluorescent quantum yield of their aggregates, strongly absorbing in the visible region, highly fluorescent in monomers and aggregates both in solution and organized media. The two types of aggregates that are known for cyanine dyes are H-aggregate recognised by their blue shifted broad absorption band and J-aggregate that exhibits a sharp red shifted absorbance with respect to the monomer absorption. The ease of formation of aggregates in conjunction with their potential applications in optical devices, photosensitises, and fluorescent probes for bio-membrane fluidity made cyanine dyes particularly interesting.

2.3. Photosensitization effect of cyanine dyes in silver halide emulsion (Mishra et al., 2000; Finar, 1990: 893-894):

Cyanine dyes (mainly refers to spectrum sensitisation added dyes) are used as an essential photography organic matter of new variety photosensitive material because of their unrivalled ability to impart light sensitivity to silver halide emulsions in a region of the spectrum to which the silver halide is normally not sensitive. Hence, by using cyanine dyes it is possible to make photographic emulsions sensitive to all parts of the visible spectrum, which are then termed as panchromatic. For instances, photographic plates of silver chloride emulsions are sensitive from 350 to 450 nm and those of silver bromide emulsions, from 350 to 530 nm. By using cyanine, the photographic plates of silver bromide emulsions sensitised from the region 350-530 nm to the green region 350-600 nm. Pinacyanol cyanine dye sensitised the emulsion to the red region 350-710 nm and kryptocyanine cyanine dye sensitised it to the infra-red radiation. Therefore, the synthesis and application research of cyanine dyes is very important for the domestic and international foreign film factory.

2.4. Photosensitization-structure correlation (Shindy et al., 2002; Shindy et al., 2006a; El-Aal et al., 1997):

Photosensitisation-structure correlation properties of cyanine dyes were usually determined by studying their electronic visible absorption spectra in 95 % ethanol solution. The dyes are thought to be better photosensitisation when they absorb light at longer wavelength (bathochromic and/or red shifted dyes) and consequently, photosensitisation of the dyes decrease in the dyes which absorb light at shorter wavelength (hypsochromic and/or blue shifted dyes).

The photosensitisation of the cyanine dyes is very markedly dependent on the structure and nature of the dyes. Generally, photosensitisation of the dyes increases (decreases) by increasing (decreasing) conjugation in the dye molecule. Also, the photosensitisation of the dyes increases (decreases) by decreasing (increasing) the electronegativity of the hetero atoms present in the heterocyclic system of the dye. Electron donating groups increase the photosensitisation of the dyes while electron accepting groups decrease the photosensitisation. Increasing number of methine groups give better photosensitisers dyes, and dyes which have two conjugated charge transfer pathways inside the dye molecule are better photosensitisers than those which have one conjugated charge transfer pathway. Also, higher planarity dyes are better photosensitisers than their contrast lower planarity dyes.

2.5. Colour spectrophotometric measurements of cyanine dyes (Finar, 1990: 869; Shindy et al., 2012):

Colour spectrophotometric measurements for the cyanine dyes can be made by measuring their electronic visible absorption spectra in 95 % ethanol solution. The dyes are thought to be darker in colour when they absorb light at longer wavelength (bathochromic shifted or red shifted dyes), and consequently the lightening of the dye colour increase when they absorb light at shorter wavelength (hypsoochromic shifted and/or blue shifted dyes). So, we may say that the colour of one dye is darker than the other one if the wavelength of the maximum absorption spectrum of the former is longer than that of the latter one. Inversely, we may say that the colour of one dye is lighter than that of the other one if the wavelength of the maximum absorption spectrum of the former is shorter than that of the latter one.

In addition, colour spectrophotometric measurements for the cyanine dyes can be investigated by measuring their electronic visible absorption spectra in pure solvents having different polarities. The dyes tend to give darker colours and longer wavelength bands (bathochromic shifted or red shifted bands) in the solvents which have higher polarity or dielectric constants. So, we can say that, this solvent is more polar than the other one when the wavelength of the maximum absorption spectra bands of the dye in the former solvent is longer than that of the latter one. Inversely, the dyes tend to give lighter colours and/or shorter wavelength bands (hypsochromic shifted or blue shifted bands) in the solvents which have lower polarity and/or dielectric constants So, we can say that, this solvent is less polar than the other one when the wavelength of the maximum absorption spectra bands of the dye in the former solvent is shorter than that of the latter one. Therefore, cyanine dyes have extensive uses as indicator for solvent polarity. Deviation from this rule occurs when there are specific solvent interactions between the dye and the solvent like hydrogen bonding and/or molecular complex formation.

Besides, colour spectrophotometric measurements for the cyanine dyes can be examined by measuring their electronic visible absorption spectra in aqueous universal buffer solutions. The dyes tend to give darker colours and/or longer wavelength bands (bathochromic shifted or red shifted bands) in the buffer solutions having higher pH media or basic media. So, we can say that this buffer solution is more basic than the other one when the wavelength of the maximum absorption spectra bands of the dye in the former buffer is longer than that of the latter one. Inversely, the dyes tend to give lighter colours and/or shorter wavelength bands (hypsochromic shifted or blue shifted bands) in the buffer solutions having lower pH media or acidic media. So, we can say that this buffer solution is more acidic than the other one when the wavelength of the maximum absorption spectra bands of the dye in the former buffer is shorter than that of the latter one. Therefore cyanine dyes can be used as indicator for the pH of the buffer solutions or as indicators in acid-base titrations in analytical chemistry.

2.6. Fluorescence spectra of cyanine dyes (lakowicz, 1983: 2-3, 5-6):

Fluorescence spectral data are generally presented as emission spectra. A fluorescence emission spectrum is a plot of the fluorescence intensity versus wavelength (in nanometers) or wave numbers (in cm^{-1}) Emission spectra vary widely and are dependent upon the chemical structure of the cyanine fluorophore and the solvent in which it is dissolved. Generally, the fluorescenec emission spectrum appears to be a mirror image of the absorption spectrum.

The emission from cyanine fluorophore generally occurs at wavelengths which are longer than those of light absorption. The loss of energy between absorption and reemission of light is called Stokes' shift. Stokes' shift is a result of several dynamic processes. These processes include energy losses due to dissipation of vibrational energy, redistribution of electrons in the surrounding solvent molecules induced by the altered (generally increased) dipole moment of the excited cyanine fluorophore, reorientation of the solvent molecules around the excited state dipole, and specific interactions between the fluorophore and the solvent or solutes. Specific interactions include hydrogen bonding and formation of charge transfer complexes.

The Stokes' shift of many cyanine dyes are in between 10-40 nm. A large Stokes' shifts between the excitation spectrum wavelength and emission spectrum wavelength of a dye can lead to greater sensitivity and higher resolution at physiological concentrations.

2.7. IR and ^{1}H NMR spectra of cyanine dyes (Moreda, Forrester, 1997):

The IR and ^{1}H NMR spectra of cyanine dyes are often distinguished by the appearance of IR bands and ^{1}H NMR signals characteristic for: N-Me, N-MeCH_2, CH=N, -CH=CH-, -CH=CH- conjugated.

In many cases the ^{1}H NMR spectra of cyanine dyes gives broad, multiple and poor resolved peaks. This may be attributed to the following reasons:

i) Cyanine dyes are complex organic compounds.

ii) Cyanine dyes are electronic charge transfer compounds. So, the signals of the^{1}H NMR spectra will be complicated with these electronic charge transfer leading to broad and multiple signals.

iii) The molecular motion of the polymethine chain inside the dyes molecules (due to the mesomeric structures of the cyanine dyes) leads to poor resolved peaks.

2.8. General view in the visible spectra of cyanine dyes (Shindy et al., 2015; Shindy et al., 2015a; Shindy et al., 2015b; Shindy et al., 2016b; Winstead, Willams, 2011):

As a general view, the electronic visible absorption spectra of cyanine dyes reveals wavelength bands in the following approximately visible range values:

i) 400-500 nm for the monomethine cyanine dyes (simple cyanine dyes).

ii) 500-600 nm for the trimethine cyanine dyes (carbocyanine dyes).

iii) 600-700 nm for the pentamethine cyanine dyes (dicarbocyanine dyes).

iv) 700-980 nm for the heptamethine cyanine dyes (tricarbocyanine dyes).

The minimum and maximum wavelength values of these bands may go up and dawn approximately by 20-50 nm according to the types of the substituents and nature of the heterocyclic nucleus in the cyanine dyes structure.

2.9. Stability of cyanine dyes (Yao et al., 2015; Shindy, 2012; Shindy, 2015; Shindy et al., 2014; Kim, 2006):

When making fluorescent tags, higher stability cyanine dyes is required, but there are lack and/or poor stability problems for cyanine dyes on light, heat, and/or oxygen. The main factors of light oxidation and fade of dye are redox active substances such as singlet oxygen, oxygen compounds, and peroxides. Lack stability of cyanine dyes against the mentioned conditions have a large influence on the application of cyanine dyes in various aspects. For example, cyanine dyes have a wide uses and application in CD-R and DVD-R industry as disc media, and the standard characteristics of CD-R were established on cyanine-based optical recording disk, but these disks have lack chemical stability. So, they are unsuitable for archival CD and DVD use, as they can fade and become unreadable in few years. In addition, most cyanine dyes are valueless as fabric dyes because their fugitive and/or lack stability to light. For these reasons, finding out the effective methods and ways to increase the stability of cyanine dyes have very important meaning. The concentration of dyes, heterocyclic mother nucleus, oxygen in atmosphere, single and/or double cyanines and stabilizers will effect on the stability of the cyanine dye.

Double-cyanine dyes are better light stability than mono-cyanine dyes (single cyanine dyes). This is probably because in double-cyanine dyes there are two single cyanine dyes can be the base of each other, that is the introduction of the substituent with high space steric, hindering the attack of singlet oxygen or ultra-oxygen anion and improving the oxidation resistance and light stability of the dye. In addition, stabilized cyanine dyes are higher stability than the non-stabilized cyanine dyes. Therefore, recent cyanine disks contain stabilizers that slow down the deterioration significantly. As general, now days the stability of many cyanine dyes have been improved by introducing some metals like Ni (Nickel), Cu (Cupper) and/or Co (Cobalt) to their structures. The cyanine dyes obtained in these cases called metal stabilized cyanine dyes.

3. Cyanine dyes in photodynamic therapy (PDT) (Shindy et al., 2012; Yao et al., 2015; Shindy et al., 2016c)

Photodynamic therapy is a new method for treatment of cancer. Due to its excellent properties, cyanine dyes are used in light power treatment. Photodynamic therapy has many advantages compared with surgery chemotherapy and radiotherapy treatment in treating cancer. First of all, it can have special light sensitive materials accumulate in tumor selectively, which will not damage the body normal tissues cells. Secondly, only local anesthetic is needed which saves a lot of medical bills. Finally, the side effect is small, which does not cause other damage in the body. Because of its light selectivity and specificity, photodynamic therapy only damage tumor tissue without harming the body normal cells.

Particularly, merocyanine dyes can distinguish some certain cells and selectively enter into cancer cells, then kill it as photosensitizers directly using for photodynamic therapy (PDT) or as radiation sensitizers for the treatment of solid tumors, where the affinity between cyanine dyes and tumor cells is much higher than that between cyanine dyes and normal cells. Merocyanine dyes are also used as antitumor drugs and combining PDT with drug therapy has become a tendency and will certainly promote the treatment of tumors.

4. Synthesis mechanisms of some cyanine dyes (Shindy, 1999; Finar, 1990; Hamer, 1964; Shindy, 2007; Koraiem et al., 1989; Shindy et al., 2006a; Shindy, Koraiem, 2008; Koraiem et al., 1990; Shindy, 2007a)

4.1. Mechanism of monomethine cyanine dyes:

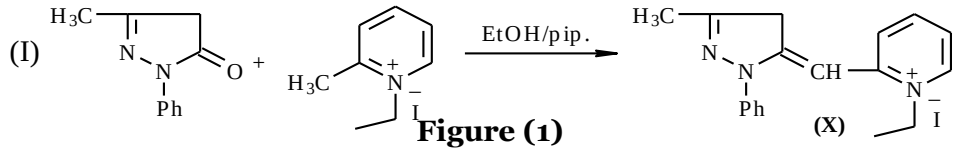

Figure (1)

The formation of the dye (X) is suggested to proceed as follows:

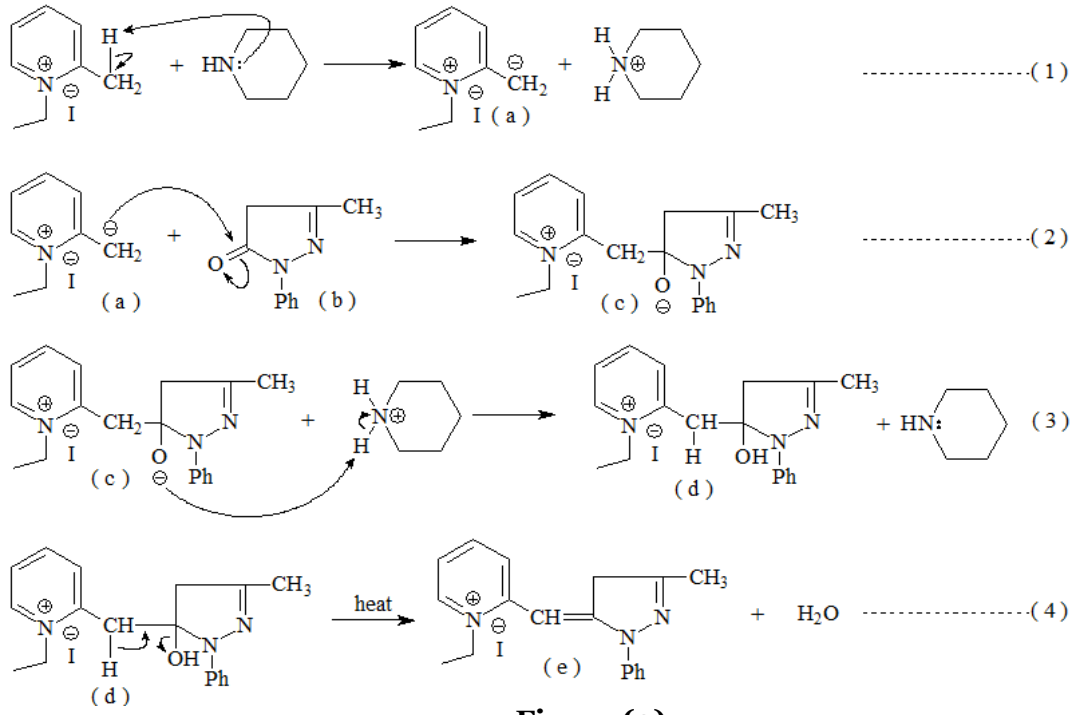

Figure (2)

The first step in this suggested mechanism is attacking of basic catalyst piperidine to the active methyl group of the quaternary salt to form the carbanion ion (a) (first step). The carbanion ion (a) attacks the positive centre of the compound (b) to obtain the intermediate compound (c) (second step). The intermediate compound (c) directly abstracts the proton $\overset{\oplus}{H}$ from piperidine-$\overset{\oplus}{H}$ to form compound (d) as intermediate compound (third step). The latter intermediate compound (d) under heat refluxing conditions gave the compound (E) (fourth step), **Figure** (2).

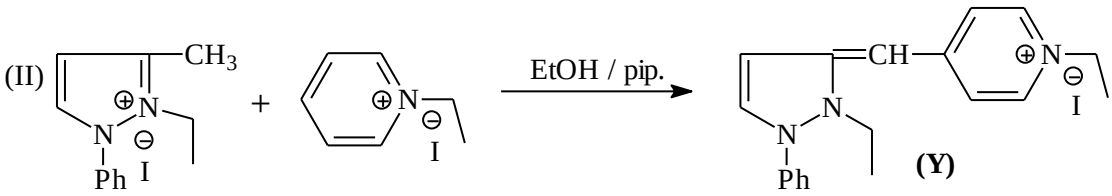

Figure (3)

The formation of the dye (Y) is suggested to proceed as follows:

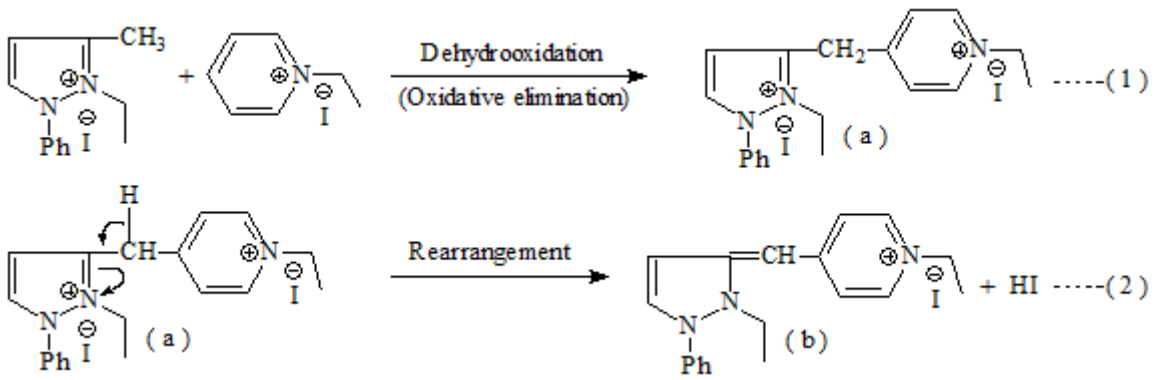

Figure (4)

The first step in this mechanism involves dehydroxidation (oxidative elimination) of the active CH_3 hydrogen atom of the pyrazolone iodide salt and the active 4-H of pyridinium iodide salt to form the intermediate compound (a). The second step involves rearrangement process of compound (a) by losing HI molecule to give the stable monomethine (b), **Figure** (4).

4.2. Mechanism of trimethine cyanine dyes:

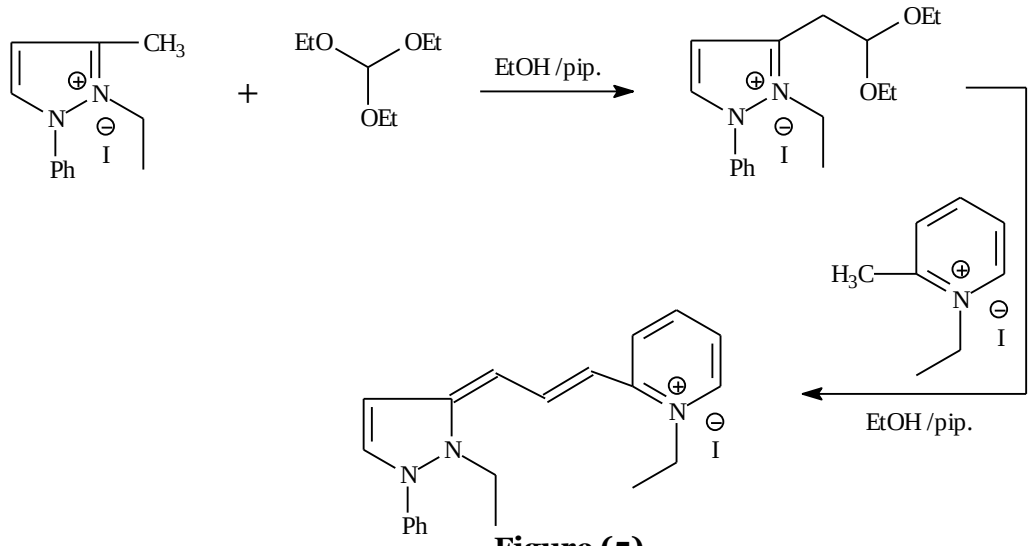

Figure (5)

The suggested mechanism for this reaction is as follows:

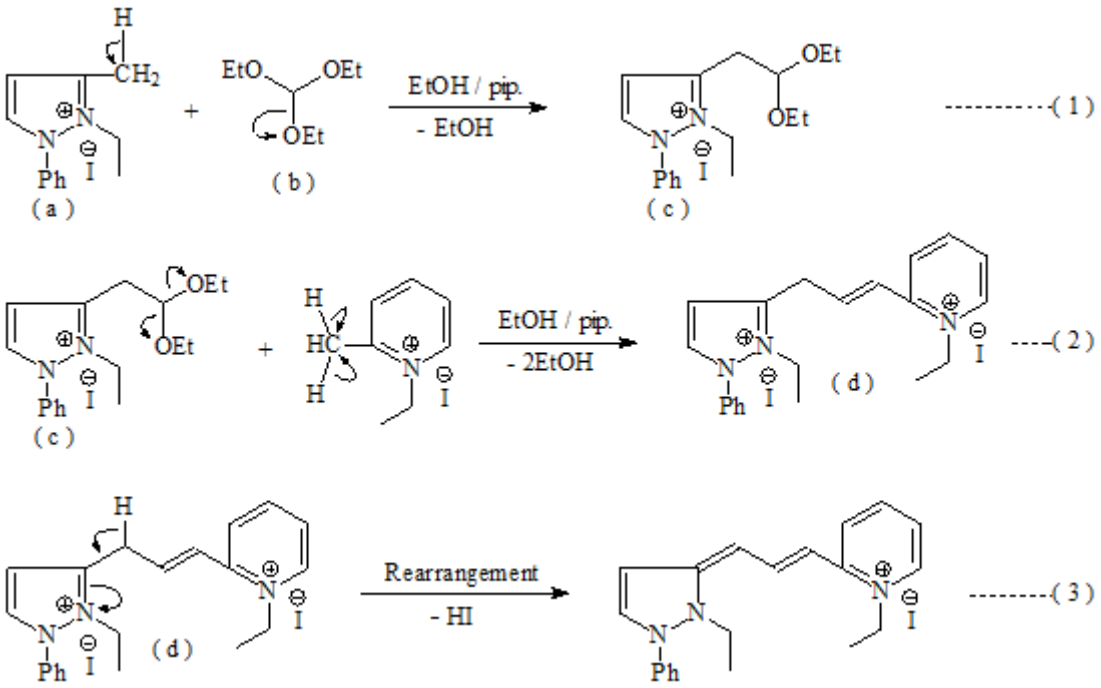

Figure (6)

The reaction proceeded via interaction of compound (a) with compound (b) losing of EtOH molecule to give compound (c), (first step). Compound (c) undergoes condensation reaction with α-picoline quaternary salt losing 2EtOH molecule to give the unstable compound (d), (second step). The unstable compound (d) undergoes rearrangement process losing HI molecule to give the trimethine compound (E), (third step), **Figure** (6).

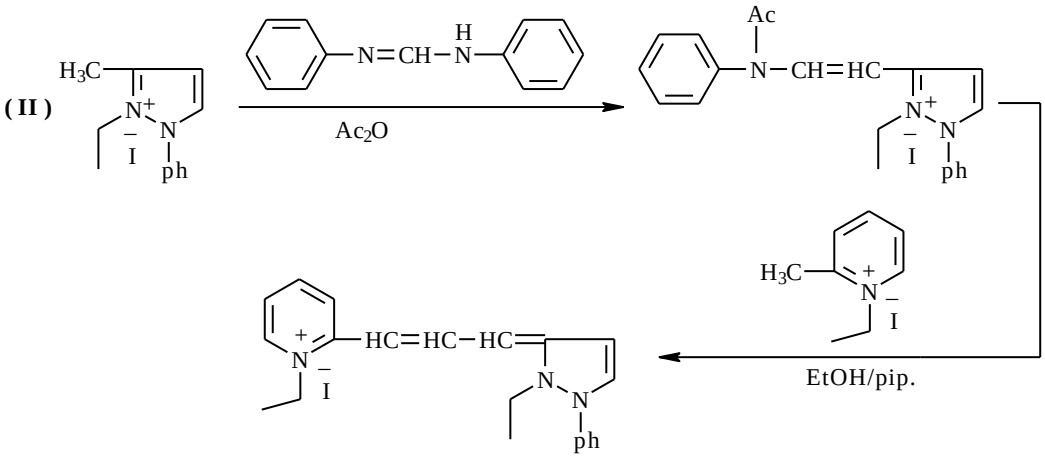

Figure (7)

The mechanism of this reaction is suggested to proceed as shown by the equations 1-7, **Figure** (8):

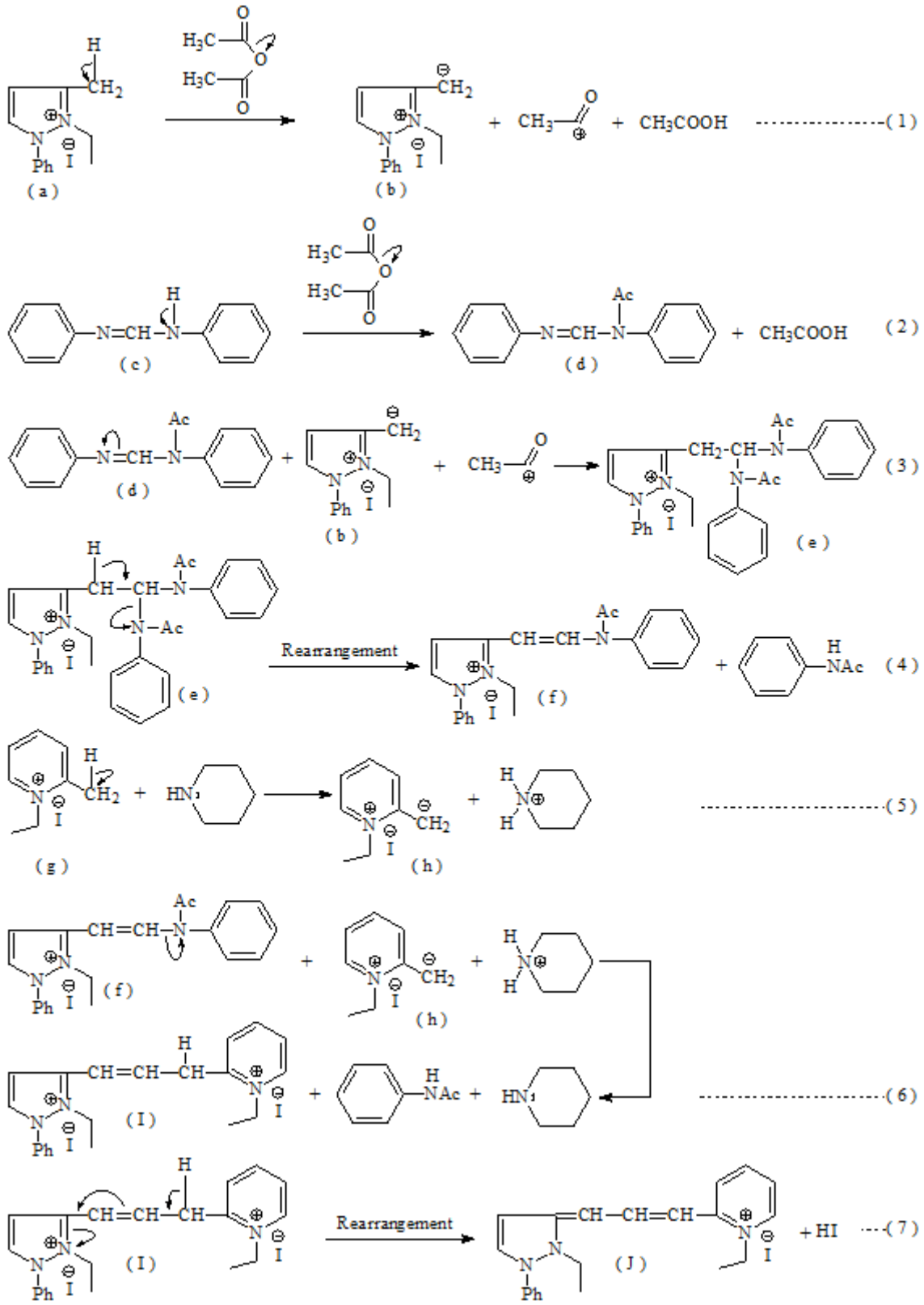

Figure (8)

5. Conclusion

The developments of cyanine dyes synthesis and their applications in photographic and non-photographic multidisciplinary areas are growing continuously and rapidly. Of course, this will make the present and the future of cyanine dyes chemistry effective, fruitful and very bright.

6. Current future developments

The current and the future research developments aim to provide novel synthetic methods for the preparation of different classes of highly antimicrobial active, Anti-tumour, p-H sensitive, highly photographic sensitizers, non toxic, high stability, light fastness, near IR (Infrared), fluorescent, anti corrosion, strong labelled DNA and extra conjugated cyanine dyes. Such as oxadiazine cyanine dyes, thiazole cyanine dyes, metal stabilized cyanine dyes, pentamethine cyanine dyes, heptamethine cyanine dyes, nonamethine cyanine dyes, undecamethine cyanine dyes and tridecamethine cyanine dyes.

7. Conflict of interest

There is no conflict of interest.

8. Acknowledgements

I am thankful to the Chemistry department, Faculty of Science, Aswan University, Aswan, Egypt for supporting this work.

References

Arjona et al., 2016 – *Arjona, A., Stolte, M., Wilerthner, F.* (2016). Conformational switching of π -conjugated junctions from merocyanine to cyanine statesby solvent polarity. *Angewandte Chemie*, 55 (7), 2470-2473.

Boto et al., 2008 – *Boto, R.E.F., Santos, P.F., Reis L.V., Almeida P.* (2008). Synthesis and characterization of new mono- and dicarboxyalkyl selenacarbocyanines. *Dyes and Pigments*, 76, 165–172.

Champagne et al., 2006 – *Champagne, B., Guillaume, M., Zutterman, F.* (2006). TDDFT Investigations of the optical properties of cyanine dyes. *Chemical physics letters*, 425 (1-3), 105-109.

Deligeorgiev et al., 1998 – *Deligeorgiev, T. G., Daphinka, D. A., Kim, Z., S. H. and Sabnis R.W.* (1998). Preparation of monomethine cyanine dyes for nucleic acid detection. *Dyes and Pigments*, 37(3), 205–211.

Dioxn et al., 2005 – *Dioxn, A., Duncan, C. and Samha, H.* (2005). Self assemply of cyanine dye on clay nanoparticles. *American journal of undergraduate research,* 3 (4), 29-33.

El-Aal et al., 1997 – *El-Aal, R. M.., Shindy, H. A., and Koraiem, A. I. M.* (1997). Synthesis and Electronic Absorption Spectra of Some New Penta-and Dimethine Cyanine Dyes. *Heteroatom Chemistry*, 8 (3), 259-266.

Fasiulla et al., 2008 – *Fasiulla, M.H., Khan, M., Harish M.N.K, Keshavayya, J., Reddy, K.R.* (2008). Synthesis spectral, magnetic and antifungal studies on symmetrically substituted metal (II) octain inophthalocyanine pigments. *Dyes and Pigments*, 76, 557–563.

Ferreira et al., 2015 – *Ferreira, D.P., Conceicao, D.S., Prostota, Y., Santos, P.F., Ferreira, L.F.V.* (2015). Fluorescene "rhodamine-like" hemicyanines derived from the 6-(N-N-diethylamino)-1,2,3,4-tetrahydroxanthylium system. *Dyes and Pigments*, 112, 73-80.

Finar, 1990 – *Finar, I. L.* (1990). Organic Chemistry, Vol. 1, *The fundamental principles*, sixth edition, 893-894.

Gadjev et al., 1999 – *Gadjev, N. I., Deligeorgiev, T. G., Kim, S. H.* (1999). Preparation of monomethine cyanine dyes as noncovalent labels for nucleic acids, *Dyes and Pigments,* 40, 181–186.

Hamer, 1964 – *Hamer, F.M.* (1964). The cyanine dyes and related compounds, *New York, interscience publishers Inc.,* 198.

lakowicz, 1983 – lakowicz, J. R. (1983). Principles of fluorescence spectroscopy, plenum press, *New York and London*, 2-3, 5-6.

Kabatc, Paczkowski, 2010 – *Kabatc J., Paczkowski, J.* (2010). Monomeric asymmetric two- and three- cationic monomethine cyanine dyes as novel photoinitiations for free radical polymerization. *Dyes and Pigments*, 86, 133–142.

Keisar et al., 2014 – *Keisar, O. R., Finfer, E. K., Ferber, S., Finaro, R., Shabat, D.* (2014). Synthesis and use of QCY7-derived modular probes for the detection and imaging of biologically relevant analytes. Nature Protocols, 9 (1), 27-36.

Kim, 2006 – *Kim, S.* (2006). Functional dyes, Elsevier B. V. 47-84.

Klochko et al., 2010 – *Klochko, O. P., Fedyunyayeva, I. A., Khabuseva, S. U., Semenova, O. M., Terpetschnig, E. A., Patsenker, L. D.* (2010). Benzodipyrrolenium–based biscyanine dyes: synthesis, molecular structure and spectroscopic characterization. *Dyes and Pigments*, 85, 7–15.

Koraiem et al., 1989 – *Koraiem, A. I. M., El-Maghraby, M. A, Khalafallah, A. K. and Shindy H. A.* (1989). Studies on the Synthesis and Solvatochromic Behaviour of Mono- and Tri-Methine Cyanines: Methine Cyanine Dyes, Synthesis And Solfatochromism, *Dyes and Pigment*, 11, 47–63.

Koraiem et al., 1990 – *Koraiem, A. I. M., Khalil, Z.H. and Abu El-Hamd, R. M.* (1990). Synthesis and spectra of some asymmetric trimethine cyanine dyes. *Dyes and Pigments*, 13 (4), 289–299.

Kovalska et al., 2010 – *Kovalska, V. B., Volkova, K. D., Manaev, A. V., Losytskky M. Y., Okhrimenko, I. N., Traven, V. F., Yarmoluk, S. M.* (2010). 2-Quinolone and Coumarin polymethines for the detection of proteins using fluorescence. *Dyes and Pigments*, 34, 159–164.

Lynch et al., 2013 – *Lynch, D. E., Chowdhury, M. Z., Luu, N, Wane, E. S., Heptinstall, J., Cox, M. J.* (2013). Water soluble bis (indolenine) squaraine salts for use as fluorescent protein – sensitive probes. Dyes and Pigments, 96, 116–124.

Mishra et al., 2000 – *Mishra, A., Behera, R. K., Behera, P. K., Mishra, B. k. and Behera, G. B.* (2000). Cyanines during the 1999s. *Chem. Review*, 100 (6), 1973-2011.

Mojzych, Henary, 2008 – *Mojzych, M. and Henary, M.* (2008). Synthesis of cyanine dyes. *Top Heterocycl Chem*, 14, 1-9.

Moreda, Forrester, 1997 – *Moreda, W. and Forrester, A. R.* (1997). Novel Heterocyclic dyes as DNA markers, part II, Structure and Biological activity. Department of chemistry, *University of Aberdeen, Meston Building, Meston Walk, Aberdeen AB9 2UE. UK.*

Moreira et al., 2015 – *Moreira, B. G., You Y., Owczarzy R.* (2015). Cy3 and Cy5 dyes attached to oligonucleotide terminus stabilize DNA duplexes: Predictive thermodynamic model. Biophysical Chemistry, 198, 36-44.

Owens et al., 2014 – *Owens, E. A., Tawney, J.G. and Henary, M.M.* (2014). 2-{(E)-2-[(3E)-2-Chloro-3-{(2E)-2-[1,1-dimethyl-3-(3-phenylpropyl)-1,3-dihydro-2H-benzo[e]indol-2-ylidene]-ethyliden}cyclohex-1-en-1-yl]ethyl}-1,1-dimethyl-3-(3-phenylpropyl)-1H-benzo[e]indolium Iodide. Molbank, 8, 1–8.

Park et al., 2013 – *Park, J., Kim, D., Lee, K., Kim, Y.* (2013). Reactive cyanine fluorescence dyes indicating pH perturbation of biomolecules. *Bull. korean chem. Soc.*, 34, 1, 1–4.

Parvathy et al., 2015 – *Parvathy, S., Liji, P.T., Kalaiyarasi A. and Venkatraman, R.R.* (2015). Synthesis of characterization of heterocyclic cyanine dyes. *Der Chemica Sinica*, 6(1), 42-45.

Rongqi, 2006 – *Rongqi C.* (2006). The development and application of green dye, *Printing and dyeing*, (6): 45.

Shindy, 1999 – *Shindy, H. A.* (1999). Synthesis and Visible Spectral Behaviour of Some New Photosensitizers: Monomethine, Dimethine, Trimethine, Styryl and Mixed Cyanine, *Dyes J. Chem. Research (S)*, 700-701., *J. Chm. Research*, (M), 3001-3017.

Shindy, 2007 – *Shindy, H.A.* (2007). Synthesis, Characterization and Visible Spectral Behaviour of some Novel Methine, Styryl, and Aza-styryl Cyanine Dyes. *Dyes and Pigments*, 75 (2). 344–350.

Shindy, 2007a – *Shindy, H. A.* (2007). Synthesis, Absorption Characteristics and Solvatochromism of some Novel Heterocyclic Cyanine Dyes. *Coloration Technology*, 123 (5), 298-305.

Shindy, 2012 – *Shindy, H.A.* (2012). Basics, Mechanisms and Properties in the Chemistry of Cyanine Dyes: A Review Paper. *Mini-Reviews in Organic Chemistry*, 9 (4), 352-360.

Shindy, 2015 – *Shindy, H. A.* (2015). Synthesis of Different Classes of Benz (Naphth) / Five Membered Heterocyclic Cyanine Dyes: A Review. *Revue Roumaine de Chimie*, 60 (1), 5-13.

Shindy et al., 2000 – Shindy, H. A., El-Aal, R. M., and Koraiem, A.I.M. (2000). Synthesis and Spectral Behaviour of Some New Uninuclear Pyrimidine 2[2(4)]-Mono (Tri)-Methine Cyanine Dyes. *Journal of the Chinese Chemical Society*, 47, 519-525.

Shindy et al., 2001 – *Shindy, H. A., Koraiem, A. I. M., Khalafallah A.K. and Soleiman, H.A.* (2001). New Cyanine Dyes from 4,9-Dioxopiperidino[2,3-g]-1,2,3,4,6,7,8,9-Octahydro-quinolinoquinone. *Indian Journal of Chemistry*, 40B, 426-429.

Shindy et al., 2002 – *Shindy, H. A. and Koraiem, A. I. M.* (2002). Synthesis and Absorption-Structure Relationship of Some New Photosensitizers Cyanine Dyes**.** *Proc. Ind. Acad. Sci. (Chem. Sci.),* 114 (2), 125-136.

Shindy et al., 2002 – *Shindy, H. A., El-Maghraby, M. A. and Eissa, F. M.* (2002). Novel Cyanine Dyes: Synthesis, Characterization and Photosensitization-Structure Correlation. *Journal of the Chinese Chemical Society*, 49, 1061-1068.

Shindy et al., 2002a – *Shindy, H. A., El-Maghraby, M. A. and Eissa, F. M.* (2002). Novel quinone cyanine dyes: Synthesis and Spectral studies. *Dyes and Pigments*, 52, 79-87.

Shindy et al., 2006 – *Shindy, H. A., El-Maghraby, M. A. and Eissa, F. M.* (2006). New Photosensitizers Cyanine Dyes: Synthesis and Properties. *Indian Journal of Chemistry*, 45B, 1197-1203.

Shindy et al., 2006a – *Shindy, H. A., El-Maghraby, M. A. and Eissa, F. M.* (2006). Synthesis, Photosensitization and Antimicrobial Activity of Certain Oxadiazine Cyanine Dyes. *Dyes and Pigments*, 70, 110-116.

Shindy et al., 2006a – *Shindy, H.A., El-Maghraby, M. A and Eissa, F. M.* (2006). Cyanine Dyes of New Heterocyclic Ring System: Synthesis and Structure-Spectra Studies. *Dyes and Pigments*, 68 (1), 11-18.

Shindy et al., 2012 – *Shindy, H. A., El-Maghraby, M. A. and Eissa, F. M.* (2012). Synthesis and Colour Spectrophotometric Measurements of some Novel Merocyanine Dyes, *Dyes and Pigments*, 92 (3), 929-935.

Shindy et al., 2014 – *Shindy, H. A., El-Maghraby, M. A. and Eissa, F. M.* (2014). Effects of Chemical structure, solvent and solution pH on the visible spectra of some new methine cyanine dyes. *European Journal of Chemistry*, 5 (3), 451-456.

Shindy et al., 2015 – *Shindy, H. A., Goma, M. M. and Harb, N. A.* (2015). Synthesis, Spectral Behavior and Biological Activity of some Novel 1,3,4-Oxadiazine Cyanine Dyes. *European Journal of Chemistry*, 6 (2), 151-156.

Shindy et al., 2015a – *Shindy, H. A., Khalafalla, A. K., Goma, M. M. and Eed A., H.* (2015). Synthesis and photosensitization evaluation of some novel polyheterocyclic cyanine dyes. *European Reviews of Chemical Research,* 5 (3), 180-188.

Shindy et al., 2015b – *Shindy, H. A., Goma, M. M. and Harb, N. A.* (2015). Novel carbocyanine and dicarbocyanine dyes: synthesis, spectral characterization and biological activity. *Revue Roumaine de Chimie*, 60 (10), 965-974.

Shindy et al., 2016 – *Shindy, H. A., Khalafalla, A. K., Goma, M. M. and Eed A., H.* (2016). Polyheterocyclic compound in the synthesis and spectral studies of some novel methine cyanine dyes. *Revue Roumaine de Chimie*, 61 (3), 139-145.

Shindy et al., 2016a – *Shindy, H. A., Khalafalla, A. K., Goma, M. M. and Eed A., H.* (2016). Novel hemicyanine and aza-hemicyanine dyes: synthesis, spectral investigation and antimicrobial evaluation. *European Journal of Molecular Biotechnology*, 13 (3), 94-103.

Shindy et al., 2016b – *Shindy, H. A., Goma, M. M. and Harb, N. A.* (2016). Novel carbocyanine and bis carbocyanine dyes: synthesis, visible spectra studies, solvatochromism and Halochromism. *Chemistry International,* 2 (4), 222-231.

Shindy et al., 2016c – *Shindy, H. A., Khalafalla, A. K., Goma, M. M. and Eed A., H.* (2016). Synthesis, photosensitization and antimicrobial activity evaluation of some novel Merocyanine dyes, *Chemistry International*, 2 (3), 114-120.

Shindy, Koraiem, 2008 – *Shindy, H. A. and Koraiem, A. I. M.* (2008). Synthesis and Colour Spectroscopic Investigation of Some Hemicyanine Dyes**.** *Coloration Technology,* 124 (5), 290-294.

Soriano et al., 2016 – *Soriano, E., Holder, C., Levitz, A. and Henary, M.* (2016). Benz [c,d] indolium-containing monomethine cyanine dyes: synthesis and photophysical properties. *Molecules*, 21 (1), 23-37.

Upadhyayula et al., 2015 – *Upadhyayula S., Nunes, V., Espinosa, E. M., Larsen, J. M., Bao, D., Shi D., Mac, J. T., Anvari, B., and Vullev, V.* (2015). Photoinduced dynamics of a cyanine dye: parallel pathways of non-radiative deactivation involving multiple excited-state twisted transitions. *Chemical Science (Chem. Sci.)*, 6, 2237-2251.

Winstead, Willams, 2011 – *Winstead, A. and Willams, R.* (2011). Application of microwave assisted organic synthesis to the development of near-IR cyanine dye probes, Enviromentals and Biosensors, Prof. V. Somerset (Ed.), 237-254.

Yakubovskyi et al., 2010 – *Yakubovskyi, V. P., Shandura, M. P., Kovtum, Y. P.* (2010). Boradipyrromethene cyanines derived from conformationally restricted nuclei. *Dyes and Pigments*, 87, 17–21.

Yao et al., 2015 – *Yao, X., Fang, R., Pang, H. and Liu, G.* (2015). Research on synthesis and properties of water-soluble symmetrical squarylium double-cyanine dyes. *The open materials science journal*, 9, 113-118.

Yashchuk et al., 2007 – *Yashchuk, V. M., Gusak, V. V., Dmytruk, I. M., Prokopets, V. M., Kudrya, V.Yu., Losytskyy, M.Y., Tokar, V. P., Gumenyuk, Ya. O., Yarmoluk, S. M., Kovalska, V. B., Kryvorotenko D. V.* (2007). Molecular Crystals and Liquid Crystals, V. 467, iss. 1, p. 325–338.

Yi et al., 2014 – *Yi, X., Wang, F., Qin, W., Yang, X., Tuan, J.* (2014). Near-Infrared fluorescent probes in Cancer imaging and therapy: an emerging field. *International Journal of Nanomedicine*, 9, 1347–1365.

Zanotti et al., 2011 – *Zanotti, K. J, Silva, G. L., Creeger, Y., Robertson, K. L., Waggoner, A. S., Berget, P. B. and Armitage, B. A.* (2011). Blue fluorescent dye-protein complexes based on fluorogenic cyanine dyes and single chain antibody fragments. *Organic Biomolecular Chemistry*, 9, 1012-1020.

Zhao et al., 2013 – *Zhao, J., Lv, Y., Ren, H., Sun, W., Liu, Q., Fu, Y., Wang, L.* (2013). Synthesis, spectral properties of cyanine dyes ß-cyclodextrin and their application as the supramolecular host with spectroscopic probe. *Dyes and Pigments*, 96, 180–188.

Zielinska et al., 2010 – *Zielinska, J., Saczko, J., Kulbacka, M., Majkowski, K., Wilk, A.* (2010). New approach to hydrophobic cyanine-type photosensitizer delivery using polymeric oil-cored nanocarriers: Hemolytic activity, in vitro cytotoxicity and localization in cancer cells. *Journal of Pharmaceutical Sciences*, 39, 322-335.